ISBN 91-628-2875-4
LUNFD6/(NFFL-7152) 1998

Luminosity Measurements and Two-Photon Physics with the DELPHI VSAT at LEP

Thesis Submitted for the Degree of
Doctor of Philosophy in Physics
by

Per M Jonsson

Department of Particle Physics
Lund University

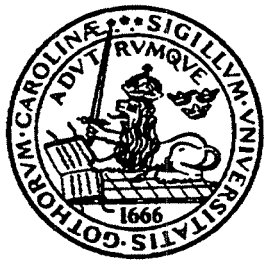

Organization **LUND UNIVERSITY** Department of Physics Professorsgatan 1, Box 118 S - 221 00 Lund	Document name **DOCTORAL DISSERTATION** Date of issue February 4, 1998 CODEN: LUNFD6/(NFFL-7152) 1998
Author(s) Per M Jonsson	Sponsoring organization

Title and subtitle
Luminosity Measurements and Two-Photon Physics with the DELPHI VSAT at LEP

Abstract

This thesis describes analysis of data from the DELPHI Very Small Angle Tagger (VSAT) calorimeter at LEP1. The VSAT consists of four Silicon-Tungsten calorimeter modules symetrically positioned 7.7 meters away from the interaction point. It measures elastically scattered electrons and positrons, Bhabha events, within the polar angular region between 5-12 mrad. Trigger efficiency and reconstruction procedures for the energy and position measurement of VSAT data are described. Off momentum electron background and online luminosity monitoring with the VSAT are also discussed. The extraction of various beam-parameters from analysis of the impact point of Bhabha pairs reveal the ability to measure variations in beam angles with a precision of 50 microrad. The relative luminosity measurement of the VSAT with a precision level of 0.1 % for the 1993-1994 Z^0 scan is also presented. Through the study of double-tag two-photon events, using the VSAT for measuring the energy of both scattered electrons, the behaviour of the total hadronic two-photon cross section is for the first time investigated up to invariant masses of 35 GeV.

Key words
LEP, DELPHI, VSAT, luminosity, two-photon physics, cross section, double-tag, Bhabha, interaction point, beam angles

Classification system and/or index terms (if any)

Supplementary bibliographical information	Language English
ISSN and key title	ISBN 91-628-2875-4
Recipient's notes	Number of pages 133 Price Security classification

Distribution by (name and address) Per M Jonsson, Department of Physics, Lund University
Professorsg 1, Box 118, S - 221 00 Lund, Sweden

Signature 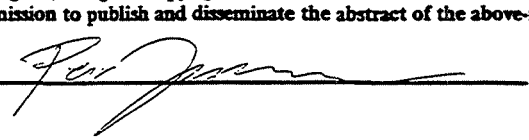 Date February 4, 1998

Luminosity Measurements and Two-Photon Physics with the DELPHI VSAT at LEP

By due permission of the faculty of mathematics and natural sciences of the
Lund University to be publicly discussed at lecture hall B of the Department of Physics,
March 6, 1998, at 10:15, for the degree of Doctor of Philosophy

by

Per M Jonsson

Department of Particle Physics
Lund University
Professorsgatan 1
Box 118
S-221 00 Lund
Sweden

This thesis is partly based on four papers, included as Appendices A to D:

A Beam parameter monitoring and interaction point measurement in DELPHI with the VSAT,
DELPHI 94-144 (1994) PHYS 453.

B Measurement of the beam parameter variations in DELPHI with the VSAT,
DELPHI 95-150 (1995) LEDI 2.

C Precision Determination of the Z^0 Resonance Parameters,
DELPHI 95-62 (1995) PHYS 497.
Submitted to the International Europhysics Conference on High Energy Physics-EPS-HEP'95 Brussels, Belgium; 27 Jul-2 Aug 1995.

D Study of multihadron production in two-photon collisions at LEP1 and LEP2,
JINR Rap. Comm. No.6(86) (1997) 55-60.

Abstract

This thesis describes analysis of data from the DELPHI Very Small Angle Tagger (VSAT) calorimeter at LEP1. The VSAT consists of four Silicon-Tungsten calorimeter modules symetrically positioned 7.7 meters away from the interaction point. It measures elastically scattered electrons and positrons, Bhabha events, within the polar angular region between 5-12 mrad. Trigger efficiency and reconstruction procedures for the energy and position measurement of VSAT data are described. Off momentum electron background and online luminosity monitoring with the VSAT are also discussed. The extraction of various beamparameters from analysis of the impact point of Bhabha pairs reveal the ability to measure variations in beam angles with a precision of 50 μrad. The relative luminosity measurement of the VSAT with a precision level of 0.1% for the 1993-1994 Z^0 scan is also presented. Through the study of double-tag two-photon events, using the VSAT for measuring the energy of both scattered electrons, the behaviour of the total hadronic two-photon cross section is for the first time investigated up to invariant masses of the $\gamma\gamma$ system of 35 GeV.

Contents

Preface

This thesis describes analysis based on data from the DELPHI VSAT detector collected during the LEP1 era at energies around the Z^0 mass peak. All descriptions refer to LEP1 conditions unless otherwise stated. The VSAT consists of four Silicon-Tungsten sampling calorimeters symmetrically placed 7.7 m away from the DELPHI interaction point. It mainly detects elastically scattered electrons, Bhabha events, at polar angles between 5 and 12 mrad. The work in this thesis gives a rather complete description of the various issues studied with VSAT data from LEP1. The author spent two-years 1994-1995 at CERN as responsible for the running of the detector and the offline processing and reconstructions of the VSAT data. After returning to Lund in 1996 my work has been concentrated on analysing two-photon events. The thesis follows in a natural way the data from the detector through all studies and corrections to the final two-photon analysis where the knowledge gained from the previous chapters are benefited from.

The first chapter describes LEP, the Large Electron-Positron Collider, and the DELPHI experiment at CERN. The VSAT detector is described in details together with the reconstruction procedures for the energy and position measurements.

The second chapter describes how Bhabha events detected by the VSAT are used to monitor variations of the interaction point coordinates. This is useful for investigating the alignment of the detector and the corrections made to the accepted Bhabha cross section, but may also serve as a cross-check of the DELPHI interaction point measurement by other detectors. A special feature is monitoring of beam-angles variations where the VSAT can measure variations of the size of 50 μrad. For completeness also monitoring of the electron background and online luminosity is mentioned in this chapter.

Chapter three describes the VSAT relative luminosity measurement for the 1993-1994 Z^0 energy-scan. Due to its high statistical precision, the VSAT was used to measure the relative luminosity at the off-peak energy points. The normalisation was done to the SAT absolute luminosity at the Z^0 peak energy. The VSAT luminosity was then used to calculate the cross-sections for the reactions $e^+e^- \to f\bar{f}$, from which various electroweak parameters were extracted.

Chapter four deals with the subject of two-photon physics and especially with the analysis of double-tag two-photon events at DELPHI. The VSAT was here used to tag both the outgoing electron and positron, thereby achieving a complete determination of the invariant mass of the hadronic system. The total hadronic two-photon cross-section was extracted from the finally selected events at invariant masses between 25 and 35 GeV.

The four appendices include papers that I have contributed to. Appendix A and B describe the measurement of various beamparameters with the VSAT. Appendix C treats the DELPHI precision measurement of the Z^0 resonance parameters from the 1993-1994

scan data. My contribution here was work on the VSAT relative luminosity used for the cross section calculation. Appendix D describes two DELPHI studies of multi-hadron two-photon events. My work was concentrated on the latter of these; the double-tag two-photon analysis.

Per M Jonsson
CERN, Geneva, February, 1998

Chapter 1

LEP, DELPHI and the VSAT

Experimental Particle Physics rely on particle accelerators for the study of the elementary constituents of matter and their interactions. Special designed detectors are also necessary for the detection and recording of the physics reactions created at the accelerators. The European Laboratory for Particle Physics, CERN, outside Geneva houses the world's largest accelerator complex (see fig. 1.1).

The latest addition to the accelerators is the LEP collider around which the four physics experiments DELPHI, ALEPH, L3 and OPAL reside.
This chapter gives a brief description of LEP and DELPHI, where I in detail describe the Very Small Angle Tagger (VSAT) calorimeter, as an introduction to the work presented in the later chapters.

1.1 The Large Electron Positron collider

The Large Electron Positron collider, LEP [1], is the largest particle-accelerator in the world. It is located on the border of France and Switzerland just outside Geneva in connection to the European Laboratory for Particle Physics, CERN. The circumference of the accelerator-ring is 26.7 km and it is situated under ground at a depth between 75 and 150 m. The whole ring consists of eight straight sections of 500 m length, connected by eight arches of 2800 m length. The radius of curvature of the arches is 3300 m. To make all of the four experimental caverns lie on firm rock ground and furthermore avoiding unnecessary excavation, the ring is inclined by 1.4%, with DELPHI at the lowest point. The inner diameter of the tunnel is between 3.8 and 5.5 m while the experimental halls have a cylindrical shape with a diameter of 23 m and a length of 80 m.

The construction of LEP was completed in 1989 and the same year the first beams were successfully brought into collisions. LEP takes advantage of the older and smaller CERN accelerators, the PS and the SPS, as injectors. When the electrons and positrons are injected into LEP they have an energy of 20 GeV. 120 Radio-frequent copper cavities are then used to accelerate the particles to the desired collision energy, while magnetic fields from combinations of dipole, quadrupole and sextupole-magnets keep the beams in their orbits. The particles are kept in 4 or 8 bunches (trains) separated by a few micro-seconds in time. In order to maximise the produced luminosity each bunch can since 1995 be divided into 2 to 4 mini-bunches (wagons) separated by a few hundred

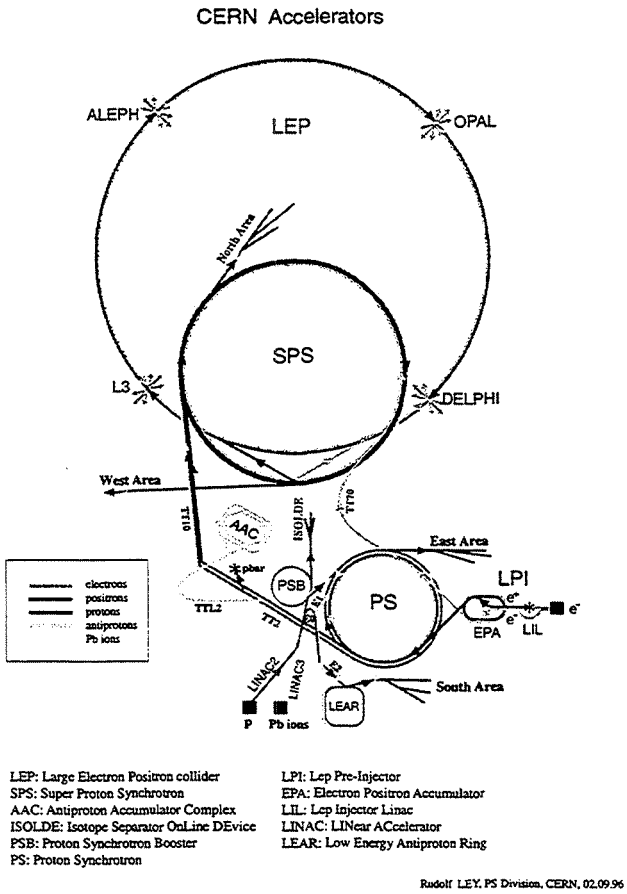

Figure 1.1: The CERN accelerator complex with the LEP collider and its four physics experiments.

nano-seconds. At the interaction-points the bunches are sharply focused by quadrupole-magnets, thereby aquiring an elliptical shape of 210 μm in width and 8 μm in height. The longitudinal length of the bunches is about 1 cm. Each bunch consists of the order of 10^{11} particles equivalent to a current of 3 mA. Typical produced luminosities at LEP1 were $\approx 10^{31}\text{cm}^{-2}\text{s}^{-1}$. In order to maximise the life-times of the beams and reduce unnecessary background from beam-gas interactions, it is crucial to have a good vacuum in the beam pipe. This is achieved by a system of independent vacuum sectors pumped by two different sets of vacuum pumps. The vacuum is normally of the order of 10^{-9} Torr during beam-operations. Since charged particles bent in a circular trajectory emit photons, synchrotron radiation, it is necessary to shield the detectors from this background source. By installing collimators made of tungsten and copper at various locations around LEP and especially around each experimental cavern, minimal photon-background can be achieved. The collimators can be maneuvered remotely to move closer to the beam if required. The LEP accelerator was constructed for precision-studies of the carrier particles of the weak

interaction. These so-called intermediate vector-bosons are the Z^0 and $W^{\pm}$ particles with masses of 91.2 GeV and 80.2 GeV. In the first stage of LEP called LEP1 in the years 1989-1995, a precision study of the Z^0 particle was performed by running LEP with energies close to the Z^0 mass. By accelerating bunches of electrons and positrons in opposite directions and letting them collide at the experimental points with an energy of 91.2 GeV (the rest-mass of the Z^0), it is possible to create Z^0 particles and to detect and study their decay-products. Fig. 1.2 shows the creation and rapid decay of a Z^0 boson.

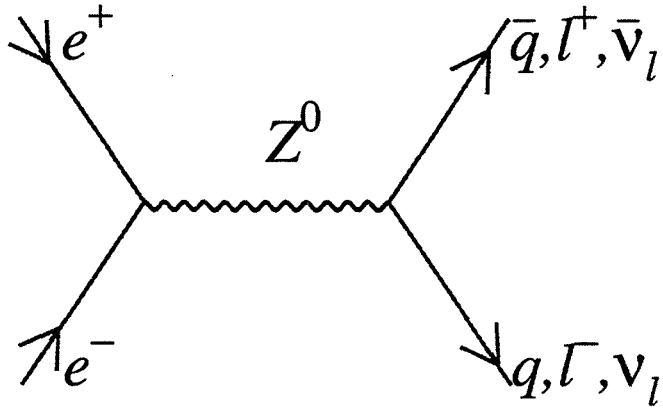

Figure 1.2: Feynman diagram of the creation and decay of a Z^0 boson at LEP1. The Z^0 has a short life-time and thus only the decay-products are detected.

From the study of Z^0 decays you gain not only information about the properties of the Z^0 particle and the associated weak interaction, but also a wide variety of other physics-issues can be investigated. An overview of the variation of physics topics studied at LEP1 can be found in [2]. In a later stage LEP has been upgraded through the installation of new super-conducting cavities to LEP2, and is since 1996 running with an energy above the W^+W^- pair production threshold. The aim is to perform a precision study of the W particles and also to search for super-symmetric and Higgs particles [3].
This thesis will mainly concentrate on LEP1 results.

1.2 The DELPHI detector

DELPHI, a DEtector with Lepton, Photon and Hadron Identification, is one of four experiments around LEP. It is a general purpose detector with special emphasis on particle identification, high granularity three dimensional information and precise vertex determination. DELPHI was completed in 1989 and is situated in a cavern 100 m under ground, in the middle of a straight section of the LEP collider. The detector has a cylindrical shape and consists of a barrel and two endcaps. The total length is about 10 m and the radius is 5 m. The largest super conducting solenoid-coil in the world, 7.2 m long and 5.2 m in diameter, surrounds the inner parts of the barrel. It provides a uniform magnetic field of 1.2 T along the beam-pipe as required by the long drift-detectors. The design

of DELPHI is made so that easy access can be achieved to the inner sub-detectors by removing the endcaps. Fig. 1.3 shows the detector layout.

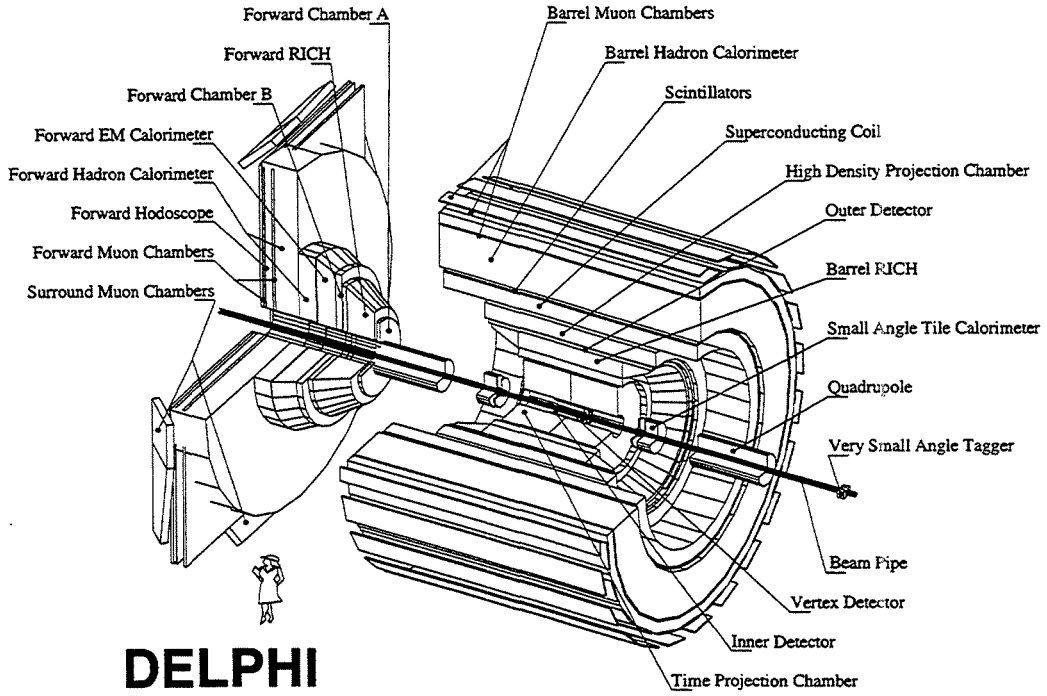

Figure 1.3: DELPHI with all of its sub-detectors.

The detector consists of around twenty sub-detectors divided into tracking detectors, calorimeters, muon detectors and the special Ring Imaging Cherenkov Counters (RICH). Each sub-detector is designed to fulfil a specific purpose, so that they together give a picture as complete as possible of the physics events. The tracking is done by the Time Projection Chamber (TPC), Vertex Detector (VD), Inner and Outer Detectors (ID and OD) and in the endcap region by the Forward Chambers (FCA and FCB). Electromagnetic showers are measured in the barrel by the High Density Projection Chamber (HPC) and in the endcaps by the Forward Electromagnetic Calorimeter (FEMC). In the forward region the Small Angle Tagger (SAT) and the Very Small Angle Tagger (VSAT) calorimeters measure electrons and positrons at small angles. In 1994 the SAT was replaced by the Small Angle Tile Calorimeter (STIC). Scintillators have been installed in the barrel region for trigger-purposes. In the region between the barrel and the endcaps additional scintillators have also more recently been installed to prevent the escape of high-energetic photons. The Hadron-Calorimeter (HAC) is placed in the iron return yoke of the solenoid. Muons are detected by the Muon Chambers (MUB and MUF), which in 1994 were complemented by the Surround Muon Chambers, which cover the glitch between the barrel and forward regions. The Ring Imaging Cherenkov Counters (RICH) in the barrel and in the forward region are responsible for particle identification. The coordinate system of DELPHI, with respect to which all coordinates are given, is defined as follows: the

z-axis is defined by the beam pipe in the direction of the electron beam, the x-axis points towards the center of LEP and the y-axis points upwards. θ corresponds to the polar angle to the z-axis and ϕ is the azimuthal angle in the plane perpendicular to the z-axis. Starting with the tracking detectors some of the sub-detectors which are of relevance for the rest of this thesis will be described more carefully. For more details on DELPHI and its performance see [4].

1.2.1 Vertex Detector (VD)

The Vertex Detector [5] is situated close to the beam-pipe in the centre of DELPHI. It consists of three concentric shells of Si-strip detectors at an average radii of 6, 9 and 11 cm, and covers a length of 24 cm along the beam-pipe. Each shell consists of 24 modules, together covering the full azimuthal angle. Each module in turn consists of 4 segments along the z-direction. The angular coverage of the VD in polar angle θ is between 37° and 143°. For each track it measures three Rϕ points with a resolution of 8 μm per single track. This ability makes it ideal for beam-spot monitoring as well as secondary vertex reconstruction. In 1994 the inner and outer layers of the VD were equipped with double-sided silicon-strip detectors for measurements of the z-coordinate. The precision of the z-measurement is on average 18 μm. In 1997 finally, the VD was upgraded for LEP2 energies and is now called the Silicon Tracker.

1.2.2 Inner Detector (ID)

The Inner Detector [6] is positioned just outside the Vertex Detector between radii of 12 and 28 cm. The detector covers the angular region between 30° and 150° in θ and is constructed as a tracking and triggering detector consisting of two parts: an inner drift chamber and an outer part of 5 layers of Multi Wire Proportional Counters (MWPC). The driftchamber part consists of 24 sectors, each covering 15° in ϕ with 24 sense-wires measuring drift time. A measure of up to 24 Rϕ points is thus obtained with an accuracy of 60 μm in R and 1.5 mrads in ϕ for a single track. The two-track separation is of the order of 1.5 mm. The MWPCs have 192 anode-wires each along the z-direction and 192 cathode-strips forming full circles at constant z. Thereby an additional 5 Rϕ points per track and also 5 z-coordinates are achieved with a precision of around 1 mm. This information is mainly used for trigger-purposes and to resolve the left/right ambiguity of the hits. The trigger efficiency of the MWPCs is better than 95% for a single track. In 1995 the MWPCs were replaced by a similar structure of straw tube detectors, thereby increasing the full angle coverage to between 15° and 165° in θ.

1.2.3 Time Projection Chamber (TPC)

The Time Projection Chamber [7] is the main tracking detector of DELPHI. It consists of two cylindrical drift volumes, separated by a high voltage anode-plane. Each half is 1.5 m long with an inner radius of 40 cm and an outer radius of 1.2 m. The whole detector covers a θ angle between 20° and 160° (see fig1.4).

Each drift volume consists of 6 sectors with 16 radial pad rows at the endcap, giving 16 space points per track with a resolution of 230 μm in Rϕ and 900 μm in z. In front

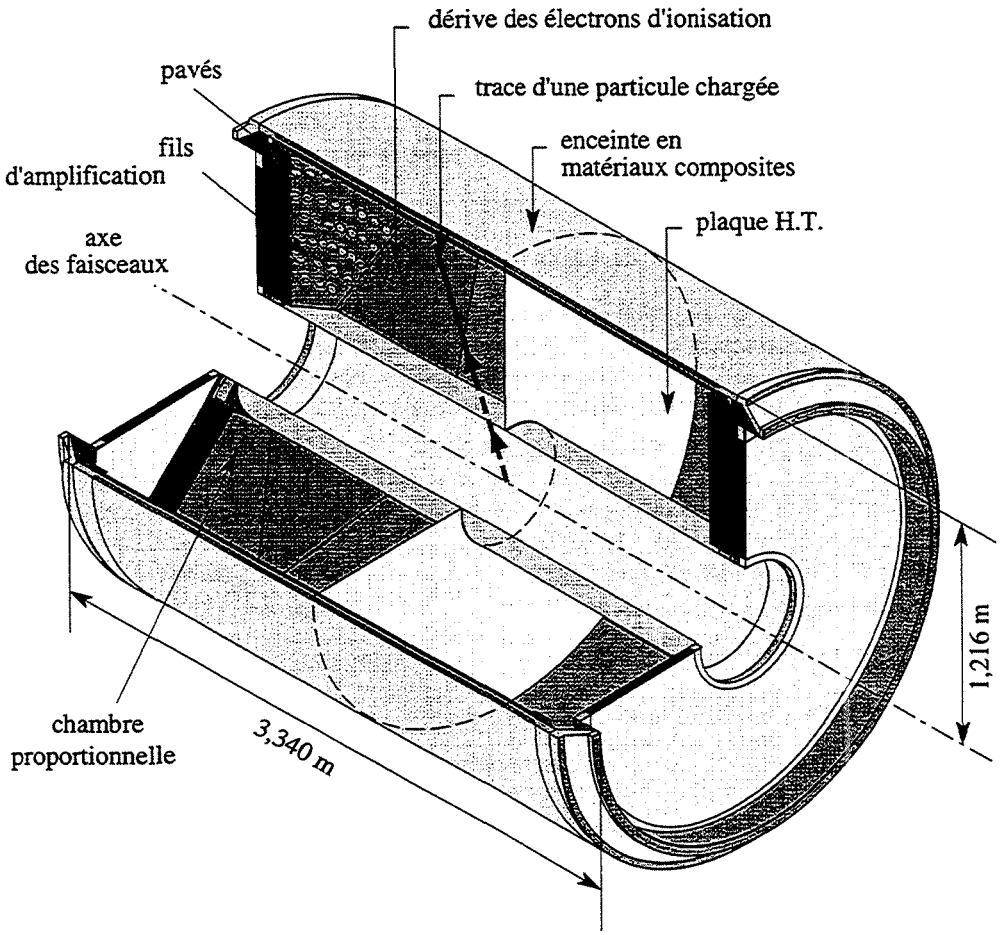

Figure 1.4: The DELPHI TPC

of the pad-rows there are three levels of grids, one of which contains 192 sense-wires for dE/dx measurements. In this way the TPC can be used for particle identification, especially low-energetic e/π separation. The TPC also provides important information for the trigger.

1.2.4 Outer Detector (OD)

The Outer Detector [8] is the third of the important trigger-detectors and also the outermost tracking detector in the DELPHI-barrel. It is situated in the radial region between 197 and 208 cm. The 24 modules, each being 4.7 m long, contain 5 radial layers of drift-tubes. The individual drift-tubes have a diameter of 1.65×1.65 cm^2. The coverage in θ is between 37° and 143°. The resolution is 110 μm for the Rϕ measurement and 3.5 cm for the z measurement, which is performed as a timing measurement of the signals in three of the layers. Apart from the Rϕ and z information used for the trigger, the OD is also

essential for the momentum resolution of fast charged particles.

1.2.5 Forward Chambers A and B (FCA, FCB)

The Forward Chambers [9] are responsible for tracking and triggering in the forward and backward regions. Forward Chambers A are mounted at the endcap on both sides of the TPC. It consists of 3×2 half-circular modules on each side with an outer radius of 120 cm. Each module consists of two staggered planes of drift-tubes and is rotated by 120° with respect to the other modules. Thus 3×2 space coordinates are obtained for each track with a resolution of 300 μm. On the outside of each module there are also additional cathode-wires for local pattern recognition. The angular coverage in θ is between 11° and 33°. Forward Chambers B are mounted on the Forward Ring Imaging Cherenkov Detector (FRICH) and consists of 4 independent conventional drift-chambers, 2 for each side. The inner and outer radii are 48 and 211 cm respectively. The chambers are divided into 12 sense-wire planes, separated by 1.1 cm, with in total 2000 wires with a spacing of 2 mm. The planes are oriented in the same way as for FCA thereby giving 12 track points with a combined resolution of 150 μm.

1.2.6 High Density Projection Chamber (HPC)

The High density Projection Chamber (HPC) [10] is the electro-magnetic calorimeter in the barrel region of DELPHI. It is a sampling calorimeter with projection chambers to collect the electromagnetic-showers. This approach has the advantage of giving both a good energy resolution and a complete picture of the energy flow. The detector is constructed from 144 modules placed in a structure of 24 sectors in ϕ and 6 sectors along the z-axis. The inner radius is 208 cm and the outer radius is 260 cm. The whole detector is placed inside the DELPHI solenoid-field. Each module consists of a trapezoidal gas-chamber with a pad-readout at one end. The pads are placed in 9 rows with different radii. Inside each chamber there are 41 lead walls, giving a total depth of 18 radiation-lengths, and functioning both as converters and as drift-field shapers. The walls consist of a fibreglass-epoxy support of 0.1 mm on which lead-wires are glued. Resistors between the lead-wires ensure a stable drift-field of 100 V/cm in the z-direction. The distance between neighbouring walls is 8 mm. An incoming electron starts showering in the lead-planes and the resulting radiation ionises the gas between the planes. The released charge then drift towards the brass-cathodes at the end of the module and is read-out. Fig 1.5 shows the detection of an electron pair in the HPC.

The granularity in ϕ is determined by the pad structure and is 1°. In z the uncertainty is about 4 mm. The energy resolution of the HPC can be expressed as $25\%/\sqrt{E} + 7\%$ where the last term is due to various systematic uncertainties.

1.2.7 Hadron Calorimeter (HAC)

The Hadron Calorimeter (HAC) [11] is a sampling gas detector installed in the iron return yoke of the DELPHI super conducting magnet. The detector consists of a barrel and two endcaps, together covering the full azimuthal angle and between 11° and 169° in the θ direction. The construction of the calorimeter is done such that the detector also works

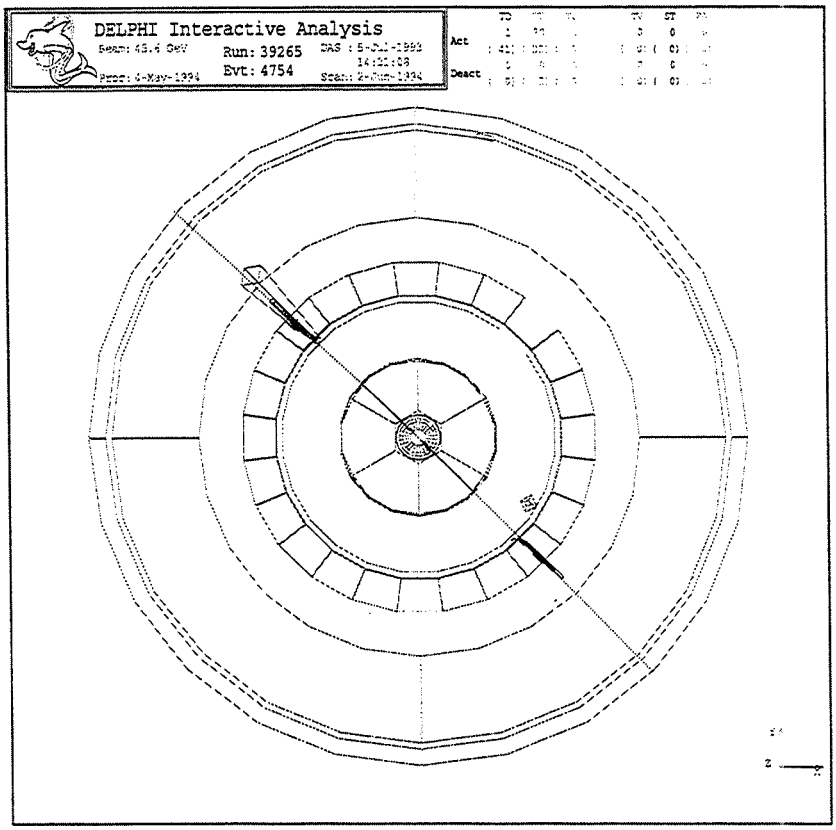

Figure 1.5: An electron pair at the Z^0 energy detected by DELPHI. The energy deposit in the HPC is clearly demonstrated, also the tracking of the VD, ID and TPC can be seen. Compare this picture to the detector response of the quark pair in fig. 1.6 to understand the barrel calorimetry-coverage of different fermions.

as a muon filter and thus is responsible for μ/π separation. Fig. 1.6 shows the detection of a quark pair through their associated jets in the HAC.

The detector consists of about $20 * 10^3$ limited streamer plastic tubes with inductive pad readout giving calorimetric information. Recently the HAC has been modified with a cathode readout, which gives some spatial information, thus improving granularity and μ identification. The upgrade also makes it possible to use the detector for fast trigger purposes, especially the cosmics trigger which is used for calibration.

1.2.8 Forward Electromagnetic Calorimeter (FEMC)

The Forward Electromagnetic Calorimeter (FEMC) [12] is the calorimeter covering the forward region of DELPHI. It consists of two circular-arrays of lead-glass counters covering polar angles between 8° and 37°, and 143° and 172° respectively. The disks are 5 m in diameter and contain 4532 counters each. The counters are mounted in steel boxes and

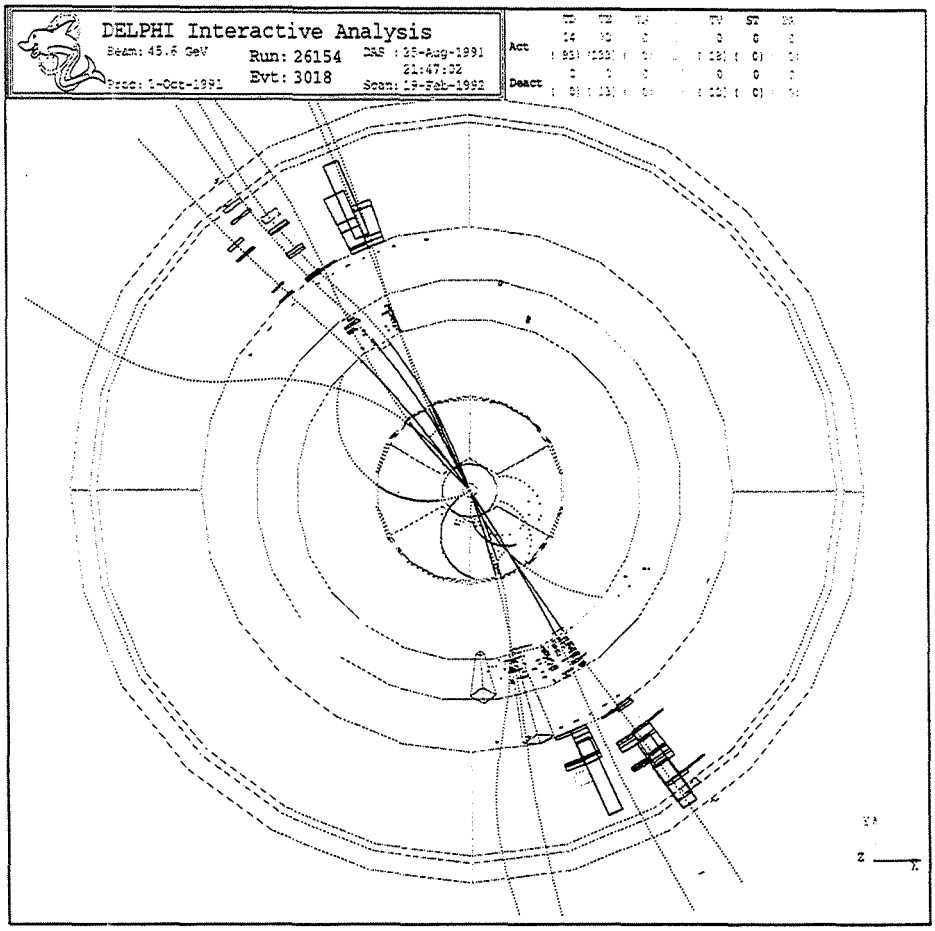

Figure 1.6: The detection of a quark pair in DELPHI. The main part of the energy is deposited in HAC.

each counter has a depth of 20 radiation lengths. The angular resolution is about 1° and the energy resolution for Bhabha events at 45 GeV is 4%. Fig. 1.7 shows the detection of a Bhabha pair through the deposited energy in the FEMC.

1.2.9 Small Angle Tagger (SAT)

The Small Angle Tagger (SAT) [13] was the luminosity monitor of DELPHI until 1994, when it was replaced by the STIC (see 1.2.10). It consisted of two cylindrical calorimeters which were placed at a distance of ±233 cm from the interaction point. The modules consisted of alternating layers of 1 mm lead sheets and 1 mm diameter scintillating fibres, with a total depth of 28 radiation lengths per module. The fibres were collected in bundles and coupled via light guides to photo diodes behind the calorimeters. The acceptance was defined by a set of precise tungsten-masks and in front of one of the calorimeters was a

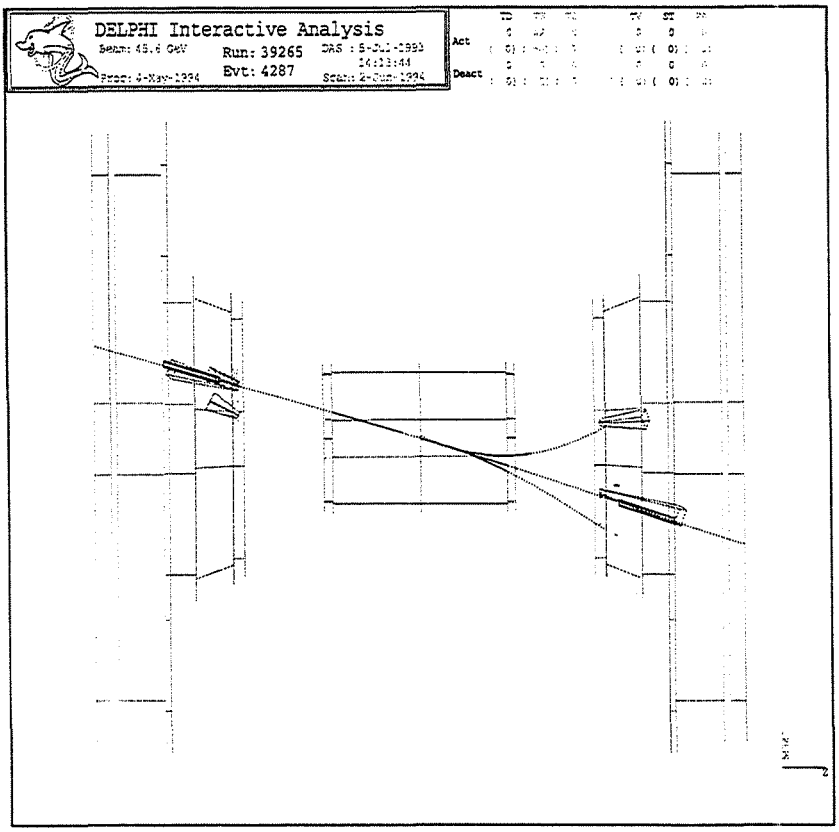

Figure 1.7: The detected energy in the FEMC from a Bhabha-pair is represented by the rectangles. The accompanying tracks in the z-direction comes from a pair-produced electron-positron, originating from a photon irradiated at the exit of the ID.

two-plane silicon-tracker for position determination. The calorimeter covered the polar-angular region from 43 to 133 mrad with an energy resolution of $11\%/\sqrt{E}$.

1.2.10 Small Angle Tile Calorimeter (STIC)

The VSAT (see section 1.3) and the Small angle TIle Calorimeter [14] are the primary luminosity detectors of DELPHI. The STIC covers an angular region between 29 and 185 mrad in θ and measures Bhabha scattered electrons and positrons within this region. The detector consists of two lead-scintillator sampling calorimeters in a pointing tower structure with optical fibres for the light collection. Figure 1.8 shows one layer of the STIC sampling-calorimeter. Each layer consists of 3.4 mm stainless steel laminated lead plates and 3.0 mm polystyrene scintillator. The total depth is 27 radiation lengths.

Two silicon strip planes are placed at a depth of 4 and 7.4 radiation lengths for measurement of the position of the electromagnetic shower. In front of each module there is a veto-counter composed of two scintillator planes in order to provide e/γ separation

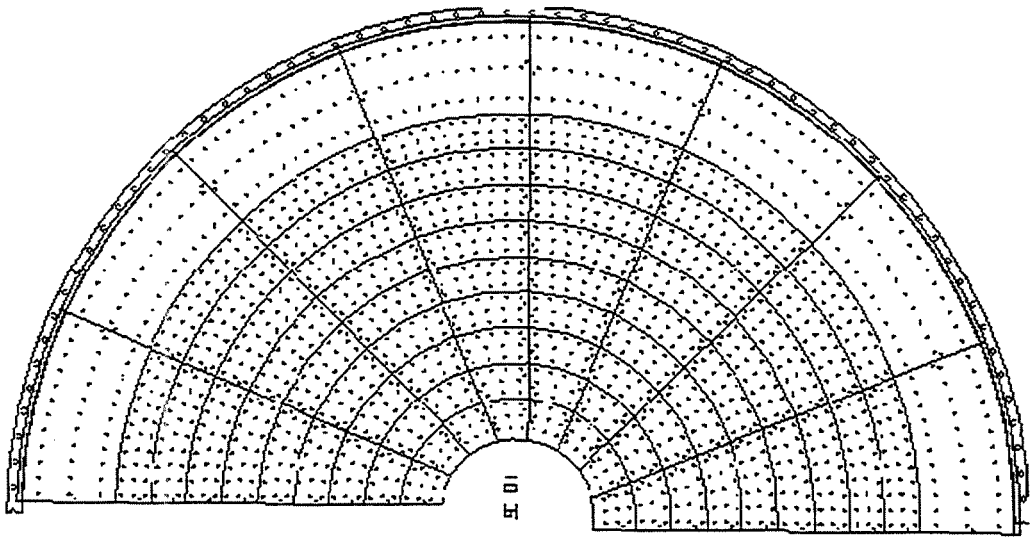

Figure 1.8: One of the 47 layers of STIC lead/scintillator. The dots show the holes for the optical fibres. The subdivision of the scintillator into tiles can also be seen.

and a neutral particle trigger. The energy resolution is 2.7% for 45 GeV electrons and the position resolution varies between 250 μm and 1.2 mm at these energies, depending on the internal structure of the detector. Since the Bhabha cross section falls like $1/\theta^3$, the inner acceptance edge is crucial to understand for a high precision luminosity determination. For the STIC this is defined by a tungsten mask. The main reason for the replacement of the SAT detector was to achieve a higher precision for the luminosity measurement. Since the installation of the STIC the statistical accuracy of the luminosity measurement has improved by a factor 2.3 due to its larger acceptance and the luminosity error is now close to 1 permille.

1.3 Very Small Angle Tagger (VSAT)

The Very Small Angle Tagger (VSAT) [15] is a Silicon-Tungsten electromagnetic sampling calorimeter. It is situated at an elliptical section of the LEP beam-pipe, 7.7 m away from the centre of DELPHI downstream the super-conducting quadrupoles. The main purpose of the detector was originally to monitor luminosity, background-conditions and beam parameters with high statistics. The process used for luminosity-measurement is Bhabha scattering (see chapter 3) and due to the smaller polar-angles covered by the VSAT, the accepted cross section is about 9 times larger than for the STIC. The bending effect of the quadrupole on the particle trajectories can be seen in fig. 1.9.

The VSAT consists of four identical modules, two on each side of DELPHI, placed in a symmetrical way in the horizontal plane. The tungsten absorbers and the full-area silicon planes are 50×50 mm^2, but the position measurements are restricted to 32×48 mm^2, i.e. in practice each module is 32 mm wide and 48 mm high and has a depth of approximately 10 cm. The detector covers a polar angle of 5 to 12 mrad for 45 GeV

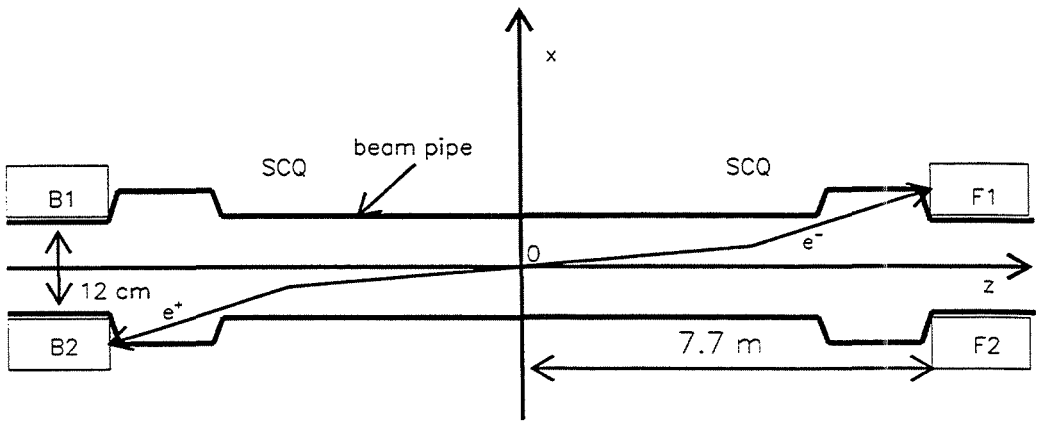

Figure 1.9: The position of the VSAT modules, showing the divergent effect of the quadrupoles (SCQ) in the x-z plane. In the y-z plane the effect of the quadrupoles is convergent.

electrons, the range depending on the energy of the particles due to the energy dependent effect of the quadrupole. The range in azimuth is about 180°. Each module consists of eleven silicon Full Area Detector planes for energy measurement, interspaced by tungsten planes of 2 radiation lengths thickness each. The energy resolution is $35\%/\sqrt{E}$. Fig. 1.10 shows the layout of a VSAT module.

The total depth of the modules is 22 radiation lengths, enough to contain the whole electromagnetic shower for 45 GeV electrons. To determine the central position of the shower there are at a depth of 5, 7 and 9 radiation lengths, where the electromagnetic shower has its maximum, placed silicon strip planes. Two of the strip planes measure the x-coordinate and one measure the y-coordinate. The strip planes have a pitch of 1 mm and are able to determine the position with an accuracy of 200 μm for electrons at an energy of 45 GeV.

1.3.1 Local trigger

The local trigger decision for the VSAT is made by looking at the summed signals from a set of FAD planes in each module. If this signal is above a threshold of about 25 GeV the event is triggered. The different trigger types of the VSAT are listed below.

- Bhabha trigger, a coincidence of signals above the 25 GeV threshold in two diagonal modules.

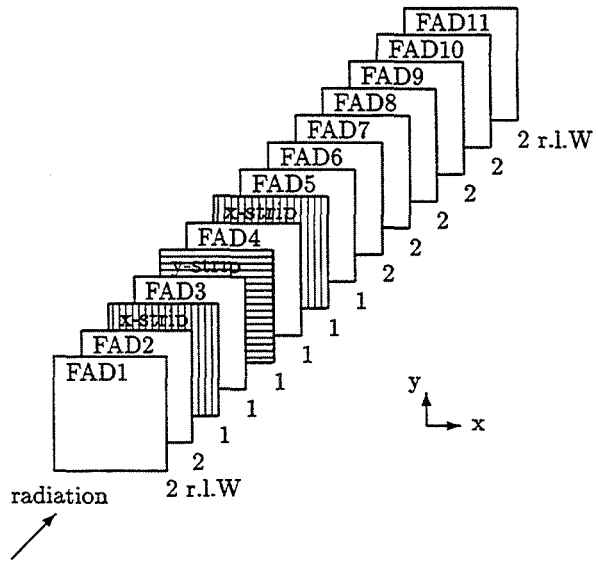

Figure 1.10: One of the VSAT detector modules in cross section, showing the FAD and strip planes. The depth in radiation lengths of Wolfram is also indicated.

- False Bhabha trigger, a coincidence of signals above the 25 GeV threshold but with a time difference of N bunch crossings between the two diagonal modules, where N is the number of bunches in LEP (N=4 or 8). The false Bhabhas are used to estimate the accidental background to the Bhabha trigger. For LEP2 this trigger-component has been removed and instead the single electrons are used for accidental background estimations.

- Single electron trigger, a signal above the 25 GeV threshold in any module. This trigger type is downscaled[1] due to the high rate.

Apart from these local trigger types, the VSAT-modules are always read out when DELPHI triggers an event. The VSAT has a hardware buffer with room for 12 events, thus the VSAT can store 11 local events between DELPHI triggers. This is necessary because of the high rate of Bhabha events. When DELPHI triggers or the buffer is full all the stored events are read out.

Trigger efficiency

To evaluate the efficiency of the local trigger, the DELPHI triggered events are used. These are events where other sub-detectors in DELPHI have caused VSAT to perform a forced read out regardless of the energy deposit in the VSAT itself. Normally there is no

[1]This means that only a few of these events are actually read out.

signal in the VSAT for these events, but for around 1% of them there are energy deposits in the modules (for instance for tagged two-photon events). Using the DELPHI triggers it is possible to see events even below the local trigger threshold in the VSAT. It is also possible to see if the VSAT has triggered itself for these events. This is used for evaluating the local trigger threshold and the Bhabha trigger efficiencies. Fig. 1.11 shows the VSAT trigger efficiency for 1993 and 1994.

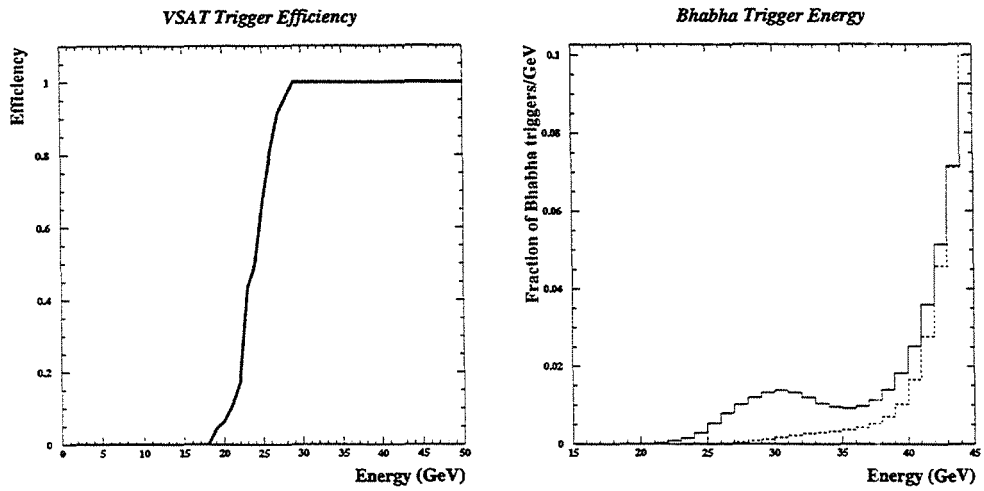

Figure 1.11: Left: The efficiency of the local VSAT trigger. Right: The different energy distributions 1993 (dotted) and 1994 (full) showing the influence from the bad vacuum in LEP for 1994.

The sharpness of the threshold is not crucial to the analysis, since the trigger threshold around 25 GeV is 5 GeV lower than the software cut used for Bhabha events when calculating the luminosity (and the two-photon events are triggered by DELPHI). However, any inefficiency above 30 GeV has to be taken into account and corrected for in the luminosity analysis. In order to evaluate the trigger-efficiency for Bhabha events, the energy spectrum of the Bhabha triggers is convoluted with the trigger-efficiency function shown in fig. 1.11. In table 1.1 the calculated total Bhabha inefficiencies above 70% of the beam energy for the different periods of 1993 and 1994 can be seen.

The reason why the Bhabha trigger inefficiency for 1994 is worse than for 1993 in module B2 and F2 is mainly due to the different shape of the energy distributions of the Bhabha triggered events, as can be seen from figure 1.11. For a long period in 1994 there were vacuum problems in LEP. This resulted in beam-gas interactions and low energy contributions to the Bhabha trigger spectrum.

Minibunch modifications

In 1995 LEP started to operate in a new mode. Instead of using the normal bunch scheme with 4 or 8 bunches of electrons and positrons, separated by some microseconds, every bunch was divided into a train consisting of 2 to 4 mini-bunches. Each of these so called

module B2				
year	1993			1994
beam energy (GeV)	91.2	89.4	93.0	91.2
inefficiency	1.4	2.1	1.0	2.6
error	0.2	0.3	0.1	0.4

module B1				
year	1993			1994
beam energy (GeV)	91.2	89.4	93.0	91.2
inefficiency	1.5	2.1	1.0	1.3
error	0.2	0.2	0.1	0.3

module F2				
year	1993			1994
beam energy (GeV)	91.2	89.4	93.0	91.2
inefficiency	0.2	0.3	0.1	1.6
error	0.1	0.1	0.1	0.3

module F1				
year	1993			1994
beam energy (GeV)	91.2	89.4	93.0	91.2
inefficiency	1.4	2.0	1.0	1.3
error	0.2	0.3	0.1	0.4

Table 1.1: Integrated Bhabha trigger inefficiencies above 70% of the beam energy in permille. The inefficiencies are corrected for in the luminosity calculation and the errors included in the systematic error.

wagons were separated by some hundred nanoseconds. The idea of using mini-bunches is to increase the total luminosity in LEP. This naturally puts tougher demands on the detectors; they have to be able to distinguish and separate events with a time difference of a few hundred ns[2]. For the VSAT the modifications necessary to accomplish this time resolution were extensive. A new fastbus card, LURFB [16], was installed during the summer of 1995 as were the changes required for the data analysis. The LURFB card looks at the summed signals from the trigger FAD-planes and, depending on where in time a peak of the pulses occur, assigns a mini-bunch number to the event individually for each module (see fig. 1.12).

[2]One cannot say that this change of mode of operation initially was successful since during 1995 the luminosity did not exceed the luminosity the previous year. In fact there were many problems associated both with LEP and with data taking modifications for the experiments. The final solution to the problems

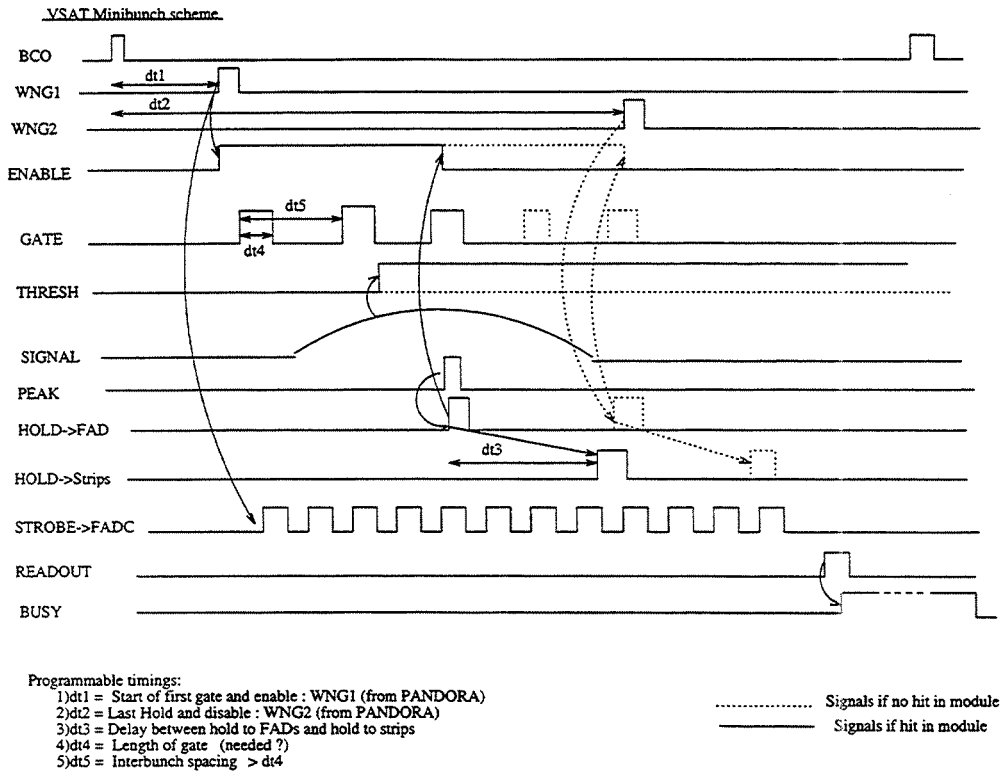

Figure 1.12: The timing of the signals from the LURFB card.

The LURFB card also decides when to issue the hold[3] on the signals depending on what minibunch the event belongs to. The pulses are also sampled by a Flash ADC every 47 nanoseconds and these samples are read out together with the assigned mini-bunch number and written in the raw-data together with other new information from LURFB according to the specifications [16]. From the FADC data it is thus possible to offline reconstruct the pulse-shape in time. This provides the possibility to correct any mistake in the mini-bunch assignment done by the hardware. Naturally these hardware changes required new software for all stages of processing.

1.3.2 Monitoring and reconstructions

No matter what kind of analysis the data will be used for, the result depends on the accuracy of the reconstructions made (just as they depend on the functionality of the detector hardware itself). Therefore it is crucial to make sure that the reconstruction routines are as accurate as possible. Any error made here will propagate to the final result of the analysis. The software of the VSAT consists of both online monitoring programs and offline programs, performing reconstructions of the measured quantities;

was to run with only 2 wagons separated by a longer time interval than the initial 247 ns.

[3] "Hold" means that the signals are frozen at that amplitude later to be read out.

position and energy. The primary objective is to transform the electronic signals from the detector, read out and stored in the raw-data, into as accurately reconstructed quantities as possible for each event, so that they can be used for physics-analyses. Specific software-routines have been developed during the years in order to achieve as high precision as possible.

Online monitoring

The on-line monitoring programs [17] are the first step in the software reconstruction and analysis chain. There are two programs: the local and the central monitors. Both run directly on the incoming data. They are designed to

- Provide an immediate check on how the hardware performs.
- Perform a rough on-line analysis of the data, discovering big effects that might have to be taken into account before running the offline analysis.
- Calculate pedestal values for all channels, strips and FADs, and check the status of each channel. Pedestals are the threshold values of each channel and they are necessary to subtract from the raw signals in order to retrieve the true amplitude of the data-signals,(see equation 1.1).

The histograms continuously produced by the monitors, (see fig. 1.13), are saved in files for each fill[4] or run[5] (if so requested), to allow comparisons of detector performance and data quality with the offline results.

The monitoring programs guarantee that any serious problem will be detected immediately. Summary files, with information about the number of Bhabha events, length of the buffers etc. for each run taken by DELPHI are also produced and can be examined afterwards if any undetected problem would be seen in the offline analysis. Since the DELPHI monitoring system, the physics of interest and also lately the VSAT-hardware itself changes, modifications are frequently necessary. Recently the local monitor has been modified for several reasons: to fit into the DELPHI standard monitoring skeleton [18], the minibunch upgrades of the detector, the high energy running of LEP2 and also for a migration from the VMS to the AXP operating system. The local monitor also calculates the pedestal values to be subtracted from each channel by the reconstruction programs. The calculated pedestals and the status of all channels are automatically updated to the database [19], with the help of a database updating program.

Pedestal calculation

The one feature of the online monitors that will be discussed here in more detail is the pedestal calculation. The event selection is done based on DELPHI triggers without any

[4]The fill number is a number given to the set of data collected during a certain LEP "fill". Each fill lasts normally 10-20 hours. After that the remaining beams are dumped and LEP prepares to be filled again.

[5]A run is a time-interval when DELPHI, or the local sub-detector, is continuously collecting data. Every fill normally consists of several runs.

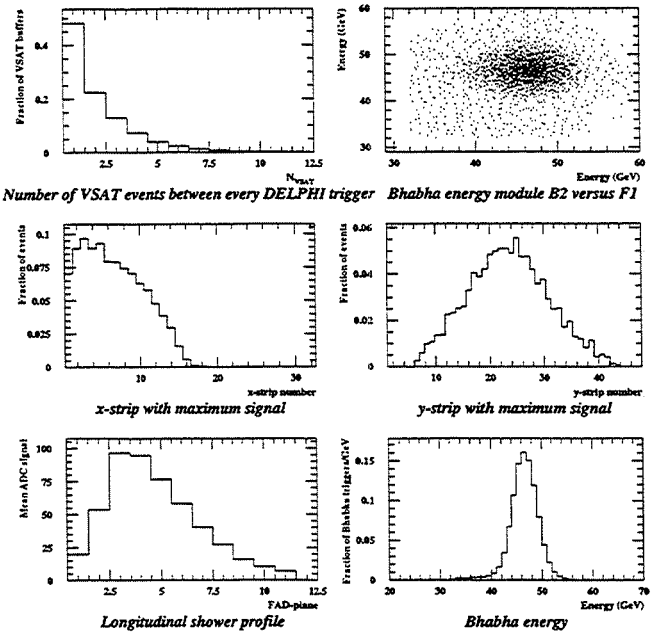

Figure 1.13: Histograms from the VSAT monitoring programs. Upper left: The length of the local trigger buffers. Upper right: Energy in one module versus energy in the diagonal module for Bhabha triggered events. Middle left: Distribution of x-strips with maximum signal from a VSAT module. Middle right: Distribution of y-strips with maximum signal from a VSAT module. Lower left: FAD plane signals, showing the longitudinal shower development. Lower right: Bhabha energy distribution from a VSAT module.

hit in the VSAT. For these events the mean values of the raw ADC signals for each channel (FADs and strips) are calculated together with the RMS of the distribution. When enough events are gathered the new pedestal and RMS values are written to a file. The data-base updating program then reads the new values and compare them to the values in the data-base. If they are different and at the same time the RMS is below a certain limit, the value is updated to the data-base. Typical values of pedestals are shown in fig. 1.14. The RMS of the measured pedestal distribution range up to 3-4 ADC counts. The influence of the pedestals on the FAD signals and the reconstructed energy is less significant.

Offline reconstructions

The offline programs take care of the reconstructions and analysis of the data in different steps. In the chain of software used for this purpose there are several different programs. Figure 1.15 shows the structure of the VSAT offline software.

In this section the energy and position reconstructions done by the routines in LUMANA, the VSAT part of the DELPHI analysis program DELANA [20], and by VS-

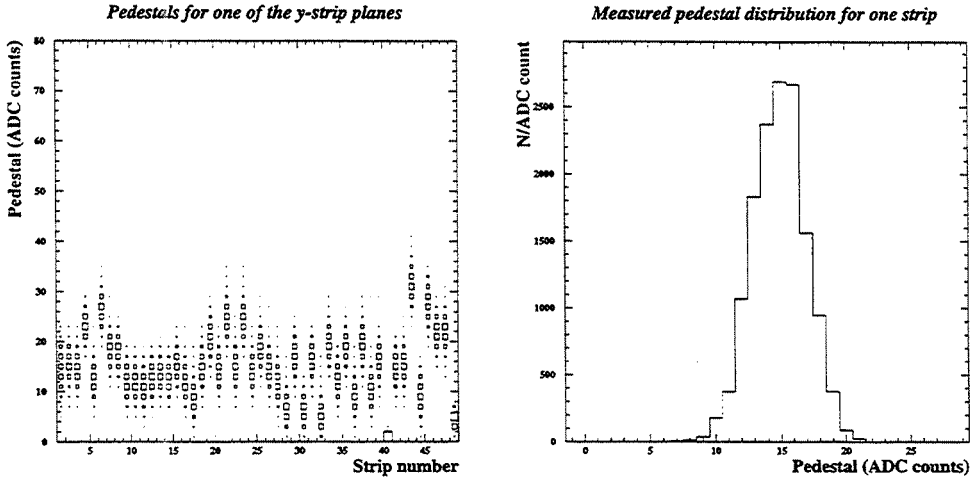

Figure 1.14: Right: The pedestals for one of the y-strip planes. Left: The distribution of the measured pedestal for one strip.

DST will be described. Other issues like calibrations and mini-bunch tagging are also discussed. DELANA is run centrally by the DELPHI analysis farm and produce the VSAT output files ("VSAT-DSTs"). When this is done the main reconstruction and selection program, VSDST, processes the data. This is where the final corrections to the reconstructed energies are made. The Bhabha acceptance cuts for the luminosity analysis are also applied here. The VSAT part of the offline analysis chain can be run automatically by a control program running in batch mode on one of the VAX-machines. It checks when a new data file has arrived on the disk and then compresses it and runs VSDST when all the files from that physics fill have arrived.

Calibrations

The raw signals from the FAD planes and strips have to be both pedestal subtracted and calibrated before they can be used for position and energy determination of the events. This is done for each channel according to the general formula:

$$SIGNAL_{calibrated} = CONST_{cal} * (SIGNAL_{raw} - PEDESTAL) \qquad (1.1)$$

The calibration constants are calculated offline. For the strips this is done by studying the signals from a set of Bhabha events. The uncalibrated signals are then fitted to the expected shape. For the strips the signals from the central strips of each shower are fitted to the mean value of the corrected energy distribution for Bhabha events in that strip (see fig. 1.16). The FADs are calibrated by fitting the signals of Bhabha events to the shower profiles of simulated events.

The calibration constants should be evenly distributed around 1 in order to minimise any uncertainty introduced. Once new calibration-constants have been produced they have to be updated to the database used by all the VSAT-software.

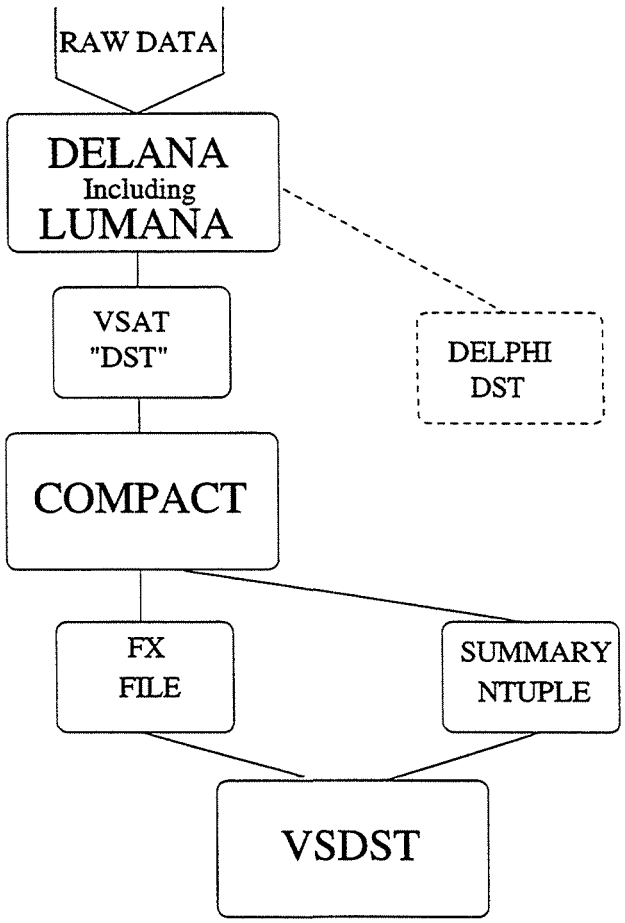

Figure 1.15: The different software-steps in the VSAT offline reconstruction chain.

The edge strips

The uncertainty of the calibration of the edge strips is a problem for the VSAT. Due to the fact that a particle with maximum signal in the edge strips may have started its shower outside the module and thus not deposited its full energy, there is a large uncertainty in the calibration constant for these strips. Events with maximum signal in the edge strips are discarded from the analysis due to the uncertainties for these events. This means that an uncertainty in the calibration constants for the edge strips could bias the acceptance of the detector, i.e. if the calibration systematically over compensates the first x-strip, events would drift towards the edge of the detector and out of the acceptance region. The VSAT would get a lower accepted cross section. This is of greatest importance for the inner x-edge where the accepted Bhabha cross section is highest. By using particles with maximum signal in the second strip for the calibration of the first x-strip this uncertainty can be strongly reduced. The signals are then calibrated to the same level as the signals of the second strip.

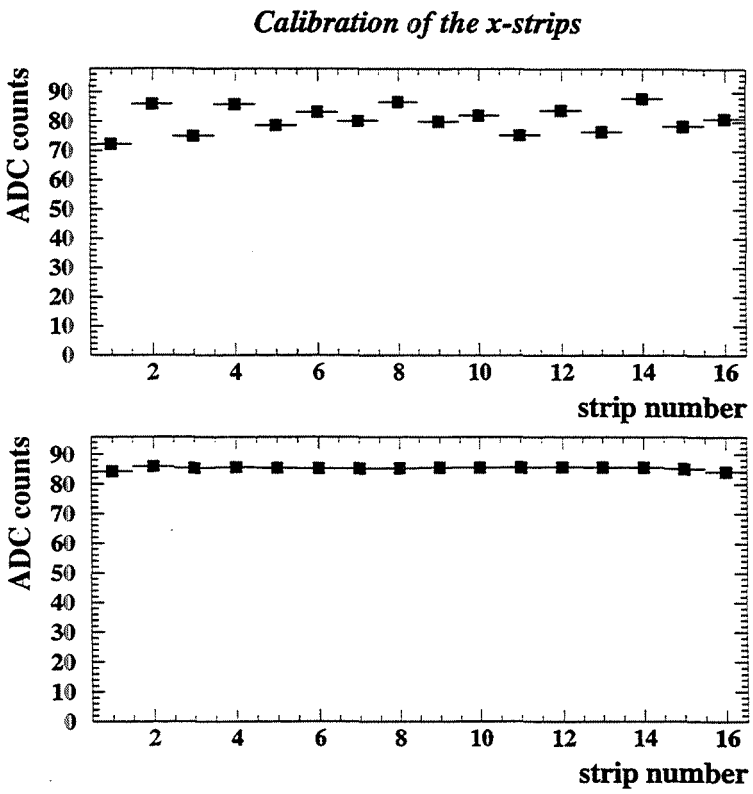

Figure 1.16: The calibration of the x-strips. Top: The uncalibrated center of shower strip signals. Bottom: The calibrated center of shower strip signals.

Position reconstruction

Based on the calibrated strip-signals, a reconstruction of the position is made. The positions of the shower maxima are fit, using the three central strips, according to the empirical formula [21]

$$ADC(R) = A(1) * e^{-R/B(1)} + A(2) * e^{-R/B(2)} \tag{1.2}$$

where R is the distance of the strip from the track and $A(1), A(2), B(1), B(2)$ are constants depending on the position of the strip-plane and the energy of the particle. Fig. 1.17 shows a comparison between equation 1.2 and experimental transversal shower profiles.

The reconstruction gives a position resolution of 200 μm for electrons at 45 GeV with the normal uncertainties on pedestals and calibration constants.

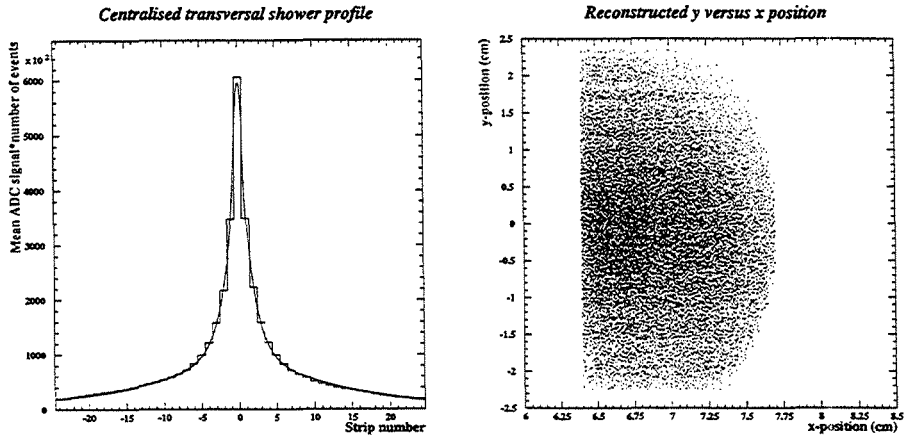

Figure 1.17: Left: The mean transversal shower profile and equation 1.2 used for the position fit. Right: Reconstructed y versus x position for Bhabha events in one of the VSAT modules.

Energy reconstruction

After the pedestal subtraction and calibration of the individual FAD planes (and the minibunch tagging of the event for data taken from 1995 and on), the energy measurement has to be corrected. The procedure is as follows for each VSAT module

$$E = C_{i,j}\epsilon_y\epsilon_x \sum_{FAD=1,11} c_{FAD}(S_{FAD} - P_{FAD}) \tag{1.3}$$

where E is the reconstructed energy of the particle, $C_{i,j}$ is the calibration constant and i and j represents the true minibunch and the minibunch assigned by LURFB. S_{FAD} is the raw FAD signal, P_{FAD} is the pedestal and c_{FAD} the FAD calibration constant. The leakage correction constants ϵ_x and ϵ_y depend on the reconstructed position. The reason for this correction is that electrons hitting the module close to the edge, will lose energy due to leakage of part of the shower out of the module, i.e. the area of the FAD plane is too small to contain the whole electromagnetic shower. This effect is larger for LEP2 energies. The size of the correction will thus depend on the reconstructed position and is theoretically determined from equation 1.2. To get the actual values of the constants a fit to data is made. Fig 1.18 shows energy versus x-position for Bhabha events before and after the leakage correction.

The final energy calibration is done fill-by-fill, by calibrating the Bhabha energy peak after all corrections, to the energy of the beam given by LEP. This calibration has to be done separately for the different minibunches for 1995, also taking into account possible mistakes in the minibunch identification from LURFB (see next section).

Mini bunch tagging

In 1995 LEP changed its running procedure, introducing minibunches, and the VSAT was upgraded as described in section 1.3.1. The procedure to distinguish between events

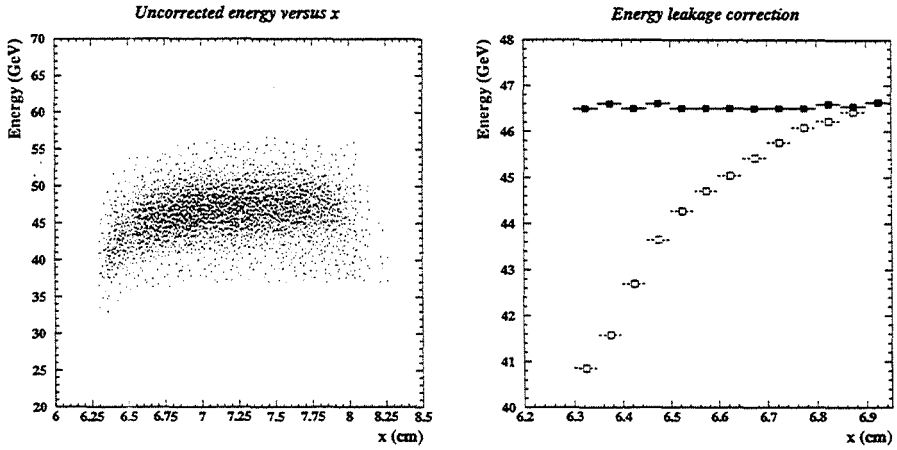

Figure 1.18: Left: Bhabha energy versus x-position before leakage correction. Right: Close up of the edge of the detector. Energy before (white) and after (black) leakage correction.

from different minibunches offline is to investigate the FADC[6] samples and determine when the pulse passes a software threshold. The threshold has to be chosen sufficiently low to allow all events to be tagged and sufficiently high to allow enough separation between the different minibunches. The steeper the rise-time of the pulses is, the better separation is achieved. An offline mini-bunch assignment with an accuracy of better than 0.1 permille is achieved. The reconstructed energy is then corrected with a set of special calibration constants [22] depending on when the hold was issued by LURFB. Fig. 1.19 shows the FADC samples and the separation between the minibunches achieved by the offline procedure.

The offline procedure for minibunch identification is installed in LUMANA and VSDST and it can easily be retuned to different energies, amplification and timing if needed.

[6]The Flash ADC samples the summed FAD signal. One sample each 47 ns gives an oscilloscope like picture of the signals in time, which is possible to study offline.

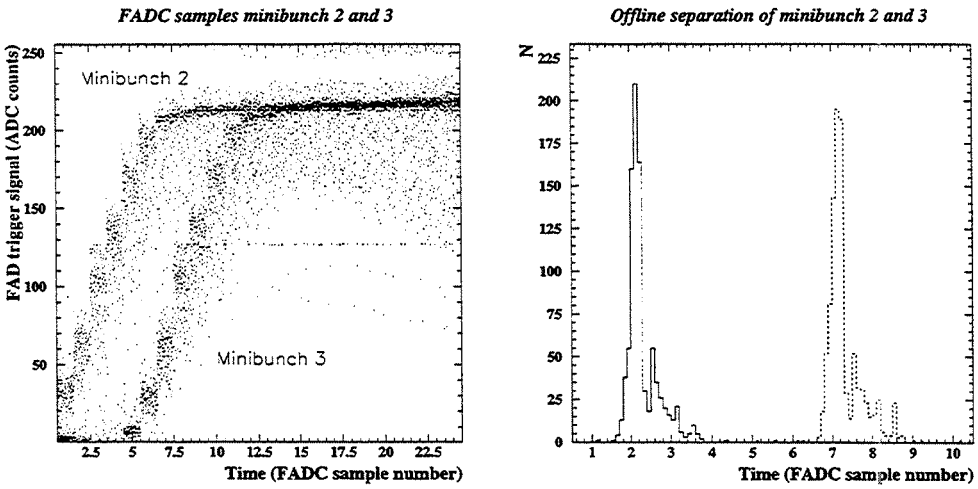

Figure 1.19: Left:The FADC samples for minibunch 2 and 3 events. Right: The separation between minibunch 2 and 3 achieved by the offline procedure.

Chapter 2

Background and interaction point measurements

This chapter deals with measurements of quantities which due to their effect as background and biases to precision physics measurements are absolutely necessary for a high energy physics experiment to have a good knowledge of. The first section describes how the electron background is measured at DELPHI with the VSAT. The following section describes measurements of variations of the interaction point and the angles of the beams by analysing the impact position of Bhabha events in the VSAT modules. This measurement is a cross check of the validity of the corrections made to the accepted Bhabha cross section for the luminosity analysis in chapter 3. The measured interaction point and beam angle variations are also used in the two-photon analysis in chapter 4.

2.1 Particle background

The VSAT has, due to its closeness to the beampipe, great possibilities to monitor the electron background[1] at DELPHI. This background source consists of electrons which have been deflected from the stable orbit of the lepton bunches for different reasons, most likely through beam-gas Bremsstrahlung (see fig. 2.1) and thereby lost part of their momenta [23].

Therefore these particles are often referred to as off-momentum electrons. If the particles lose less than one percent of their energy they stay in the stable orbit, but if they lose between 1 and 3 percent they keep an unstable orbit and are eventually lost, some of them showing up as particle-background at the experiments. Particles losing more than 3 percent of their energy are immediately lost at the local point. The off-momentum electrons hitting the VSAT are sharply focused in the y-plane due to the effect of the quadrupole and this fact is used for alignment of the modules and the beam axis in chapter 4. Since a major part of the electron background originates from beam-gas interactions, the background rate is dependent on the vacuum quality in the beampipe. A bad vacuum can cause serious background problems. The experiments are shielded from the off-momentum electrons by remotely operated lead-tungsten collimators at various

[1] The photon background, mainly synchrotron radiation, is much softer and is totally absorbed by the first VSAT planes. Thus it is better detected by other DELPHI sub-detectors for instance the TPC.

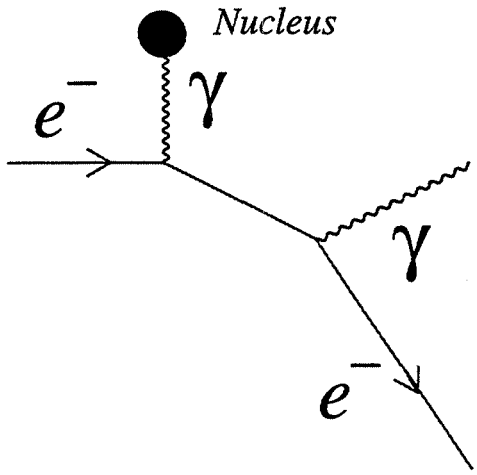

Figure 2.1: An electron in the LEP beam losing energy through beam-gas Bremsstrahlung.

locations around the LEP ring. The setting of the collimators can be optimised for the current background situation. If the level of the background gets too high, the particles can not only blur the detection of physics events by blinding the detectors or causing dead-time by too high trigger-rates, but they can also cause physical damage to the innermost subdetectors of DELPHI. It is therefore of highest importance to keep a good watch at the rate of off-momentum electrons. Each experiment monitors the electron and photon backgrounds continuosly and feeds the information back to the LEP control-room. VSAT is monitoring the electron background for DELPHI. For the analysis of VSAT data itself it is also necessary to record the off-momentum electrons because of their role as accidental Bhabhas and background to single- and double-tag two-photon events. This is done by the false Bhabha and single elctron triggers.

2.1.1 Trigger scalers

The instrument which the VSAT uses for background monitoring is the MIG-scalers [24]. The MIG-scalers are counters counting each time there is a signal above the trigger-threshold in any VSAT module. The signals monitored are the same, consisting of a chosen set of FAD-planes, which are used for the local trigger decision. There are 16 different scalers, counting events individually for each VSAT module and trigger-type. There are also separate counters for if the signal is gated by the DELPHI readout or not. Thus it is also possible to evaluate how efficient DELPHI's data acquisition is. The different values monitored by the MIG-scalers are:

- BHGAT and BHUNG 1-2, gated and ungated Bhabha events in VSAT diagonal 1 and 2.
- FBGAT and FBUNG 1-2, gated and ungated false Bhabha events in VSAT diagonal 1 and 2.

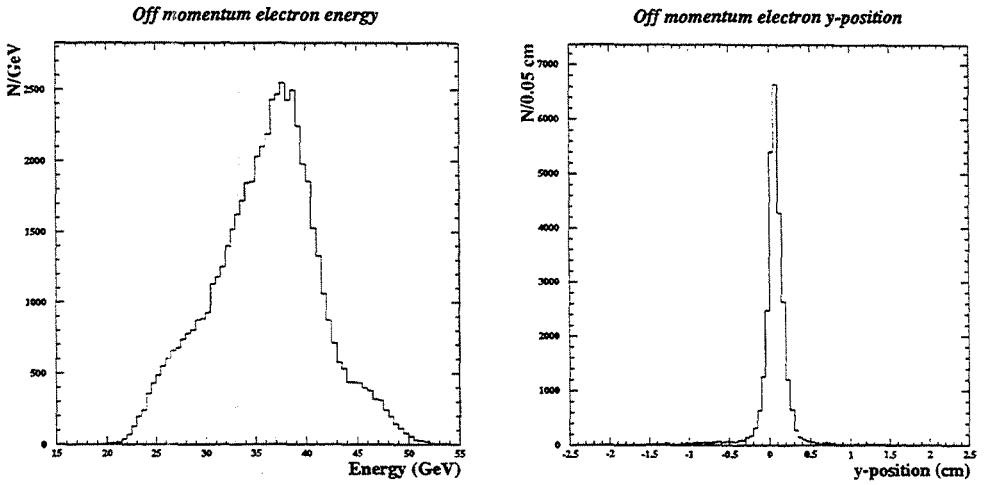

Figure 2.2: Left: The energy spectrum of the off-momentum electron background in the VSAT. Right: The sharply focused y-positions of the particle background.

- SEGAT and SEUNG 1-4, gated and ungated single electrons in VSAT module 1 to 4.

The values of the MIG-scalers are accessible either as the rate, updated every 15 seconds, or as the integral count over a run. The total count is written to the DELPHI rawdata for each run and can be analysed offline.

Background monitoring

The MIG-scalers are active even when DELPHI is not taking data. By extracting the rates of the scalers it is thus possible to monitor the development of the background online during the sensitive filling and adjusting phases of LEP without having DELPHI active, i.e. it is possible to watch and wait until the background levels go down before ramping up the voltages of the DELPHI detector. The counters used for the background monitoring are the Single Electrons UNGated. They are scaled by a normalisation constant according to:

$$BKG2 = CONST * (SEUNG1 + SEUNG2 + SEUNG3 + SEUNG4) \tag{2.1}$$

This corresponds to counting all hits in any VSAT module and normalise it to a scale which indicates how dangerous the particle-background is for the experiment. This scale is chosen so that it is equivalent for all the four LEP experiments. If the background-rate reaches the value 10 on this scale, it means danger to the detector and the beams are dumped. Normal physics conditions correspond to values well below 5. The development of BKG2 is displayed as a traceplot in the DELPHI control-room.

Online luminosity

Luminosity is a fundamental quantity of a collider physics experiment and the offline calculation of the luminosity will be treated in chapter 3. The ability to get a good estimate of the achieved luminosity at run time is also essential both for the experiment and the accelerator. The VSAT MIG-scalers are used to evaluate the online luminosity [24]. For this purpose the ungated Bhabha and False Bhabha counters are used:

$$\mathcal{L} = CONST * (BHUNG1 - FBUNG1 + BHUNG2 - FBUNG2) \qquad (2.2)$$

The constant here contains all information about the accepted Bhabha cross section, which varies with the running conditions. For the online luminosity the statistical fluctuations during the short time intervalls, i.e. 15 seconds, used to evaluate the trigger rate, are more significant and instead an average value of the accepted cross section is used. The measurement is also normalised to the STIC online luminosity. This normalisation usually has to be redone every year due to shifts in the geometry in between the years. These shifts affect the relative accepted cross section in a non negligible way. The VSAT online luminosity is displayed together with the STIC value as a traceplot in the DELPHI control room. The gated MIG-scaler values can also be used offline for a quick estimate of the luminosity at LEP2 energies.

2.2 Interaction point measurements

Besides the background rates and the luminosity, other necessary quantities for an experiment to know, is the geometry of the interaction point in respect to the detector. This information comprises both the coordinates and spread of the interaction point and the angles of the incoming beams. The coordinates and size of the interaction point is measured with high accuracy at DELPHI by the Vertex Detector and the Time Projection Chamber [25]. Due to its close position to the beampipe, and the sharp drop of the Bhabha cross section with polar angle, the VSAT is also sensitive to changes in these beamparameters. The extraction of beamparameters from VSAT data is not only valuable as a cross check of the interaction point information provided by the VD and TPC, but it also provides new information about the beam angles. The origin of the VSAT studies of the beamparameters, was a need to correct the VSAT luminosity calculation for variations in different beamparameters (see chapter 3). This study was continued after the correction formula for the Bhabha cross section was found and ended up in an improved understanding of the effect of various beamparameters on VSAT data. This is described in detail together with studies of 1993 and 1994 variations in appendix A and B. The knowledge of the beam angle variations that emerged from these studies also plays a role in the reconstruction of angles and momentum transfer for the double-tag two-photon analysis discussed in chapter 4.

2.2.1 Transport equations

The Bhabha process is elastic and therefore strictly symmetric in forward-backward direction. By knowing the transport equation for the particles from the interaction point

and up to the VSAT modules and in addition knowing the exact VSAT and DELPHI geometry [2], it would be possible to deduce the coordinates of the interaction point from the reconstructed position of a Bhabha pair. Equations 2.3-2.6 describe how the x coordinates of the Bhabhas as they hit the VSAT, depend on the interaction point coordinates and the beam angles.

$$x_{F1} = f_x(x_b - z_b(\theta_1^x + \theta_-^x)) + l_x(\theta_1^x + \theta_-^x) \tag{2.3}$$

$$x_{B2} = f_x(x_b - z_b(\theta_1^x + \theta_+^x)) - l_x(\theta_1^x + \theta_+^x) \tag{2.4}$$

$$x_{B1} = f_x(x_b + z_b(\theta_2^x - \theta_+^x)) + l_x(\theta_2^x - \theta_+^x) \tag{2.5}$$

$$x_{F2} = f_x(x_b + z_b(\theta_2^x - \theta_-^x)) - l_x(\theta_2^x - \theta_-^x) \tag{2.6}$$

Similar equations are valid for the y coordinates

$$y_{F1} = f_y(y_b - z_b(\theta_1^y + \theta_-^y)) + l_y(\theta_1^y + \theta_-^y) \tag{2.7}$$

$$y_{B2} = f_y(y_b - z_b(\theta_1^y + \theta_+^y)) - l_y(\theta_1^y + \theta_+^y) \tag{2.8}$$

$$y_{B1} = f_y(y_b + z_b(\theta_2^y - \theta_+^y)) + l_y(\theta_2^y - \theta_+^y) \tag{2.9}$$

$$y_{F2} = f_y(y_b + z_b(\theta_2^y - \theta_-^y)) - l_y(\theta_2^y - \theta_-^y) \tag{2.10}$$

The indices F1, B2, B1, F2 corresponds to the four different VSAT modules as shown in fig. 2.3.

f_i stands for the magnification factor experienced by displacements in the i plane, due to the superconducting quadrupole between the interaction point and the VSAT modules. The effect is actually demagnifying in the y plane and the size of the factor is found from simulations [26] with different interaction points. The influence of the quadrupole field on the particle trajectories are highly energy dependent but for non radiative Bhabha events it can be assumed to be constant. x_b, y_b and z_b stand for the x, y and z coordinates of the interaction point. The angular dependence of the transport equations are considered under the small angles approximation and θ_j^i, where $i = x, y$ and $j = 1, 2$, denotes the polar scattering angle in the i plane of VSAT diagonal j. The angles θ_j^i, where $i = x, y$ and $j = -, +$, denotes the tilt angles of the electron (-) and positron(+) beams in the i plane. l_i, where $i = x, y$, is the effective length, taking into account the quadrupole effect, between the interaction point and the VSAT in the x- and y-plane respectively. The values of l_i are found through the extensive simulation studies of Bhabha events which have been performed for the luminosity analysis.

[2]The distance between the two neighbouring forward and backward VSAT modules is measured with an accuracy of 200 micrometer at the begining and end of the data taking every year. The uncertainties in the absolute alignment to the DELPHI coordinate system are larger.

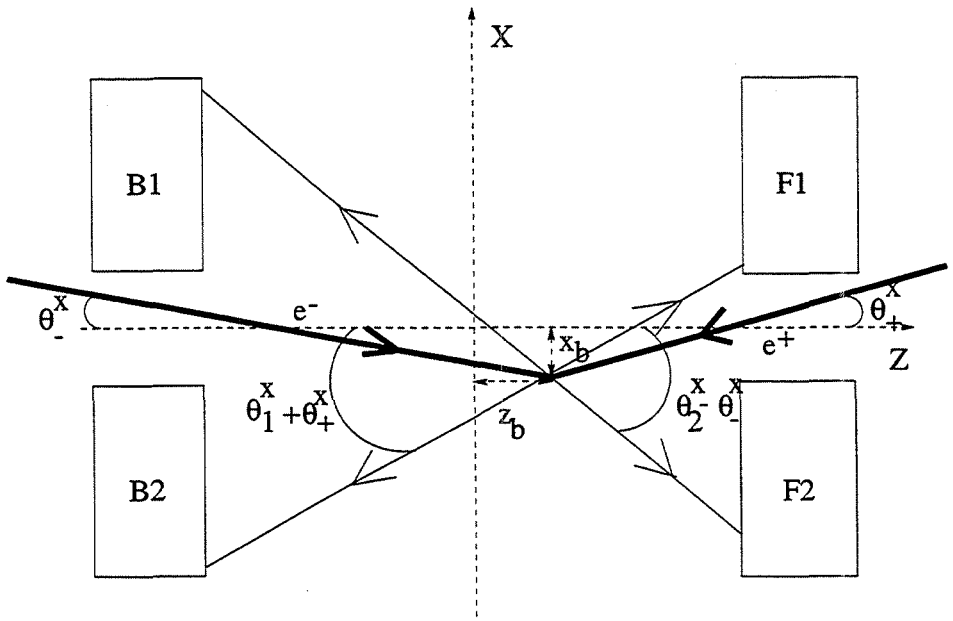

Figure 2.3: The geometry of the four VSAT modules also showing the effect of interaction point fluctuations and non zero beam angles on Bhabha events in the x-plane. The tilt angles θ^x_+ and θ^x_- are positive in the counterclockwise direction. The effect of the quadrupole field is not shown in this picture. A similar picture is applicable to the y-plane.

2.2.2 The z-coordinate

Equations 2.3-2.10 show that there is a direct influence from the interaction point coordinates on the position of the Bhabha events measured by the VSAT. By combining these equations in a proper way it is possible to extract information about the interaction point coordinates. The z-coordinate of the interaction point can be extracted by combining the measured x-positions of Bhabha events in the four VSAT modules. From equations 2.3-2.6 follows

$$x_{F2} + x_{B1} - x_{F1} - x_{B2} = 2f_x z_b(\theta^x_1 + \theta^x_2) \tag{2.11}$$

$$\theta^x_1 + \theta^x_2 = \frac{x_{F1} + x_{B1} - x_{B2} - x_{F2}}{2l_x} \tag{2.12}$$

combing equations 2.11 and 2.12 gives

$$z_b = \frac{l_x(x_{F2} + x_{B1} - x_{F1} - x_{B2})}{f_x(x_{F1} + x_{B1} - x_{B2} - x_{F2})} \tag{2.13}$$

It is here convenient to use the measurable quantities Δx_1 and Δx_2, the sum of the reconstructed x-position for Bhabha pairs

$$\begin{aligned} \Delta x_1 &= x_{F1} + x_{B2} \\ \Delta x_2 &= x_{F2} + x_{B1} \end{aligned} \tag{2.14}$$

Δy_1 and Δy_2 are defined in an analog way. The Δx_1 and Δx_2 distributions of Bhabha events are measured over a time intervall and the mean values used in equation 2.13. Thereafter a measure of the mean z coordinate of the interaction point in the VSAT coordinate system can be extracted. The precision of this measurement is restricted by the accuracy in the reconstructed x positions of the Bhabha events but there is also an influence from the dispersion of the beams as can be seen directly from equations 2.3-2.6. The accuracy of the relative VSAT measurement is on the average 2 mm, to be compared to 1.5 mm for the TPC. Figure 2.4 shows the variations of the z-positions during 1994 measured by the VSAT and the TPC. To the right you can see the difference between the VSAT and TPC measurements normalised to the combined statistical error.

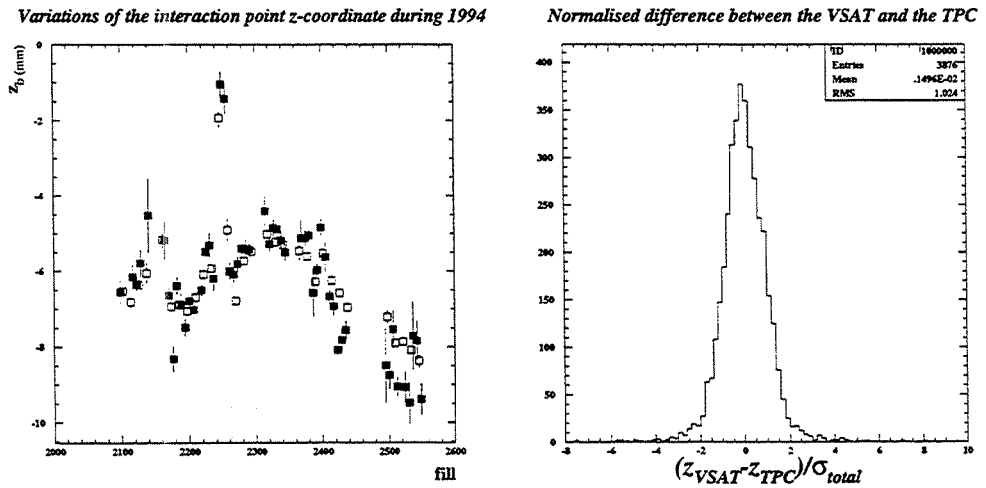

Figure 2.4: Left: The z-variations of the interaction-point during 1994 as measured by the VSAT (black) and the TPC (white). The VSAT measurement has been aligned to the TPC. Right: The difference between the VSAT and TPC measurements normalised to the combined statistical error.

Due to the uncertainty in the absolute position of the VSAT modules in respect to the rest of DELPHI, the VSAT measurement has to be aligned to the absolute measurement from the TPC. Relative changes in the z-coodinate, however, can be accurately monitored by the VSAT itself, providing a cross check to the interaction point measurements from the TPC.

2.2.3 Beam angles

Apart from measurements of the z-coordinate of the interaction point,the VSAT can also measure some quantities connected to the angles of the beams at the interaction point. From the transport equations 2.3-2.10 a direct dependence from the beam angles on the impact point of the Bhabha events at the VSAT modules can be seen. It is however not possible to isolate the individual beam angle dependence from equations 2.3-2.10. The mean tilt of the beams in the x-plane, θ_x, can instead be measured by the diagonal

counting asymmetry, A_D, for Bhabha events in the two VSAT diagonals

$$\theta_x = cA_D = c\frac{N_1 - N_2}{N_1 + N_2} \tag{2.15}$$

where N_i is the number of Bhabha events in VSAT diagonal i; $i = 1, 2$ and $c = 20$ μrad. The reason is of course the sharp drop in the Bhabha cross section with polar angles. Therefore a tilt of the beam in the x-direction will increase the accepted cross section in one VSAT diagonal and decrease it in the other. This measure only gives information about the size of the *mean* tilt of the two beams, but does not say anything explicitly about the individual beam angles. For the y-plane the transport equations suggest that it is possible to measure the mean tilt, θ_y, of the beams as:

$$\theta_y \approx \frac{y_{F1} + y_{F2} - y_{B1} - y_{B2}}{4 * l_y} \tag{2.16}$$

This equation comes straight from equations 2.2.7-2.2.10 under the assumption of a mean production angle, $\theta^y_{1,2}$, equal to zero.

Acollinearities

The difference in angles between the two beams is called the acollinearity, ϵ_i

$$\epsilon_i = \theta^i_+ - \theta^i_-; i = x, y \tag{2.17}$$

Ideally this quantity should be equal to zero, corresponding to head on collisions in LEP. In real life deviations from this situation of the order of 0.1 mrad occur frequently. The transport equations give

$$\Delta y_1 + \Delta y_2 \approx 4 f_y y_b + 2 l_y \epsilon_y \tag{2.18}$$

and similar for the x-coordinates

$$\Delta x_1 + \Delta x_2 \approx 4 f_x x_b + 2 l_x \epsilon_x \tag{2.19}$$

In equation 2.19, $2 * x_b >> z_b(\theta^x_1 - \theta^x_2 - 2 * \theta_x)$ is assumed. This assumption agrees well with data where the two production angles are approximately equal and the mean beam-tilt of the order of milliradians. Thus equations 2.18 and 2.19 describe similar situations in the two different planes.

The y-plane acollinearity

As evident from equation 2.18 the effect seen by the VSAT in the y-plane is a linear combination of displacements in the y-coordinate of the interaction point and the acollinearity of the beams in the y-plane. The values of the magnification factor and effecitve length, $f_y = 0.10 \pm 0.02$ and $l_y = 3.50 \pm 0.02$ m, are given from simulation studies. Thus $f_y << l_y$ and since the variations in the y coordinate of the interaction point observed so far during a year are less than 0.5 mm (see [25]), effectively all the observed variations are due to the acollinearity. The acollinearity in the y-plane may vary by several hundred μrad during a

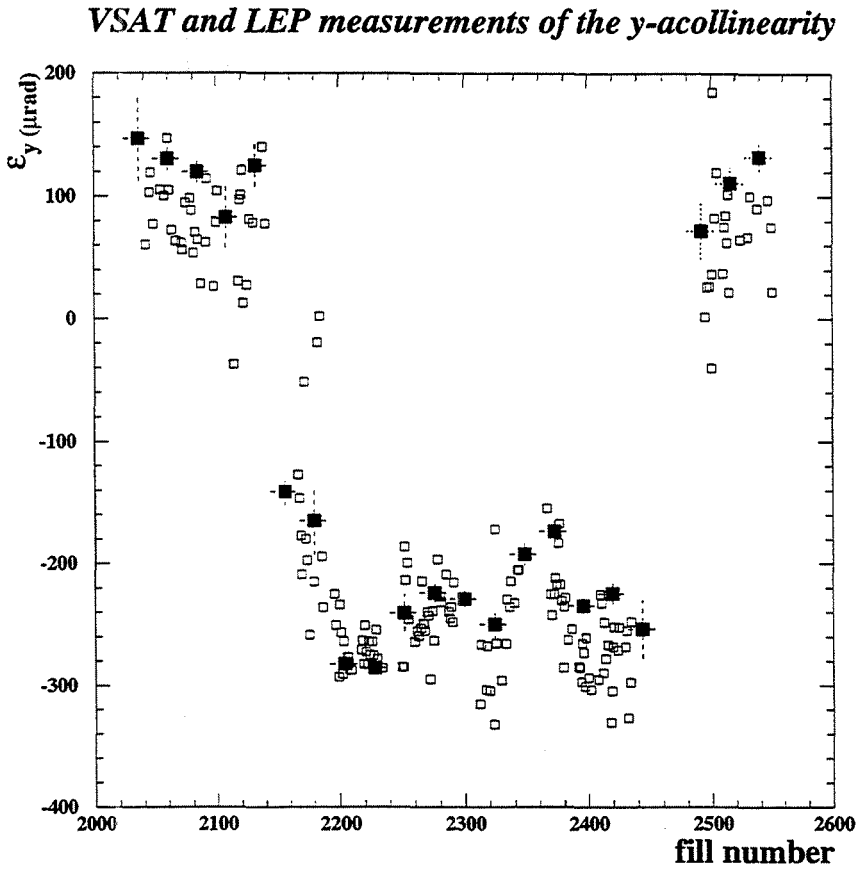

Figure 2.5: The y-acollinearity measured by the VSAT (white) and the same measurement by LEP (black) versus the fill number for 1994 data.

year. To give an effect of the same order in the VSAT, the y-coordinate of the interaction point would have to vary by approximately 5 mm. Fig 2.5 shows a comparison of the y-acollinearity measurement from the VSAT and the LEP Beam Orbit Monitors for 1994 data.

The VSAT can measure relative acollinearity variations with an accuracy of better than 50 μrad in the y-plane. In order to be able to extract the absolute beam angles, just as for the z-coordinate of the interaction point, the VSAT measurement has to be aligned to the central DELPHI coordinate system.

The x-plane acollinearity

In the x-plane the situation is different due to the different values of l_x and f_x (2.1 ± 0.1 and 12.60 ± 0.02 m). Here the two terms representing the displacement and the angles in

equation 2.19 give rise to approximately the same size contributions. It is hence impossible to distinguish a shift in the x-coordinate of the interaction point from an acollinearity in the beams in the x-plane from VSAT data alone. By inserting the x-coordinate of the interaction point as measured by the VD in equation 2.19 it is however possible to extract the acollinearity variations (see fig 2.6).

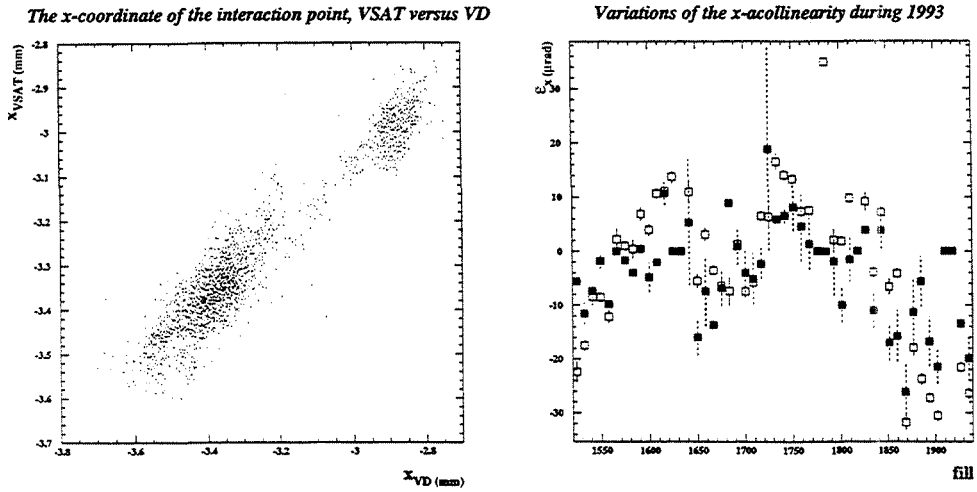

Figure 2.6: Left: The left side of equation 2.19 versus the VD measurement of the x-coordinate of the interaction point. The VSAT measurement is affected by the acollinearity. Right: The acollinearity of the beam extracted from the VSAT measurement (white) compared to the values from LEP (black).

2.2.4 Summary

The VSAT is able to measure relative variations of the main interaction point parameters. The z-coordinate fluctuations can be monitored with an accuracy of 2 mm and the acollinearity of the angles in the y-plane with an accuracy of 50 μrad. By combining the VSAT measurement with the x-interaction point measurement from the VD also the acollinearity of the beam angles in the x-plane can be monitored. The measured variations have thus not only been used as a cross check of the TPC and VD measurements but has also contributed new information about the beam-angles variation. This information is of interest for physics analysis, e.g. reconstruction of Q^2 for two-photon events (see chapter 4). Through the extraction of the various beamparameters from VSAT data the variations in measurable quantities seen in the VSAT has been successfully mapped to interaction point fluctuations. This validates the corrections to the accepted Bhabha cross section done in the luminosity analysis (see chapter 3). The cross check of the measured interaction point coordinates with the VD and TPC also improves the understanding of the VSAT geometry.

Chapter 3

Luminosity measurements

The main objective when LEP was built, was to precision study the decays $e^+e^- \rightarrow f\bar{f}$ and hereby measure the resonance parameters of the Z^0 particle. This precision measurement is performed by running LEP at different energypoints close to the Z^0 resonance energy[1] and measure the hadronic and leptonic cross sections and the leptonic forward-backward charge asymmetries at each energy-point. By making fits to the measured quantities various electroweak parameters can be extracted. In 1993 LEP was running at three different energypoints. At the Z^0 peak energy and at 1.76 GeV above and below, the so called peak ± 2 points. Before the scan started, a smaller sample of data was also collected at the so called pre-scan at 91.3 GeV. In 1994 LEP was running the whole year at Z^0 peak energy. The main purpose of the VSAT from the beginning was to measure the luminosity with high statistics for LEP1. Luminosity is the proportionality constant between interaction rate and cross section and is together with the beam energy the main accelerator performance parameter of a collider experiment. Good accuracy of the luminosity measurement is crucial for a high precision determination of the Z^0 line-shape but is also desired for other physics analyses. Due to its high statistical precision for Bhabha events, the VSAT is ideal for luminosity measurements. The online luminosity has already been briefly mentioned in the previous chapter. For the Z^0 measurement the aim is to have a luminosity error smaller than the statistical error from the number of hadronic Z^0 decays. Since the number of hadronic Z^0 events for the LEP experiments is of the order of 10^6, the error on the luminosity has to be around 0.1% [27]. A lot of effort has been made during the years to understand and reduce the uncertainties in the VSAT luminosity [28, 29].

3.1 Theory

Luminosity is defined as the interaction rate, $\dot{N}$, per unit cross section, σ, of the relevant e^+e^- reaction

$$\mathcal{L} = \frac{\dot{N}}{\sigma} \tag{3.1}$$

[1] This procedure is called an energy scan.

In principal the luminosity is possible to determine directly from the beam quantities according to the following. If the particles in an electron-positron collider are colliding in bunches head on, the luminosity is given by

$$\mathcal{L} = \frac{fN^+N^-}{4\pi N_b \sigma_x \sigma_y} \tag{3.2}$$

with f the revolution frequency, N^+ the number of positrons, N^- the number of electrons, N_b the number of particle bunches in each beam and σ_x, σ_y the transverse dimensions of the bunches. In real life these quantities are not known to high enough precision to match the demands. Instead the rate of events of a well-known reaction are measured and divided by the calculated theoretical cross section. Since the luminosity is dependent on parameters which may change with time, the integrated luminosity is defined as

$$\bar{\mathcal{L}} = \int \mathcal{L} dt \tag{3.3}$$

This quantity is the interesting one to measure, the integration time may vary from 15 sec in the online luminosity (see chapter 2) upto years (see fig. 3.1), depending on the purpose. The VSAT luminosity is integrated on a cassette basis corresponding to some 10 minutes[2]. Fig 3.1 shows the integrated luminosity provided by LEP to the experiments for the different years from 1993 to 1995.

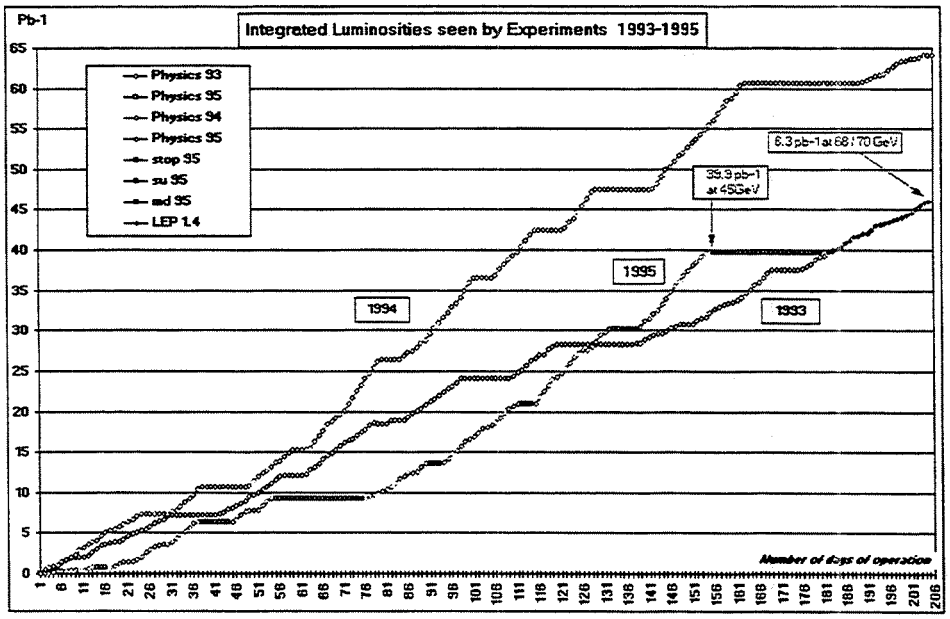

Figure 3.1: Integrated luminosity from LEP 1993-1995.

From equation 3.1 it can be seen that the dimension for luminosity is $[area \times time]^{-1}$. The dimension for integrated luminosity is therefore $[area]^{-1}$. For practical reasons the

[2]The time it takes for DELPHI to collect a cassette of data. This corresponds to an integrated luminosity of approximately 5 nb^{-1}.

unit cm^{-2} is often substituted by the unit $barn^{-1}$ ($1\ barn = 10^{-28}m^2$) with an apropriate prefix.

3.1.1 Bhabha scattering

The reaction used to measure the luminosity at LEP is Bhabha scattering, (see fig. 3.2).

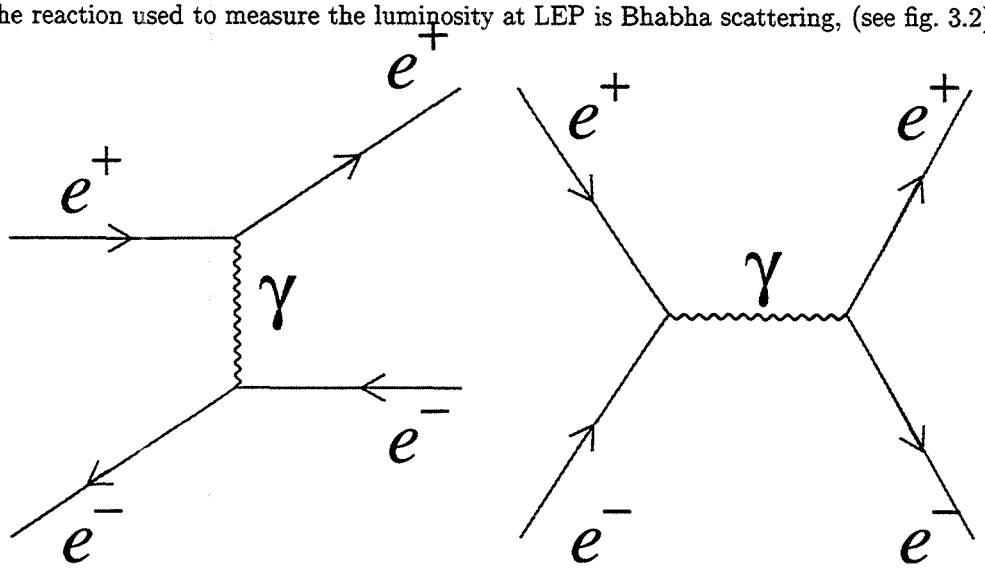

Figure 3.2: The two leading order diagrammes for Bhabha scattering.

Bhabha scattering is elastic e^+e^- scattering, where the outgoing particles are scattered into equal angles retaining their incident energy. The differential cross section for lowest order Bhabha scattering at high enough energies to neglect the lepton masses, is given by quantum electrodynamics

$$\begin{aligned}\frac{d\sigma_0^{QED}}{d\Omega} &= \frac{\alpha^2}{s}\left(\frac{1}{2}\frac{1+cos^4\theta/2}{sin^4\theta/2}+\frac{1}{4}(1+cos^2\theta)-\frac{cos^4\theta/2}{sin^2\theta/2}\right)\\ &= \frac{\alpha^2}{16s}\frac{(3+cos^2\theta)^2}{sin^4\theta/2}\end{aligned} \tag{3.4}$$

where θ is the polar scattering angle and s the centre of mass energy squared. From equation 3.4 it is clear that the Bhabha cross section falls rapidly with θ. To achieve a high Bhabha counting rate the measurement should hence be done at small polar angles. The corrections to the Bhabha cross section due to the contribution of weak diagrammes, where the photon is replaced by a Z-boson, are also smaller at small angles. These diagrammes result in 7 extra terms to the cross section which at LEP1 energies cannot be neglected. For the precision required for the Z^0 scan, also radiative corrections of higher order are necessary to the cross section [28]. A detector for luminosity measurements must be able to detect the coincidence of the two Bhabha scattered leptons and measure their direction and energy. The reason to use Bhabha scattering is that it is well known theoretically

and the kinematics is simple, so that no unknown parameters influence the measurement. Furthermore it has a large cross section at small angles providing a high counting rate. This means that there is no statistical limitation in studying the experimental systematic. Finally, the background contamination is rather low, typically less than 1% for LEP1. The VSAT uses the false Bhabha trigger (see section 1.3.1) to measure the accidental background. The steep drop of the cross section with angles also implies that a precise understanding of the inner acceptance edge of the detector is crucial for the precision of the luminosity measurement.

3.2 VSAT luminosity

The VSAT fulfils all the requirements mentioned in the previous section for a high precision Bhabha luminosity monitor. In this section the VSAT luminosity measurement from 1993 and 1994 is described. The knowledge gained from the detailed studies of the Bhabha events is not only used in the relative luminosity determination but also, as shown in chapter 4, useful for e.g. background rejection for double-tag two-photon events.

3.2.1 Accepted cross section

The accepted Bhabha cross section of the VSAT is determined by convoluting the theoretical cross section with the geometrical acceptance of the VSAT. An analytical calculation will lead to very complicated calculations based on different assumptions [28]. The natural way to proceed is instead to use computer simulations. Bhabha events are generated with the Monte Carlo generator BABAMC [30] and then passed through the detector simulation of FASTSIM [26]. BABAMC is a complete $O(\alpha)$ event generator for Bhabha scattering, including initial and final state radiation as well as weak corrections of first order. Simulations, with a consistent result, were also performed with the BHLUMI [31] generator including higher order corrections and with a stated theoretical uncertainty of 0.11%. FASTSIM tracks the particles from the interaction point and uses a parametrization of the electromagnetic shower development to describe the energy deposit in the VSAT. Due to its position at small polar angles the VSAT is sensitive to beamparameter variations (see chapter 2). This affects the accepted Bhabha cross section and contributes the main correction to the luminosity calculation. The accepted Bhabha cross section, σ_{acc}, has been found from the simulation studies to vary with the beamparameters in each VSAT diagonal according to [32]

$$\begin{aligned}\sigma_{acc} = \sigma_0[1 + A(\Delta x - \overline{\Delta x})^2 + B(D\Delta x - \overline{\Delta x}) + C(\sigma\Delta x - \overline{\sigma\Delta x}) \\ + D(\Delta y - \overline{\Delta y}) + E(A_D - \overline{A_D})]\end{aligned} \tag{3.5}$$

σ_0 is the accepted cross section at the expansion point defined by the coordinates ($\overline{\Delta x}$, $\overline{\sigma\Delta x}$, $\overline{\Delta y}$, $\overline{A_D}$). Δx is the mean of the distribution of the sum of the x-positions of the Bhabha pairs in cm, $\sigma\Delta x$ the RMS of the Δx distribution in cm, A_D is the diagonal counting asymmetry in the VSAT in % and Δy is the mean of the distribution of the sum of the y-positions of the Bhabha pairs in cm. Equation 3.5 corrects the accepted Bhabha cross section of the VSAT directly in the mesured quantities under the assumption that the

variations experienced originate from interaction point or beam angles variations (which was investigated in chapter 2).

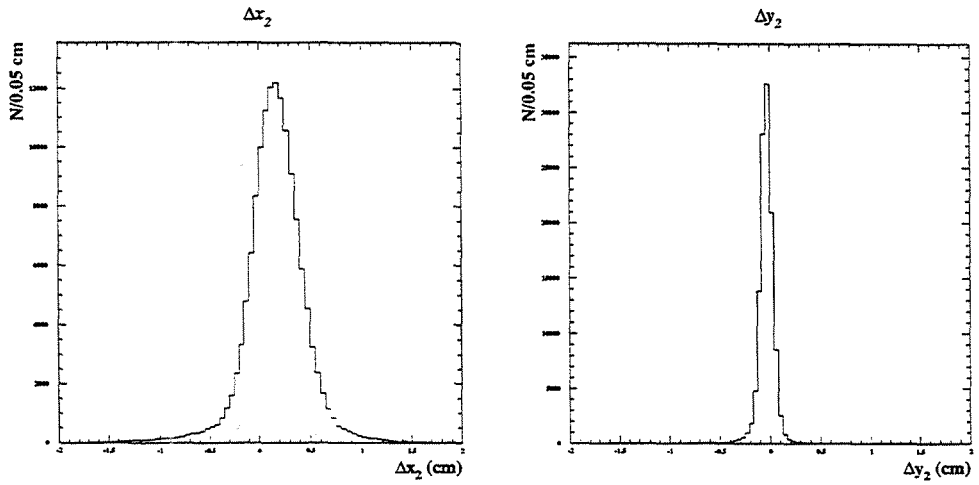

Figure 3.3: The distribution of the measured quantities Δx and Δy. The variations of these measurables are used to correct the accepted Bhabha cross section for beamparameter variations. The variations in RMS of the Δx distribution is also corrected for in equation 3.5.

The expansion point in equation 3.5 is chosen so that the corrections are minimised on the mean for the peak energy point. The exact values of the correction factors are found from fits to simulations, where the beamparameters are varied to cover the range of values seen in real data. For the 1993 luminosity the simulation studies contained more than $4*10^6$ accepted Bhabha events, thereby reducing the errors on the fitted parameters substantially. Table 3.1 shows the correction factors for the two VSAT diagonals for 1993. The accepted cross section also has to be corrected for the s^{-1} energy dependence in equation 3.4. Additional energy dependence due to the interference of weak diagrammes are negligible [28].

	diagonal 1		diagonal 2	
	parameter	error	parameter	error
A	1.58	0.05	1.21	0.04
B	0.315	0.004	0.200	0.003
C	0.90	0.02	0.66	0.02
D	0.001	0.001	-0.001	0.001
E	-1.01	0.04	0.99	0.04

Table 3.1: Correction factors to the accepted cross section from the FASTSIM simulation.

The accepted Bhabha cross section is calculated for each DELPHI cassette according to equation 3.5. When calculating the luminosity therefore also the number of accepted

Bhabhas are counted on a cassette basis. The calculated luminosity per cassette is then summed for each energy point.

3.2.2 Acceptance cuts

The Bhabha events used for the luminosity calculation were selected using the following criteria:

- an energy cut of 70% of the beam energy imposed on both the scattered electrons.
- a fiducial volume cut where the outer edge was determined by a radius of 7.8 cm and the inner edge was determined by a cut on the sum of the x-positions ($SX = |x_{forward}| + |x_{backward}|$) of the two particles greater than 13.2 cm (see fig. 3.4).

The reason for using this acceptance volume is mainly due to an uncertainty in the effects of a flange in the beampipe in front of the VSAT. The simulation description of this flange led to discrepancies with data. Especially the inner region of the detector, closer to the beampipe, was relatively more populated in Monte Carlo than in data. Studies of the calibration of the edge strip (as mentioned in chapter 1) ruled out the possibility that the effect was caused by the drifting of events from strip 2 to strip 1, i.e. out of the acceptance region. Due to this problem several different acceptance cuts were tried in order to eliminate the discrepancy. Finally the best choice appeared to be the position cuts described above. The radial cut conforms better with the geometry of the Bhabha process and together with the low SX cut it eliminates acceptance border effects sensitive to the absolute alignment of the detector. A better stability is also achieved due to smaller corrections and less sensitivity to beamparameter variations for this volume. The loss in statistics by using this cut amounts to 12 % compared to using the full VSAT volume.

3.2.3 The relative luminosity

After the acceptance cuts the number of Bhabhas are corrected for trigger efficiencies and hardware corruptions, and the false Bhabhas passing the same cuts are subtracted. The luminosity is then calculated by division with the calculated accepted cross section for each cassette and summed per energy point. Due to the uncertainty in absolute cross section, approximately 0.8% mainly due to geometrical uncertainties, the VSAT luminosity measurement was normalised to the SAT luminosity at peak energy for 1993. The SAT has a systematic absolute luminosity uncertainty of 0.29 % but the accepted Bhabha cross section for the VSAT is 16 times higher than for the SAT. Therefore the VSAT was used for the relative luminosity at the other energypoints. The lower statistical error makes a significant reduction in the statistical contribution to the error when calculating the hadronic cross sections. The resulting energy point-to-point uncertainty of the VSAT relative luminosity measurement consists of contributions from

- The errors in the measured quantities of equation 3.5.
- The errors in the correction factors in equation 3.5.
- Uncertainties from the acceptance cuts.

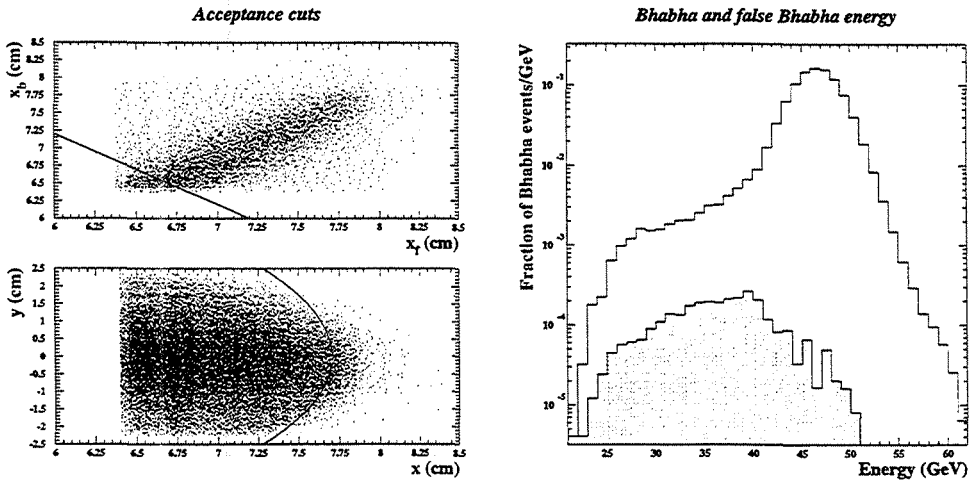

Figure 3.4: Left: The x versus x plot for a VSAT diagonal and the y versus x plot for one module, showing the SX and radius cuts. Right: The energy distribution for Bhabha events in logarithmic scale. The false Bhabha contribution is superimposed.

- Uncertainties from trigger-efficiency and Bhabha selection.
- Statistical errors from the number of accepted Bhabhas.

Table 3.2 shows the magnitudes of the contributions from the different uncertainties to the total point-to-point systematic error.

Source	Contribution
Measured quantities	0.15
Correction factors	0.20
Acceptance cuts	0.25
Trigger efficiency	0.20
Total systematic error	0.40

Table 3.2: Contributions to the VSAT point-to-point systematic error in permille for the 1993 scan.

Table 3.3 shows the VSAT relative luminosity summed per energy point for 1993 together with the statistical errors.

Compared to the 1991 luminosity [29] the improvement in uncertainties is due to the better understanding of the VSAT geometry, better determination of the correction factors and the usage of the more stable fiducial acceptance region.

energypoint	pre-scan	peak	peak -2	peak +2
VSAT luminosity (nb^{-1})	5562	9755	9181	9494
statistical error	0.65	0.49	0.51	0.50

Table 3.3: VSAT relative luminosity and statistical errors in permille for the off-peak and prescan energy points of the 1993 scan.

Comparison to the STIC

In 1994 LEP was only running at the Z^0 peak energy. This was also the first year of the new DELPHI STIC [14] luminosity detector. The STIC has a larger accepted Bhabha cross section than the SAT, improving the statistical accuracy with a factor 2.3, and the error on the absolute luminosity is 0.09 %. The VSAT luminosity was used to check the stability of the absolute luminosity measurement from the STIC (see fig. 3.5).

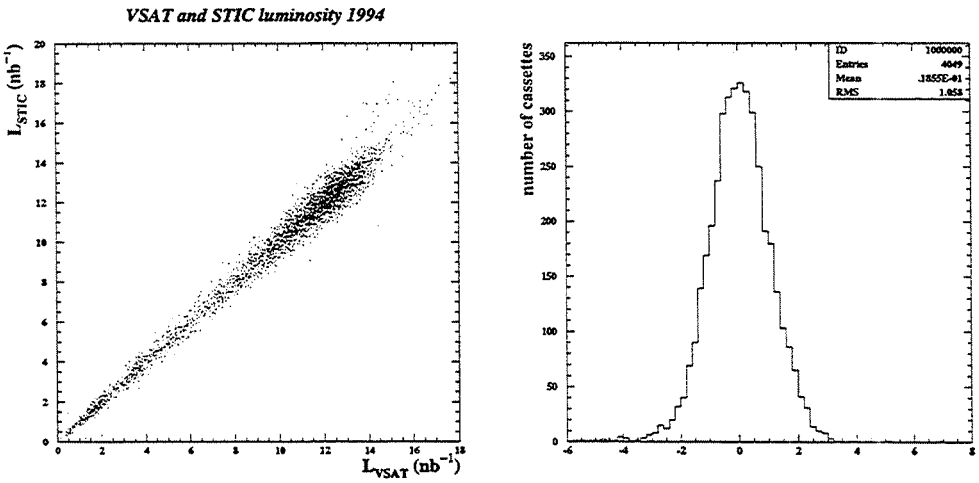

Figure 3.5: Left: The STIC luminosity versus the VSAT luminosity on a cassette basis. Right: The normalised difference of the VSAT and STIC luminosities on a cassette basis.

The agreement between the two detectors was found to be very good. As a stability check, the difference between the measurements on a cassette basis normalised to the combined statistical errors can be investigated. The VSAT luminosity was here normalised to the STIC in order to have a mean zero of the distribution.

$$f = \frac{\mathcal{L}_{VSAT} - \mathcal{L}_{STIC}}{\sqrt{\sigma^2_{VSAT} + \sigma^2_{STIC}}} \tag{3.6}$$

An RMS value of more than one would signal a bias in the measurement. As seen in fig. 3.5 the RMS value is consistent with 1, which means that all statistical fluctuations are accounted for properly. Possible systematic errors affecting the whole sample would not be discovered by this investigation.

The Z^0 lineshape

Appendix C gives a detailed description of the extraction of various electroweak parameters from the 1993-1994 Z^0 scan data. Previous DELPHI results from this measurement has been reported in [33]. Here only a short summary to point out the use of the VSAT luminosity will be made. The VSAT relative luminosity was used for the off-peak energy points when calculating the hadronic cross sections. The reduction in statistical error of the hadronic cross section when using the VSAT relative luminosity is about 20% [29]. Another advantage is the small influence from weak corrections for the VSAT which makes the luminosity measurement free from uncertainties related to the energy dependence of the electroweak interference. The hadronic event selection is based on charged tracks only, with a selection efficiency of $95.18 \pm 0.11\%$. A total of $6.87 * 10^5$ hadronic events were selected in 1993 and $1.144 * 10^6$ in 1994. The resulting cross sections were fitted with the model independent program ZFITTER [34] and the small corrections coming from γ -exchange and $\gamma - Z$ interference were calculated within the Standard Model. The accuracy of the energy determination of the LEP beams [35] was also taken into account in the fit. The cross section for $e^+e^- \rightarrow$ hadrons, without QED corrections, can be expressed as

$$\sigma(s) = \sigma_0 \frac{s\Gamma_Z^2}{(s - M_Z^2)^2 + (s^2/M_Z^2)\Gamma_Z^2} \tag{3.7}$$

where M_Z and Γ_Z are the mass and width of the Z^0 boson. The hadronic cross section at the Z^0-pole, σ_0, can be written

$$\sigma_0 = \frac{12\pi\Gamma_e\Gamma_{had}}{M_Z^2\Gamma_Z^2} \tag{3.8}$$

where Γ_e and Γ_{had} are the electronic and hadronic partial widths. The resulting values of M_Z, Γ_Z and σ_0 from the fit can be found in table 3.4.

Results from the Z^0 resonance	
M_Z	91.1849 $\pm$0.0034 GeV
Γ_Z	2.4913 $\pm$0.0053 GeV
σ_0	41.40 $\pm$ 0.10 nb

Table 3.4: The resulting values of M_Z, Γ_Z and σ_0.

Chapter 4

Two-photon physics

When electrons and positrons are travelling at high energy they are surrounded by a cloud of virtual Bremsstrahlung photons. These photons are generated according to a well known $1/E_\gamma$ like spectra, concentrated at small polar angles θ [36]. At e^+e^- colliders the intensity of these photons get high enough to enable studies of the interactions between them.

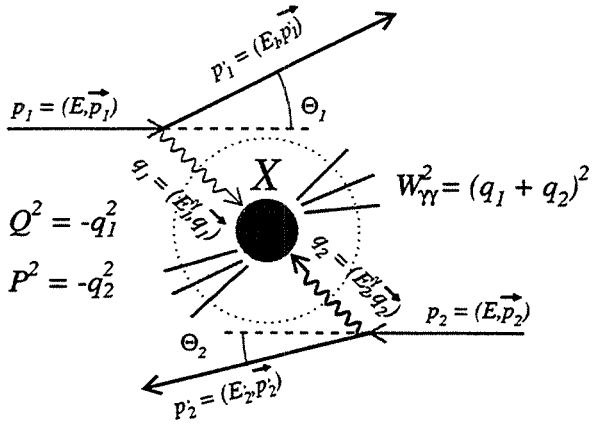

Figure 4.1: A two-photon collision at LEP resulting in a hadronic final state. The process marked X can due to the complicated nature of the photon be of several different kinds, which will be described in this chapter. The kinematic nomenclature is also defined in the figure.

Inelastic two-photon collisions, forbidden by classical electromagnetic theory, occur because the photon can fluctuate into a quark-antiquark pair of the same quantum numbers. The quarks can then interact strongly, giving rise to various kinds of reactions. The photons can also fluctuate into lepton-antilepton pairs, but since these interact electromagnetically or with less probability through the weak force and their interactions are calculable by QED to a high accuracy, they will not be treated here. Competing diagrams to the two-photon reaction $e^+e^- \rightarrow e^+e^-X$, virtual Bremsstrahlung processes and the γ cascade process, can all be neglected at LEP1 when tagging the leptons at small polar angles [17].

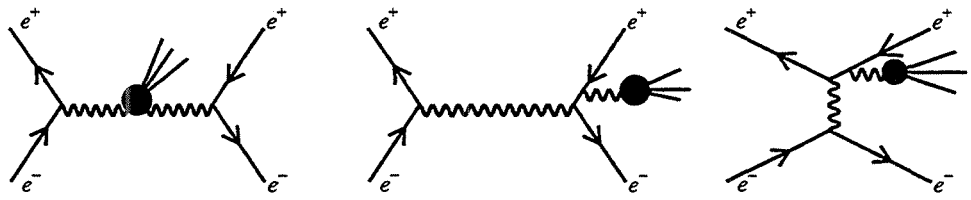

Figure 4.2: Competing diagrams to the two-photon reaction $e^+e^- \rightarrow e^+e^-X$. Left: The γ cascade process. Middle: The virtual Bremsstrahlung process with e^+e^- annihilation. Right: The virtual Bremsstrahlung process with e^+e^- scattering.

The interest in two-photon physics comes not only from the fact that it is a reaction of high cross section at all collider experiments but it also displays a wide range of different interactions due to the complicated nature of the photon. This chapter will start by briefly describing some relevant theoretical background for experimental two-photon physics and thereafter treat the DELPHI analysis of double-tag events for LEP1, where the VSAT was used to tag the electrons.

4.1 Theory

This section will outline the basic theoretical background for two-photon physics necessary to understand the experimental part presented in this thesis. The section starts with a description of the kinematics of a two-photon collision. Issues like two-photon models, cross sections and photon structure functions will also be discussed. More detailed descriptions can be found in [37–39] and other references in this section.

4.1.1 Kinematics

Refering to fig. 4.1 the kinematics of the two-photon process is defined according to the following [40]. The momentum transfer, Q^2 and P^2, in the $e\gamma$ vertices is calculated from

the four momenta of the photons

$$Q^2 = -q_1^2 \qquad (4.1)$$
$$P^2 = -q_2^2$$

where

$$\begin{aligned} q_i^2 &= (p_i - p_i^{'})^2 \\ &= 2m_e^2 - 2E_i E_i^{'}(1 - \sqrt{1 - \frac{m_e^2}{E_i}}\sqrt{1 - \frac{m_e^2}{E_i^{'}}}\cos\theta_i) \end{aligned} \qquad (4.2)$$

At LEP1 m_e/E_i is of the order of 10^{-5} and the smallest detectable θ is of the order 10^{-3} therefore equation 4.2 can be approximated to

$$Q^2 = -q_i^2 \approx 4E_i E_i^{'} sin^2\frac{\theta_i}{2} \qquad (4.3)$$

The invariant mass, $W_{\gamma\gamma}$, of the particle system X is calculated from the four-momenta of the photons

$$W_{\gamma\gamma}^2 = (q_1 + q_2)^2 \qquad (4.4)$$

so that

$$W_{\gamma\gamma}^2 = 4E_1^{\gamma}E_2^{\gamma} - 2E_1^{'}E_2^{'}(1 - \cos\theta_1\cos\theta_2 - \sin\theta_1\sin\theta_2\cos\Phi) \qquad (4.5)$$

The photon energy is here given by $E_i^{\gamma} = E_i - E_i^{'}$ and Φ is the angle between the planes defined by the two $e\gamma$ vertices. At very small angles, θ, equation 4.5 can be approximated by

$$W_{\gamma\gamma}^2 \approx 4E_1^{\gamma}E_2^{\gamma} \qquad (4.6)$$

4.1.2 The photon wavefunction

Photons show a multitude of different characteristics due to their complicated nature. As already mentioned photons can apart from interacting as bare photons, fluctuate to lepton-antilepton or quark-antiquark pairs. Furthermore the quark-antiquark pair fluctuations can be subdivided into high and low virtuality fluctuations by a suitably chosen transverse momenta, p_T, cut-off, where the high virtuality fluctuations are calculable through perturbative QCD, whereas the low virtuality part is accounted for by summing over vector-meson states. The wave-function of the photon can thus be written as [41]

$$|\gamma\rangle = c_{bare}|\gamma_{bare}\rangle + \sum_{V=\rho^0,\omega,\phi,J/\psi} c_V|V\rangle + \sum_{q=u,d,s,c,b} c_q|q\bar{q}\rangle + \sum_{l=e,\mu,\tau} c_l|l^+l^-\rangle \qquad (4.7)$$

The last term in equation 4.7 corresponds to fluctuations into lepton pairs and will, due to reasons mentioned above, be disregarded in this description. The coefficients c_i depend both on the scale which the photon is probed at and the mass of particle i, and are all of the order of α_{em}, except c_{bare} which is close to unity.

4.1.3 Photon-photon interactions

The hadronic two-photon interactions can take place by combinations of the different terms in equation 4.7. Each of these interactions in turn, proceed through different parton level processes, e.g. $\gamma\gamma \rightarrow q\bar{q}, \gamma q \rightarrow qg$ etc. Depending on the parton level processes the main interactions may be subdivided according to the following classification [42]

- **Vector Meson Dominance processes**, soft interactions where the photon act as a bound vector-meson state. These are the dominating processes at low p_T (see fig. 4.3).
- **Direct processes**, where both photons couple pointlike to the quarks. These processes dominate at high p_T.
- **Single Resolved processes**, where one direct photon reacts with the partons from a photon, perturbatively fluctuating into a quark-antiquark pair (being *resolved* into its hadronic constituents). This results in one low p_T spectator jet and two higher p_T jets.
- **Double Resolved processes**, where the partons of two photons, fluctuating into quark-antiquark pairs, interact with each other. The result is two low p_T spectator- and two higher p_T jets.

For comparisons with data the processes above are described by different Monte Carlo models. In the case of this thesis the comparison was made with the TWOGAM [43] generator. Below follows a short description of the three two-photon models included in TWOGAM to describe DELPHI two-photon data [44].

The VDM model

The VDM model describes the Vector Meson Dominance processes in the first group above. Diagrams of this type are not calculable by perturbative QCD, neither the Q^2 of the photons nor the p_T of the partons are large enough, instead the two-photon interactions are treated in a non-perturbative phenomenological way as hadron-hadron interactions replacing the photons by vector mesons. Hence VDM predicts photon-photon scattering to have the characteristics of hadron-hadron scattering. This description is dominant for small p_T where the quark-antiquark pairs have long enough lifetime to exchange gluons and thus react as a bound vector-meson state. The cross section dependence on p_T^2 is described as

$$\frac{d\sigma_{\gamma\gamma}^{VDM}}{dp_T^2} \sim e^{-\alpha p_T^2} \tag{4.8}$$

The VDM model contributes the major part of the total two-photon cross section and the partial VDM cross section can be parametrized as [45]

$$\sigma_{\gamma\gamma}^{VDM}(Q^2, P^2, W_{\gamma\gamma}^2) = F_{VDM}(Q^2)F_{VDM}(P^2)[A + \frac{B}{W_{\gamma\gamma}}] \tag{4.9}$$

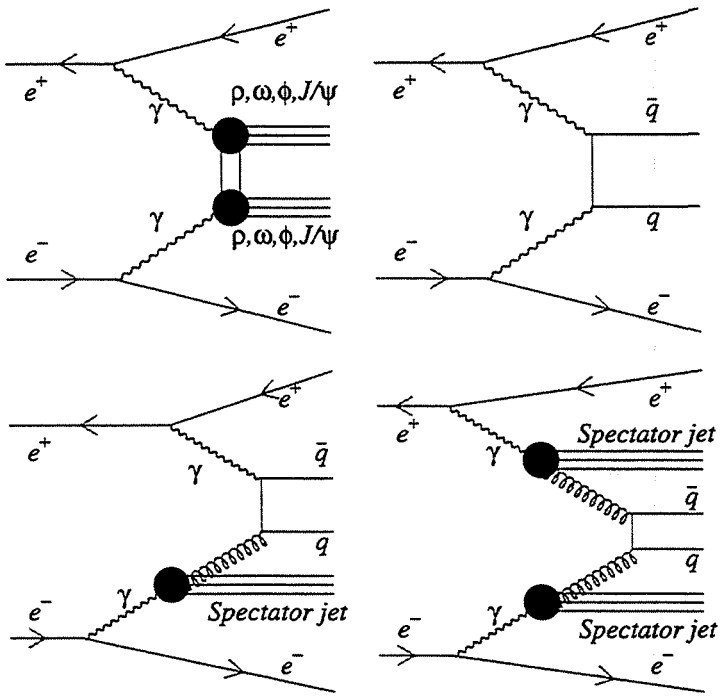

Figure 4.3: Upper left: A Vector Meson Dominance process, where photons interact as bound vector meson states. The most likely of these is ρ followed by ω, ϕ etc. The vector-mesons with higher masses are heavily suppressed. Upper right: The direct process, described by the Quark Parton Model, where the photons couple directly to a quark-antiquark pair. Lower left: A diagram showing a leading order single resolved process. Lower right: A diagram showing a leading order double resolved process.

Where Q^2 and P^2 are the squared momenta of the two photons and $A = 275$ nb and $B = 300$ nb·GeV were found from data [46] to describe the invariant mass ($W_{\gamma\gamma}$) dependence. F_{VDM} is the generalized VDM formfactor [47] describing the cross section dependence on Q^2 and also the coupling between the photon and the different vector-mesons.

$$F_{VDM}(Q^2) = \sum_{V=\rho,\omega,\phi} r_V \frac{1 + Q^2/4m_V^2}{(1 + Q^2/m_V^2)^2} + \frac{0.22}{1 + Q^2/m_0^2} \tag{4.10}$$

m_V is the mass of vector-meson V and r_V is related to its coupling to the photon. In TWOGAM the values $r_\rho = 0.65, r_\omega = 0.08$ and $r_\phi = 0.05$ are used. The last term represents radial excitations of the vector mesons and the value m_0= 1.4 GeV was used.

The QPM model

The Quark Parton Model (QPM) describes the direct photon processes by perturbative calculations. The model treats the splitting of the photon to quarks similarly to the QED

reaction $e^+e^- \to e^+e^-\mu^+\mu^-$. The resulting events show typical two jet topologies, but contrary to the VDM model the jets have high p_T. The QPM model is only applicable at high Q^2, high p_T^2 or large quark masses and its relative contribution to the cross section grows with Q^2. The leading order invariant mass dependence can be found to be $\sigma_{\gamma\gamma}^{QPM} \sim \frac{1}{W_{\gamma\gamma}^2}$ and the p_T^2 dependence is $\frac{d\sigma_{\gamma\gamma}^{QPM}}{dp_T^2} \sim \frac{1}{p_T^4}$.

The QCD-RPC model

The single and double resolved processes are described by the QCD-Resolved Photon Contribution model. The necessity for the use of the contribution from the QCD-RPC model to describe DELPHI two-photon data has been proved in previous two-photon studies [44]. Since the spectator jets produced in this model are concentrated at small angles and mainly go undetected, the detected event toplogy resembles the high p_T two-jet structure of the QPM model. The QCD-RPC model uses a set of Parton Density Functions (PDF), describing the density of different partons $(q, \bar{q}, g)$ in the photon as a function of x and Q^2, where x is defined as the fraction of the total momentum of the hadron (photon) carried by the parton. There are several different parametrisations of the PDFs available. Since the hard scattering sub-processes are considered as perturbative in the QCD-RPC model each PDF has a cut, p_T^{min}, determining the lower transverse momenta of the outgoing partons for which the associated processes can occur. This p_T^{min} cut separates the model from the contribution of the non-perturbative region. For the studies in this thesis the Gordon-Storrow [48] parametrisation was used with a $p_T^{min} = 1.88$ GeV/c found to reproduce the visible two-photon cross section from experimental data. The asymptotic p_T^2 dependence of the QCD-RPC model is similar to the QPM model.

4.1.4 Cross section

The cross section for the two-photon reaction $e^+e^- \to e^+e^- + X$ can in the Equivalent Photon Approximation[1] be written as [38]

$$\frac{d\sigma(e^+e^- \to e^+e^- X)}{dW_{\gamma\gamma}} = \frac{d\mathcal{L}_{\gamma\gamma}}{dW_{\gamma\gamma}} \sigma_{\gamma\gamma}(W_{\gamma\gamma}) \tag{4.11}$$

$\mathcal{L}_{\gamma\gamma}$ here stands for the two-photon luminosity function describing the photon-flux at the e^+e^- collider and is given by QED (see fig. 4.4). The photon flux rises logarithmically with the beam energy for a given $W_{\gamma\gamma}$. The steep drop of the photon flux with increasing $W_{\gamma\gamma}$ puts a limit on the accessible $W_{\gamma\gamma}$ values to less than half the e^+e^- energy.

The total hadronic two-photon cross section, $\sigma_{\gamma\gamma}$, which is the interesting quantity to experimentally measure, is composed of the contributions from the different two-photon processes.

$$\sigma_{\gamma\gamma} = \sigma_{\gamma\gamma}^{VDM} + \sigma_{\gamma\gamma}^{direct} + \sigma_{\gamma\gamma}^{1-resolved} + \sigma_{\gamma\gamma}^{2-resolved} \tag{4.12}$$

[1] EPA treats the photons in the limit $q^2 \to 0$.

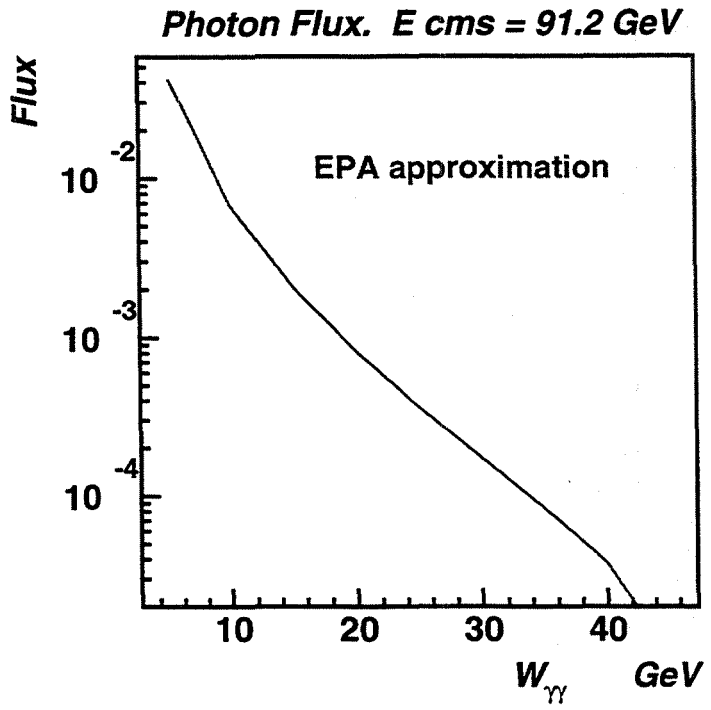

Figure 4.4: The photon flux at LEP1 as a function of $W_{\gamma\gamma}$.

The VDM part which contributes the major part of the visible cross section is described by parametrisations of hadronic cross sections. For the perturbative processes calculations of the contributions of the different hard sub-process diagrams can be made [41]. The perturbative cross sections diverge for $p_T \to 0$ why a p_T^{min} cut is needed to define the minimum value for which the calculation is valid.
Another way of approaching the invariant mass dependence of $\sigma_{\gamma\gamma}$ is given by considering Regge parametrisation seriously for photons. Hadronic cross sections have been found to be described by the parametrisation

$$\sigma_{tot}^{AB}(s) = X^{AB}s^{\epsilon} + Y^{AB}s^{-\eta} \tag{4.13}$$

Fits to all hadronic total cross sections $A + B \to X$ give results compatible with a universal value of $\epsilon \approx 0.0808$ and $\eta \approx 0.4525$ [49]. The coefficients X^{AB} and Y^{AB} are process dependent. Equation 4.13 can be interpreted within Regge theory where the two terms represent the exchange of Regge trajectories. The first term, which is dominant for

high energies, then represents Pomeron exchange and the second term Reggeon exchange. Equation 4.13 has been successful in describing γp data from HERA [50]. Thus to first approximation the Regge theory ansatz seems to be valid for the photon, at least when it comes to describing cross sections. A derivation of a Regge parametrisation for the total $\gamma\gamma$ cross section results in [41]

$$\sigma_{\gamma\gamma} \approx 211 s^{\epsilon} + 215 s^{-\eta} [nb] \tag{4.14}$$

where $s = W^2_{\gamma\gamma}$ and $\epsilon \approx 0.0808$ and $\eta \approx 0.4525$ are the universal values from fits to hadronic cross sections. The difference in total cross section between the Regge model and perturbative calculations of contributing diagrams plus the VDM parametrisation is found to be approximately 10% from a few GeV and onwards [41]. The Regge parametrisation has no real predictive power about the physics components behind the cross section, but it seems to describe data well. An interesting test would therefore be to measure the total two-photon cross section experimentally and investigate which model describes data better. Experimental measurements has so far been performed below 20 GeV with limited statistics [51].

4.1.5 The photon structure function

One of the main areas of interest in two-photon physics is studies of the *photon structure functions*. These functions describe the partonic content of the photons and are thus related to the constants c_i in equation 4.7. When one of the photons in the two-photon collision of fig. 4.1 is quasi-real with a squared momenta, P^2, around zero, the cross section can be expressed as [36]

$$\frac{d\sigma}{dxdy} = \frac{4\pi\alpha^2 s}{Q^4} \left[\left(1 + (1-y)^2\right) F_2^{\gamma}(x, Q^2) - y^2 F_L^{\gamma}(x, Q^2) \right] N_{\gamma}(z, \theta_{max}) z dz \tag{4.15}$$

where

$$\begin{aligned} s &= 4E_1^2 \\ y &= 1 - (E_1'/E_1)\cos^2(\theta_1/2) \\ x &= \frac{Q^2}{Q^2 + W^2_{\gamma\gamma}} \\ z &= \frac{E_{\gamma}}{E_1} \end{aligned} \tag{4.16}$$

The whole reaction can be viewed as deep inelastic scattering of an electron off the quasi-real target photon. $N_{\gamma}(z, \theta_{max})$ describes the flux of the target photons and θ_{max} is their maximum scattering angle. $F_2^{\gamma}(x, Q^2)$ and $F_L^{\gamma}(x, Q^2)$ are the photon structure functions describing the partonic content of the photon. Experimentally y is normally very small so that only F_2^{γ} is measurable.

In the simple parton model F_2^{γ} can be written as

$$F_2^\gamma = \sum_q [x e_q^2 q^\gamma(x,Q^2) + x e_{\overline{q}}^2 \overline{q}^\gamma(x,Q^2)] \tag{4.17}$$

where $q^\gamma(x,Q^2)$ and $\overline{q}^\gamma(x,Q^2)$ are the quark and antiquark densities, e_q is the fractional charge of the quark and the sum runs over all light quark flavours. The Altarelli-Parisi equations describe the Q^2 evolution of PDFs. For photons, compared to hadrons, there is an additional term corresponding to the splitting of a photon to a quark-antiquark pair. This term makes the equation become inhomogenous and the structure function depend linearly on ln Q^2 in leading order. As mentioned in the previous section the photon can form bound states of vector mesons described by the VDM model or interact through a point-like coupling to the quark-antiquark pair. Thus the photon structure function can be subdivided into a perturbative point-like part and a non-perturbative VDM part [38]

$$F_2^\gamma = F_2^{\gamma,VDM} + F_2^{\gamma,point} \tag{4.18}$$

It is clear that the VDM part of the structure function is not calculable by perturbative models. Instead it behaves like hadron structure functions, showing no rise with ln Q^2. $F_2^{\gamma,VDM}$ is decreasing with increasing Q^2. The perturbative part of the structure function is in the leading log approximation, neglecting gluon Bremsstrahlung, given by

$$F_2^{\gamma,point} = \frac{3\alpha \sum e_q^4}{\pi} x[x^2 + (1-x)^2] ln \frac{Q^2}{Q_0^2} \tag{4.19}$$

Q_0 is here the lower limit where $F_2^{\gamma,point}$ is valid and the sum runs over all quark flavours. To calculate the leading order QCD corrections from gluon emission and exchange the Altarelli-Parisi evolution equations are solved, resulting in the same asymptotic ln Q^2 dependence at not too small x. Measurements of the photon structure function in a Q^2 range between 4 and 30 GeV^2/c^2 has previously been reported by DELPHI [44] where the rise with ln Q^2 was confirmed. Lately a lot of interest has been attracted by the effects of non zero virtuality, $P^2 \neq 0$, of the target photon [52]. The influence of the VDM part of the structure function is predicted to go away at sufficiently high P^2 allowing a purely perturbative measurement of $F_\gamma^2(x,Q^2,P^2)$. The fall-off of the non-perturbative part is theoretically uncertain and model dependent. Experimental measurements are therefore required to clarify the situation.

4.2 Experimental methods

Since the photons in two-photon collisions generally have low energy, the electrons will be scattered into small angles. The detection of the scattered electrons thus rely on the forward and very forward calorimeter coverage. Moreover the final state hadronic particles will also to great extent be concentrated in the forward direction making detection of two-photon events at e^+e^- colliders a difficult business. The detectors at these facilities are mainly designed for different purposes, e.g. Z^0 decays at LEP. The experimental methods for measuring two-photon events at e^+e^- colliders can be grouped depending on the detection of the outgoing electrons.

- **No Tag**, none of the two electrons are detected and thus the whole measurement is dependent on the reconstruction of the hadronic system. Normally this means that the electrons are scattered into very small angles, meaning small Q^2 and small $W_{\gamma\gamma}$. The advantage for this kind of studies is the high statistics.

- **Single Tag**, one of the scattered electrons are detected by a calorimeter in the forward direction. Thereby a good measure of the Q^2 of one of the photons is achieved. This kind of measurements are used for photon structure function studies [44] assuming that the target photon is quasi-real. In order to achieve a good $W_{\gamma\gamma}$ determination advanced unfolding methods have to be used.

- **Double Tag**, both of the scattered electrons are detected by forward calorimeters. The accepted cross section for double tag events are generally lower than for no tag and single tag. By measuring both the outgoing electrons a complete picture of the kinematics of the two-photon collision is achieved thereby improving the invariant mass determination.

- **Anti tag**, a strict requirement for no-tag data that no electron is detected in any forward calorimeter. This way the Q^2 range is restricted to small values. For single tag data an anti-tag requirement can also be applied to the undetected electron.

4.3 DELPHI double tag analysis

Appendix D describes two studies of DELPHI two-photon data. The first part deals with a study of the visible two-photon cross section as a function of the e^+e^- centre-of-mass energy at LEP1 and LEP2 energies. The events were selected according to the anti-tag mode described above and with the same experimental setup and selection criteria at all energies. Hence the systematics was almost the same. Various event properties were examined and compared to simulations (see fig. 4.5). The behaviour of the Monte Carlo in the forward region led to some discrepancies with data. The visible cross section was found to depend linearly on the e^+e^- centre-of-mass energy above the Z^0 peak.

The second part of appendix D deals with DELPHI double-tag analysis using the VSAT for tagging the electrons and will be described in detail in this section. The aim of this analysis is to investaigate the total cross section for the reaction $\gamma\gamma \rightarrow q\bar{q}$ at LEP1. At LEP2 also studies of the photon structure function will be performed in this mode. By measuring both the scattered electrons with the VSAT a definite determination of the energy and momenta of the photons is achieved. The key to a succesful analysis therefore lies in a good precision in the VSAT measurement. An accurate rejection of the background sources is also essential due to the relatively low statistics. For this purpose DELPHI posseses several advantages through its VSAT.

- The VSAT covers a region at small enough polar angles, 3-15 mrad, to collect data in a region of kinematical interest.

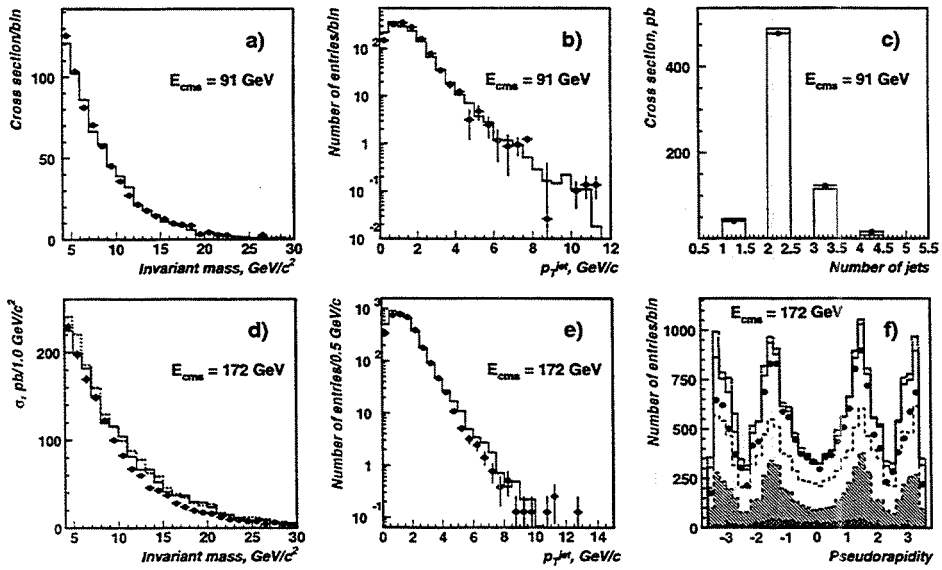

Figure 4.5: Comparisons of no-tag data and Monte Carlo for 91 and 172 GeV. Points are data, solid and dotted lines are the full VDM+QPM+QCD-RPC predictions. Dashed line is the QCD-RPC contribution. Hatched histogram is the VDM part, double hatched is the QPM part. a: The invariant mass distribution for no-tag data and Monte Carlo at 91 GeV. b: p_T of the jets at 91 GeV. c: Number of jets at 91 GeV. d: Invaraint mass at 172 GeV. e: p_T of the jets at 172 GeV. f: Pseudo rapidity at 172 GeV.

- The precision and reconstruction methods of the VSAT are well known from the luminosity analysis. The huge sample of Bhabha events provides an excellent calibration source for the two-photon analysis.
- The influence of the interaction point variations and other beam-parameters are well measured and their effect on VSAT data is well understood. The variations in beam angles are necessary to consider when determining Q^2.
- Variations and behaviour of the main background source, Bhabha events (in coincidence with no-tag two-photon events), are well known from the luminosity studies.

The simulated events where generated with the TWOGAM [43] generator and the fragmentation of the hadronic system was performed with JETSET7.3 [53]. The events were thereafter processed through the full DELPHI detector simulation [54]. For the VSAT part of the events the FASTSIM [26] detector simulation was used.

4.3.1 Corrections to the VSAT data

In addition to the position and energy reconstructions, described in chapter 1, some additional corrections were applied to the VSAT data. The aim was to be able to reconstruct the angles of the electrons at the interaction point as precisely as possible. Through the

determination of these angles a measure of Q^2, which is necessary for structure function measurements can be achieved.

$$Q^2 \approx 4E_{beam}E_i' sin^2\frac{\theta}{2} \tag{4.20}$$

The reconstruction of the angles is sensitive to several parameters and a number of careful corrections had to be made in order to determine the exact position of both the VSAT modules and the interaction point.

- The position of the VSAT modules is measured in respect to each other with a precision of 200 μm at the beginning and end of each data taking year. The variations between different years are of the order of millimeters in the x and y directions, while larger variations occur in the z direction.

- By studying the sharply peaked impact point of the off-momentum electrons in the horizontal-plane, it is possible to align the y-coordinate of the modules with respect to the beam axis (see fig 2.2).

- The accurate position of the interaction point is as essential to know as the position of the VSAT modules. The angles reconstruction was corrected for the variations in the coordinates of the beam-interaction point, as recorded by the DELPHI interaction point measurements on a run by run basis.

- During 1991-1993 the spread in the relative angles of the beams was less than 100 μrad. For 1994 however the acollinearity of the beam-angles showed variations of 400 μrad with clear systematic differences between different runs (see fig. 2.5). The effect on the VSAT data is variations in the measured y-coordinate of the order of mm. This variation was also corrected for.

Angles reconstruction

Based on the determination of the energy and position of the tagged electrons after all geometrical corrections, the angles at the vertex were reconstructed. The particles are traced backwards in an iterative procedure from the detector, through the quadrupole and DELPHI solenoid magnetic fields, to the interaction point. The precision of this procedure is best for high energetic particles hitting close to the middle of the detector. The accuracy of the angles reconstruction was checked by comparing the reconstructed angles with the true angles for simulated events. Table 4.1 shows the influence of different uncertainties from the corrections on the accuracy of the angles reconstruction. The resulting precision in reconstructed Q^2 is better than ± 0.02 GeV^2/c^2.

4.3.2 Event selection

The events used for the double tag analysis are selected on the basis of requirements on both the detected hadronic system and the tagged electrons. Below follows a description of the selection of the final events used for the cross section determination.

Correction	Size	Uncertainty	$\Delta\phi$	$\Delta\theta$ (mrad)
Energy reconstruction	<5 GeV	3 GeV	1°	0.15
Geometrical survey (x,y,z)	$\approx$ 1 mm	200 μm	0.5°	0.07
Off-momentum electron position (y)	$\approx$ 1 mm	600 μm	1.5°	0.1
Interaction point correction (x)	$\approx$ 3 mm	20 μm	-	0.03
Beam angles correction	$\approx$ 200 mrad	$\approx$ 50 mrad	2.5°	0.16
Angles reconstruction procedure	-	-	8°	0.6

Table 4.1: The size of the geometrical and energy corrections applied to the VSAT part of the analysed events. In the last two columns the resulting uncertainty in ϕ and θ are given for each correction. The fluctuations of the interaction point was corrected for in the y and z direction as well, there the effect on θ and ϕ is smaller.

Run quality requirements

For the double-tag two-photon analysis the accurate running of the TPC, OD and ID is essential. These detectors are necessary for the triggering and detection of the hadronic system, which for the double tag VSAT events mainly are concentrated in the DELPHI barrel. Therefore these three detectors in addition to the VSAT were demanded to have perfect run quality status for each run in the data set used. Loser demands were applied for the rest of the DELPHI sub-detectors. Table 4.2 shows the integrated luminosity for each year after the run quality selection was made.

	1991-1992	1993	1994
Integrated Luminosity (pb^{-1})	32.3	25.5	44.1

Table 4.2: Integrated Luminosity for the data set used for the double-tag analysis.

Selection cuts

The selection of individual events is based on the following requirements

- Two electrons detected in the VSAT modules as required for double-tag studies. One of the electrons should be in the forward direction and one in the backward direction.
- More than 2 charged tracks in the DELPHI barrel or forward region. The limit of more than two tracks is set in order to eliminate the background from leptonic decays.
- In addition there were cuts on the maximum number of charged tracks, the maximum neutral energy and the maximum hadronic energy. These cuts were applied to eliminate possible background from Z^0 decays.

4.3.3 Background sources

The visible cross section for double tag events is rather low compared to the background sources. To be able to perform the analysis a good knowledge of the various background sources and a set of cuts to eliminate them are required.

Bhabha rejection

The main background source to the double-tag two-photon events are Bhabha events in the VSAT in coincidence with for example no-tag two-photon events in the DELPHI barrel. In order to reject these events from the analysis, a set of cuts for the tagged leptons were applied to the data. These cuts are customised to cut the Bhabha background as efficiently as possible, thereby taking advantage of the strict linearity and elasticity of the Bhabha scattering process.

- The extensive studies of Bhabha events provided by the luminosity analysis reveal that they are confined in a narrow region in the plane of Δx and Δy, where Δx denotes the sum in measured x coordinates for the two leptons and Δy similarly for the y coordinates (see fig. 3.3). For the true two-photon events these two quantities show uncorrelated and significantly flatter distributions.

- A cut was applied at $\leq 2 \times \sigma$ of the measured Bhabha distribution for these two quantities. The cut was applied on a fill by fill basis, since these quantities fluctuate with the specific beam-conditions (see chapter 2). Events within this region and with a measured energy in the VSAT of more than 70% of the beam energy were marked as Bhabha events and rejected (see fig. 4.6).

- In addition to the Bhabha cut a cut on the total event energy was applied, since any completely detected background event consisting of a Bhabha pair and some hadronic event, will result in a higher event energy than the beam-energy (see fig. 4.7). The upper energy cut was set at 115 GeV, due to the limited VSAT energy resolution.

Studies of Bhabha events show that the Δx-, Δy- cut, as described above, rejects 90% of the Bhabha background while the true two-photon events are not affected. Finally the cut on total energy rejects 93% of the remaining Bhabha events, while again the true two-photon events are not affected. In total the Bhabha-background is reduced with 99.3% without losing any statistics.

Single tag background

Another source of background is the coincidence between single tag two-photon events and an off-momentum electron. This background component will not be rejected by the previously described Bhabha-cut. The number of these events can however be estimated from the number of accepted events with the electrons in two forward or two backward VSAT modules. Preliminary estimates show that this background component is negligible.

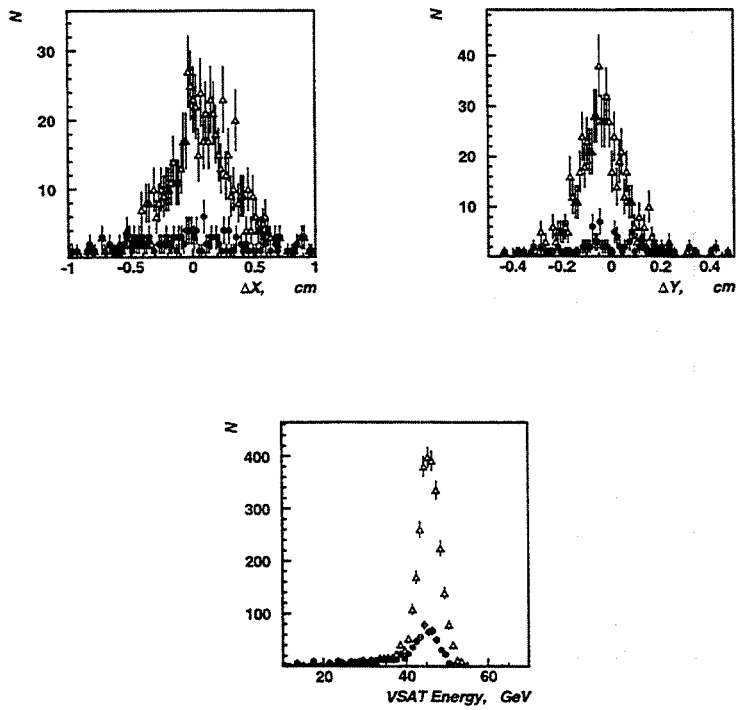

Figure 4.6: Upper left: The Δx distribution for VSAT double tag data before the Bhabha cut (triangles), compared to the same distribution after the Bhabha rejection cut (circles). Upper right: The same comparison for Δy. Bottom: Energy deposited in the VSAT for data before and after the Bhabha cut.

Leptonic background

The leptonic reactions $\gamma\gamma \to l^+l^-$ are as mentioned background to our measurement. The cut on charged tracks greater than 2, ensures that the electron and muon channels are rejected. Decays from tau pairs created in gamma-gamma collisions can give rise to more than 2 charged tracks, thereby looking like a hadronic event. From simulation studies the tau-channel can be found to be approximately 10% of the QPM-component. Since the QPM part of the events in the region of the VSAT double-tag data is very small, the tau background is negligible.

4.4 Results

The agreement between the final events and the simulated sample from the three TWOGAM components, was found to be good in all measureble quantities (see fig. 4.8).

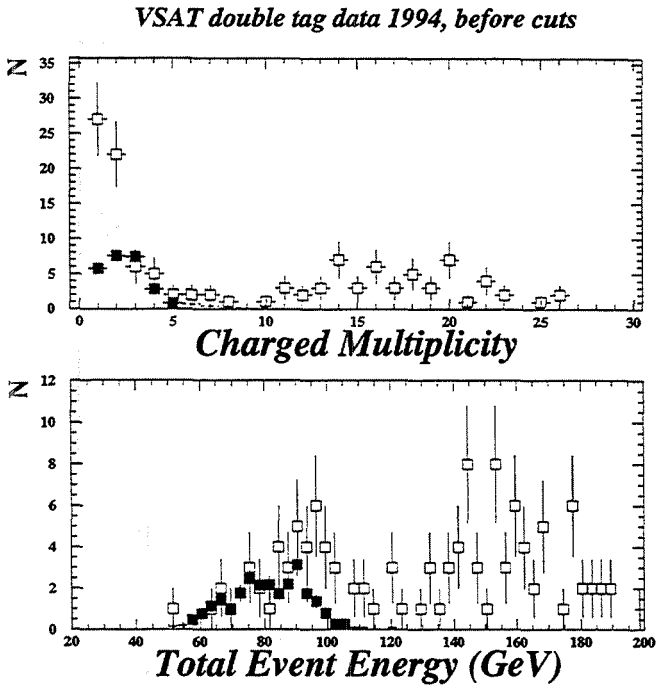

Figure 4.7: Upper: The charged multiplicity distribution for double tag data (white) and simulated events (black) before any cuts. Lower: The total event energy for data (white) and simulated events (black) before any cuts. Notice the large excess at event energies above 90 GeV in data. This originates from coincidences of Bhabha events and e.g. notag two-photon events.

The finally accepted events can be grouped into invariant-mass bins, where the invariant mass of the two-photon system is completely determined from the energy of the tagged electrons measured by the VSAT

$$W_{\gamma\gamma} = 2\sqrt{E_1^{\gamma} E_2^{\gamma}} \tag{4.21}$$

where $E_i^{\gamma} = E_i - E_i'$. The precision of the $W_{\gamma\gamma}$ determination from the VSAT is better than ± 5 GeV. In the range of $W_{\gamma\gamma} > 20$ GeV in total 26 events are found grouped in two bins. The resulting cross section of these two points can be found in table 4.4 with the statistical error. Fig. 4.9 compares the DELPHI result to previous measurements by other experiments [51] and the parametrisation of equation 4.13.

4.5 Conclusions and outlook

- The DELPHI experiment has through the study of double-tag two-photon collisions from LEP1, at an average e^+e^- center of mass energy of 91 GeV, explored the

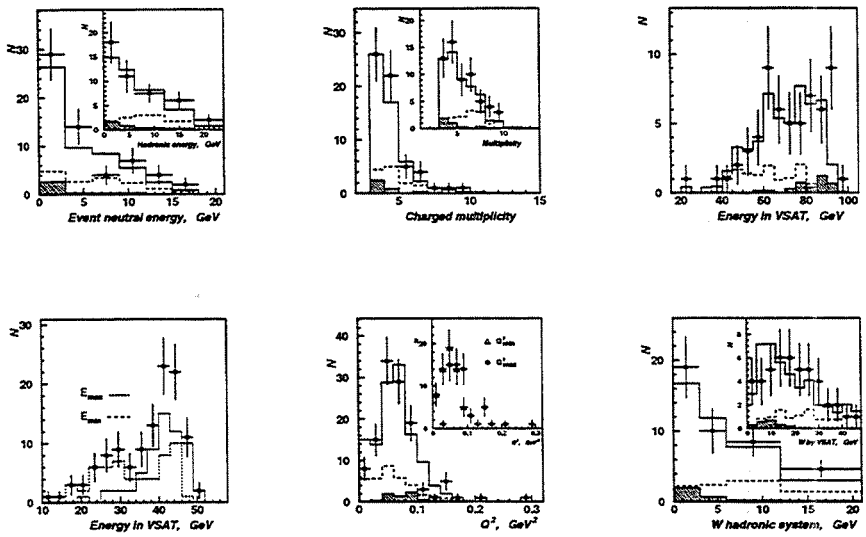

Figure 4.8: Comparison of double-tag data and Monte Carlo for various quantities. Upper left: Event energy. Upper middle: Event multiplicity. Upper right: Energy of the two tagged electrons in the VSAT. Lower left: Maximum and minimum energy in the VSAT. Lower middle: Q^2 in the VSAT. Lower right: $W_{\gamma\gamma}$ from the hadronic system and from the VSAT. Points are data, solid lines are the full VDM+QPM+QCD-RPC predictions. Dotted lines are the QPM+QCD-RPC contribution and hatched histogram is the QPM part.

behaviour of the total hadronic two-photon cross section up to invariant masses of 35 GeV.

- The resulting cross section is in agreement with theoretical predictions.
- The precision of the Very Small Angle Tagger,± 5 GeV in $W_{\gamma\gamma}$ and ± 0.02 GeV^2/c^2 in Q^2, proven in this analysis is promising for future studies of LEP2 data.

In 1998 the VSAT will be upgraded to a position closer to the beampipe [55] thereby increasing the accepted cross section for two-photon events with a factor 2. This will highly improve the measurement of the total two-photon cross section. Invariant mass energies of upto 70 GeV will be accessible for cross section studies. The aim is also to enable studies of the P^2 dependence of the photon structure function, $F_2^\gamma(x, Q^2, P^2)$ in the double-tag mode at LEP2. The STIC will then be used to tag one of the electrons measuring Q^2 while the other will be tagged by the VSAT measuring P^2. Estimates show that for 500 pb^{-1} of data at LEP2 about 800 double tag events of this kind can be expected [52]. This thesis shows that all the tools required for corrections and background rejection for this analysis are available and that both $W_{\gamma\gamma}$ and Q^2 can be measured with good precision by the VSAT.

$\sqrt{s}\ (GeV)$	$No\ of\ events$	$Total\ \sigma^{\gamma\gamma}_{Tot}\ (nb)$
25	16	356 ± 90
35	10	325 ± 105

Table 4.3: Resulting $\gamma\gamma$ hadronic cross-section from the DELPHI double tag analysis.

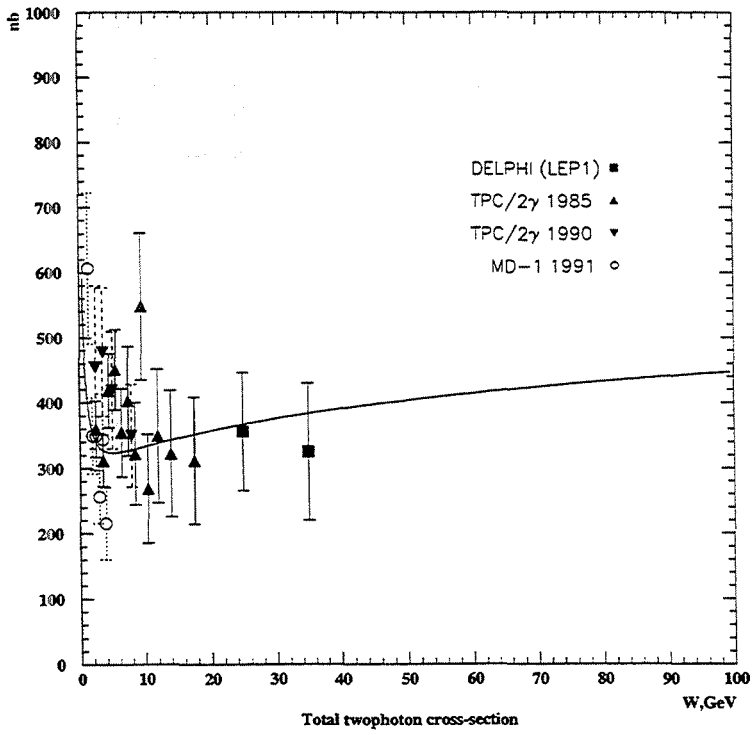

Figure 4.9: Total hadronic two-photon cross-section from the DELPHI measurement, comparedto other experiments and the Regge parametrisation (see equation 4.13).

Acknowledgement

The work in this thesis would not have been possible without the magnificent performance of the DELPHI detector. I am therefore in debt to all the people working at DELPHI. The financial support from the University of Lund is gratefully acknowledged. I would like to thank my supervisor Göran Jarlskog for his support, advice and patience during all the years needed for this work. I owe a lot to Nikolai Zimin for all the time he has spent on helping me. Working together with him has been a true pleasure. A big thanks also to Guiseppina Rinaudo for all her help and advice. Many thanks to Christina Jarlskog, Andreas Nygren, Luca Zanini, Erik Vallazza and all the others who have worked with the VSAT during the years. Everybody at the Department of Particle Physics in Lund deserves my gratitude. Ulf Mjörnmark and Henrik Carling especially for all the efforts of the minibunch upgrade and other hardware connected items. I am also in special debt to Olof, Lisa, Ivan, Göran T., Magnus L., Oxana and Ulrik for friendship and help of various kind. I am grateful to Kristina Gunne for helping me with the printing of the thesis. Finally, thanks to all my friends and family, especially Michelle. Without you this thesis would not have been possible.

Bibliography

[1] CERN, LEP the large electron-positron collider, CERN 1996.
S.Myers, Conclusions of the Sixth LEP Performance Workshop, CERN-SL-96-06-DI (1996).
S.Myers, LEP status and plans, CERN-SL-95-66-DI (1995).

[2] G.Altarelli (ed.) *et al.*, CERN 89-08(1989) Z physics at LEP1.

[3] G.Altarelli (ed.) *et al.*, CERN 96-01(1996) Physics at LEP2.

[4] DELPHI Collaboration, P.Aarnio *et al.*, Nucl. Instr. and Meth. **A303** (1991) 233.
DELPHI Collaboration, P.Abreu *et al.*, Nucl. Instr. and Meth. **A378** (1996) 57.

[5] N.Bingefors *et al.*, Nucl. Instr. and Meth. **A328** (1993) 447.
V.Chabaud *et al.*, Nucl. Instr. and Meth. **A368** (1996) 314.

[6] F.Hartjes *et al.*, Nucl. Instr. and Meth. **A256** (1987) 55.

[7] C.Brand *et al.*, Nucl. Instr. and Meth. **A283** (1989) 567.
C.Brand *et al.*, Nucl. Instr. and Meth. **A252** (1986) 413.
G.Darbo and B.W.Heck, Nucl. Instr. and Meth. **A257** (1987) 567.
O.Bärring, Thesis, Lund Univ., LUNFD6/(NFFL-7071) 1992.

[8] A.Amery *et al.*, Nucl. Instr. and Meth. **A283** (1989) 502.

[9] W.Bartl, Nucl. Instr. and Meth. **A337** (1994) 295.

[10] M.Berggren *et al.*, Nucl. Instr. and Meth. **A225** (1984) 477.
H.G.Fischer, Nucl. Instr. and Meth. **A265** (1988) 218.

[11] I.Ajinenko *et al.*, IEEE Trans. on Nucl. Science **NS-43** (1996) No.3.
O.Smirnova, Thesis, Lund Univ., LUNFD6/(NFFL-7127) 1996.

[12] P.Checcia *et al.*, Nucl. Instr. and Meth. **A248** (1986) 317.
G.Barichello *et al.*, Nucl. Instr. and Meth. **A254** (1987) 111.
P.Checcia *et al.*, Nucl. Instr. and Meth. **A275** (1989) 49.

[13] L.Bugge *et al.*, DELPHI 91-104 PHYS 147 (1991) unpublished.

[14] T.Camporesi *et al.*, CERN-PPE/92-212 (1992).
T.Camporesi *et al.*, DELPHI 97-8 PHYS 667 (1997) unpublished.
E.Falk *et al.*, DELPHI 97-60 CAL 137 (1997) unpublished.

[15] S.Almehed *et al.*, Nucl. Instr. and Meth. **A305** (1991) 320.

[16] H.Carling *et al.*, The VSAT bunch train scheme (1995) unpublished.

[17] J.Bjarne, Thesis, Lund Univ. LUNFD6/(NFFL-7089) 1994.

[18] V.Chorowicz, DELPHI 95-32 DAS 165 (1995) unpublished.

[19] F.Bianchi and I.Kronkvist, DELPHI 92-116 PROG 190 (1992) unpublished.

[20] DELPHI Collaboration, DELPHI 89-44 PROG 137 (1989) unpublished.
J.Wickens, DELPHI 95-38 PROG 213 (1995) unpublished.
J.Wickens, DELPHI 95-39 PROG 214 (1995) unpublished.

[21] G.Barbellini *et al.*, Nucl. Instr. and Meth.**A235** (1985) 55.

[22] Ch.Jarlskog, LUNFD6/(NFFL-7129) 1996.

[23] Minutes of the 6th meeting of the LEP interaction Region Working Group from August 15, 1997.

[24] S.J.Alvsvaag *et al.*, DELPHI 93-3 DAS 137 (1993) unpublished.

[25] W.J. Murray, DELPHI 96-6 PHYS (1996) unpublished.

[26] J.Cuevas *et al.*, DELPHI 87-26 PROG 71 (1987) unpublished.
I.Kronkvist, LUNFD6/(NFFL-7061)1990.
P.Jonsson, LUNFD6/(NFFL-7075)1993.

[27] G.M.Dallavalle, Review of Precision Determinations of the Accelerator Luminosity in LEP experiments, Contribution to CRAD96, August 1-5, 1996, Cracow, Poland.

[28] A.Håkansson, Thesis, Lund Univ. LUNFD6/(NFFL-7077)1993.

[29] S.Almehed *et al.*,DELPHI 92-77 PHYS 188 (1992) unpublished.

[30] F.A.Berends *et al.*, Nucl. Phys **B304** (1988) 712.

[31] S.Jadach *et al.*, Phys. Lett. **B353** (1995) 349.

[32] A.Håkansson, DELPHI 93-49 PHYS 279 (1993) unpublished.

[33] DELPHI coll., P. Abreu *et al.*, Nucl. Phys. **B367** (1991) 511.
DELPHI coll., P.Abreu *et al.*, Nucl. Phys. **B417** (1994) 3.

[34] D.Bardin *et al.*, CERN-TH 6443 (1992).

[35] R.Assmann *et al.*, CERN-PPE/95-10 (1995).

[36] V.M.Budnev *et al.*, Phys. Rep. **15C** (1975) 181.

[37] Proc. Workshop on Two-Photon Physics at LEP and HERA, Lund , Sweden, 1994, eds. G.Jarlskog, L.Jönsson.

[38] Proc. IXth International Workshop on Photon-Photon collisions, UC, San Diego, La Jolla, CA, USA, eds. D.O.Caldwell, H.P. Paar.

[39] H.Kolanoski, P.Zerwas, "Two-photon Physics", High Energy Electron-Positron Physics, eds. A.Ali, P.Söding, (1998) 695, ISBN 9971-50-260-7.

[40] I.Kronkvist, Thesis, Lund Univ. LUNFD6/(NFFL-7128) 1996.

[41] G.A.Schuler and T.Sjöstrand, CERN-TH/96-119.

[42] A.Finch, Mod. Phys. Lett. **A35**(1993)3303-3315.

[43] S.Nova *et al.*, DELPHI 90-35(1990) unpublished.

[44] DELPHI collaboration, P.Abreu *et al.*, Phys. Lett. **B342** (1995) 402.
DELPHI collaboration, P.Abreu *et al.*, Z. Phys. **C62** (1994) 357-366.
DELPHI collaboration, P.Abreu *et al.*, Z. Phys. **C69** (1996) 223-234.

[45] J.Rosner, NBL report 17522 (1972) 316.

[46] I.F.Ginzburg, V.G.Serbo, Phys.Lett. **B109** (1982) 231.

[47] S.J.Sakurai, D.Schildknecht, Phys. Lett. **B41** (1972) 489.

[48] L.E.Gordon, J.K.Storrow, MC-TH 91-29 (1991).

[49] A.Donnachie, P.V.Landshoff, Phys. Lett. **B296** (1992) 227.

[50] H1 Collaboration, Phys. Lett. **B299** (1993) 374.

[51] TPC/Two-Gamma Collaboration, H.Aihara *et al.*, Phys. Rev. **D41** (1990) 2667.
TPC/Two-Gamma Collaboration, J.C.Armitage *et al.*, Phys. Rev. Lett. 54-8 1985.
S.E.Baru *et al.*, Z. Phys. **C53** (1992) 219-224.

[52] Report on '$\gamma\gamma$ Physics' in Proc. Physics at LEP2, eds. G.Altarelli, T.Sjöstrand and F.Zwirner, CERN 96-01, Vol.1.

[53] T.Sjöstrand, JETSET 7.3 manual, CERN-TH 6488/92 (1992).

[54] DELPHI collaboration, DELPHI 89-67 PROG 142 (1989) unpublished.

[55] S.Almehed *et al.*, DELPHI 96-63 PHYS 624 (1996) unpublished.

Appendix A

Beam parameter monitoring and interaction point measurements in DELPHI with the VSAT

DELPHI Collaboration

DELPHI 94-144 PHYS 453
31 October, 1994

Beam parameter monitoring and interaction point measurement in DELPHI with the VSAT

S. Almehed [2], G. Jarlskog [2], P. Jonsson [2], F. Cossutti [4], P. Poropat [4], G. Rinaudo [3], E. Vallazza [1], L. Zanini [3]

Abstract

The measurement of the beam parameter variations during 1993 data taking, obtained by the measurements of the Very Small Angle Tagger (VSAT) luminometer, is presented; a comparison with the Micro Vertex Detector (VD) and the Time Projection Chamber (TPC) measurements of the interaction point is also shown.

[1]CERN
[2]Lund
[3]Torino
[4]Trieste

Beam parameter monitoring and interaction point measurement in DELPHI with the VSAT

October 20, 1994

S. Almehed[2], G. Jarlskog[2], P. Jonsson[2], F. Cossutti[4],

P. Poropat[4], G. Rinaudo[3], E. Vallazza[1], L. Zanini[3]

[1] *CERN*, [2] *Lund*, [3] *Torino*, [4] *Trieste*

Abstract

The measurement of the beam parameter variations during 1993 data taking, obtained by the measurements of the Very Small Angle Tagger (VSAT) luminometer, is presented; a comparison with the Micro Vertex Detector (VD) and the Time Projection Chamber (TPC) measurements of the interaction point is also shown.

1 Introduction

The Very Small Angle Tagger (VSAT) is an electromagnetic sampling calorimeter for the luminosity measurement in DELPHI. It is composed of four modules adjacent to the beam pipe, in the elliptical section located at about 7.7 m from the interaction point, downstream of the low beta superconducting quadrupoles (SCQ), two in the forward region and two in the backward region (Fig. 1).

The distance between two neighbouring modules is about 12 cm, corresponding to

the smaller beam pipe dimension in that region. The dimensions of the four calorimeters, composed of planes of silicon detectors alternated to tungsten blocks ($X_0 = 0.38$ cm), are 3 cm in the transverse horizontal direction (x), 5 cm in the vertical direction (y) and about 10 cm along the beam direction (z). The energy measurement of the shower produced inside the modules is made using the signals of 11 silicon Full Area Detectors (FAD), whereas the shower position is measured using 3 silicon strip planes, with a pitch of 1 mm, placed at 5, 7 and 9 radiation lengths (X_0). The strip planes at 5 and 9 X_0 measure the x coordinate and that at 7 X_0 measures the y coordinate. More details are given in references [1] and [2].

Since the physical process studied for the luminosity measurement is the Bhabha scattering, where electrons and positrons are emitted back to back, the trigger of the VSAT is based on the coincidence of signals in two opposite modules, that is between the modules F1-B2 (diagonal 1) or F2-B1 (diagonal 2).

Due to the very small emission angle of the bhabha events accepted in the VSAT, in spite of the restricted angular acceptance of the detector (between 5 and 7 mrad in polar angle and about 180 degrees in azimuth), the accepted bhabha cross section is very large (about 500 nb): this allows to monitor with high statistics, besides the luminosity, also the beam background and the variation of beam parameters.

The beam parameters that can be monitored to some extent by the VSAT are:

- the average values of the coordinates x_{int}, y_{int} and z_{int} of the interaction point;
- the corresponding beam widths σ_x, σ_y and σ_z;

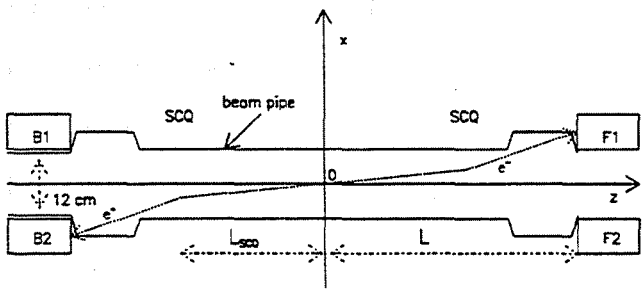

Figure 1: *Layout of the position of the VSAT modules with respect to the DELPHI origin in the (x, z) plane: the distance L_{SCQ} of the center of the SCQ from the interaction point is about 4 m, the distance L of the front of the VSAT modules from the interaction point is about 7.7 m.*

- the average values of the incident positron and electron beam directions at the interaction point, in the (x, z) and in the (y, z) planes (we will call them briefly *tilts*), respectively θ_{+x}, θ_{-x}, θ_{+y} and θ_{-y};

- the beam divergence in the two planes, that is the spread around the above average directions.

The quantities that can be measured by the VSAT are not sufficient to determine unambiguously all these parameters: we will show which information can be obtained by VSAT data alone and by the comparison of VSAT with VD and TPC measurements. We will mainly discuss measurements in the (x, z) plane, which are more important for the VSAT, and comment briefly on quantities in the other plane.

The effect of the variation of beam parameters on the quantites measured by the VSAT will be discussed in section 2. In section 3 the procedure used to obtain the information on the beam displacement from VSAT measurement will be described, as well as a comparison with the values measured by the VD and by the TPC. In section 4 the reconstruction, from VSAT, VD and TPC data, of the average evolution of the beam parameters in the fill will be discussed.

2 Beam parameters in the (x, z) plane

Limitations on the amount of information about beam parameters that can be extracted from the VSAT come from the fact that in the VSAT we cannot measure directions but only coordinates of impact points of bhabha events in the opposite modules.

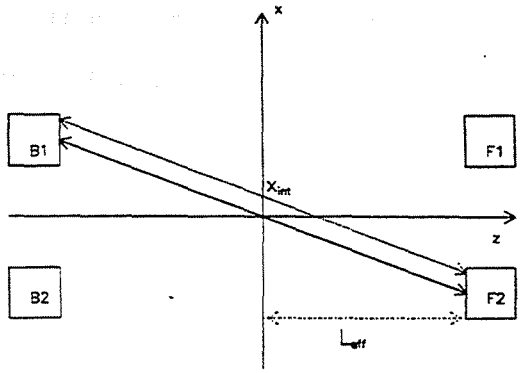

Figure 2: *Relation between the x coordinates of the impact points on opposite modules and the x position of the interaction point, x_{int}, for $x_{int} = 0$ (full line) and $x_{int} > 0$ (dotted line). The divergent effect of the SCQ is taken into account in first approximation by moving the modules to the effective distance L_{eff} (see text): this allows to represent the particle trajectories as straight lines. The scale of the x axis is magnified about 50 times with respect to that of the z axis.*

While the values of the coordinates are related to the bhabha scattering angle, their difference depends both on the coordinates and on the directions of the incident tracks at the interaction point. This is illustrated in Figs. 2, 3 and 4, where bhabha events produced by incident tracks with nominal values of the beam parameters are compared with events produced with the same emission angle but with incident tracks displaced respectively in x, z and θ_x. In all the figures the divergent effect of the SCQ is taken into account in first approximation by moving the VSAT modules to an effective distance ($L_{eff} \approx 12$ m) from the interaction point: this allows to treat the particle trajectories as straight lines.

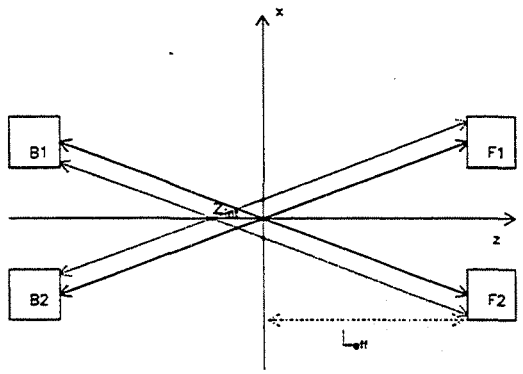

Figure 3: *Relation between the x coordinates of the impact points on opposite modules and the z position of the interaction point, for $z_{int} = 0$ (full lines) and $z_{int} < 0$ (dotted lines).*

We define the quantities:

$$\Delta x_1 = |x_{F1}| - |x_{B2}| \; ; \; \Delta x_2 = |x_{B1}| - |x_{F2}| \tag{1}$$

that is the differences between the x coordinates of the impact points of Bhabha particles on the inner module (F1 or B1) and on the outer module (F2 or B2) of the diagonal.

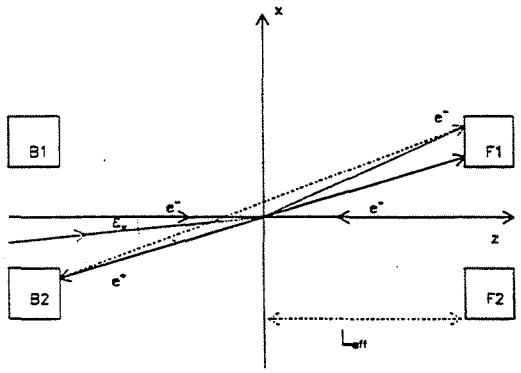

Figure 4: *Effect of the acollinearity ϵ_x on the impact point on the VSAT modules: full lines show trajectories for zero acollinearity, dotted lines for non zero acollinearity. The dot-dashed line shows an event with zero acollinearity and non zero x_{int} which has the same impact points on the VSAT modules as the one with non-zero acollinearity.*

As evident from Fig.2, a variation of x_{int} induces opposite variations of the x coordinates of the opposite modules, so that their difference Δx changes. The change is of the same sign and about of the same size in the two diagonals.

The z displacement is instead related to the difference between Δx_1 and Δx_2:

e.g., as shown in Figure 3, as z_{int} moves to negative values, Δx_1 increases and Δx_2 decreases.

Finally, a variation in the direction of any of the incident beams, has an effect very similar to that of a displacement of x_{int}. The important quantity is not the value of each tilt angle but the difference between the two tilts, that is the acollinearity ϵ_x in the (x, z) plane between the incident beams:

$$\epsilon_x = \theta_{-x} - \theta_{+x} \tag{2}$$

An example is shown in Fig.4: the same incident points in modules F1 and B2 can be obtained either with x_{int} displaced towards positive values or with a positive difference between the incident beam directions.

Since beam parameters are statistical quantities, mean values of Δx_1 and Δx_2 are calculated, averaging over the events corresponding to suitable time intervals (in this analysis we generally use the time needed to write a DELPHI cassette). From the values of Δx_1 and Δx_2 we calculate the overall average:

$$\Delta x = (\Delta x_1 + \Delta x_2)/2 \tag{3}$$

and the difference:

$$\delta = \Delta x_1 - \Delta x_2 \tag{4}$$

We will see in section 3 that, as suggested by the qualitative argument presented above, the former quantity is practically affected only by variations of x_{int} and ϵ_x, but is not affected by variations of z_{int}, while the opposite holds for the latter. In any case it

is already clear that, since we measure only two independent quantities, we can only obtain two of the three beam parameters x_{int}, z_{int} and ϵ_x.

There is a third quantity that can be measured by the VSAT and which carries informations on the tilt angles in the (x, z) plane, that is the difference in the counting rates of the two diagonals. When the average tilt angle changes, the average values of the production angles of the bhabha events accepted in the two diagonals change in an opposite way. As an example, we illustrate in Fig.5 the effect of a positive variation of both θ_{-x} and θ_{+x}: bhabha events accepted in diagonal 1 (F1-B2) have on the average a smaller production angle, compared with the case of zero tilts, while the opposite holds for the other diagonal.

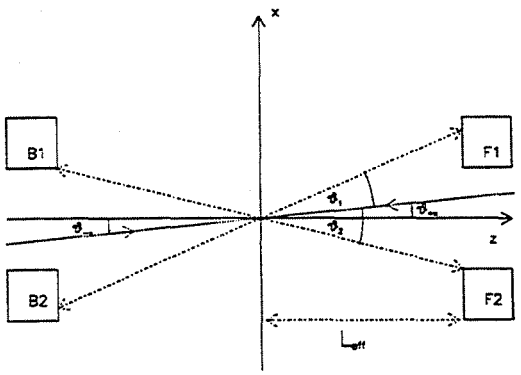

Figure 5: *Effect of positive tilt angles θ_{+x} and θ_{-x}: for the same values of the impact points on the VSAT modules, the production angle θ_1 of a bhabha event in the diagonal F1-B2 is smaller than the production angle for zero tilts of the incident beams, while the production angle θ_2 in the diagonal B1-F2 is larger than the angle for zero tilts.*

This results in a variation of the difference between the number N_1 and N_2 of accepted bhabhas in the two diagonal, due to the rapid decrease of the bhabha cross section with the angle. We monitor this through the following quantity:

$$A_D = \frac{N_1 - N_2}{N_1 + N_2} \tag{5}$$

which will be called in the following *diagonal asymmetry*. However the diagonal asymmetry is only affected by the average tilt angle:

$$\theta_x = (\theta_{-x} + \theta_{+x})/2 \tag{6}$$

and not by the separate values of θ_{-x} or θ_{+x}: therefore it cannot provide information on the acollinearity ϵ_x, which is not determined unambiguously by the average tilt.

Finally, the widths $(R\Delta x_1, R\Delta x_2)$ of the Δx_1 and Δx_2 distributions are related to the widths σ_x and σ_z of the incident beams at the interaction point and to their divergences in the (x, z) plane: the arguments are the same as presented above for the average values of the beam displacement and tilt. Due to the large distance of the VSAT from the interaction point and to the divergent effect of the SCQ, the beam divergence is the main responsible for the large $R\Delta x_1$ and $R\Delta x_2$ values: these are of the order of 3 mm, much larger than the measurement error, which is of the order of 0.3 mm.

Most of these considerations apply also to the (y, z) plane. However the measurements in this plane are less interesting for the VSAT essentially because the SCQ has a convergent in y instead of a divergent effect. As we will show, this squeezes the

trajectories in the y direction and the VSAT measurements lose sensitivity.

3 Measurement of the beam displacement

As discussed in the previous section, there are four VSAT quantities which carry information on beam parameters in the (x, z) plane, namely Δx, $(\Delta x_1 - \Delta x_2)$, $R\Delta x$ and the diagonal asymmetry.

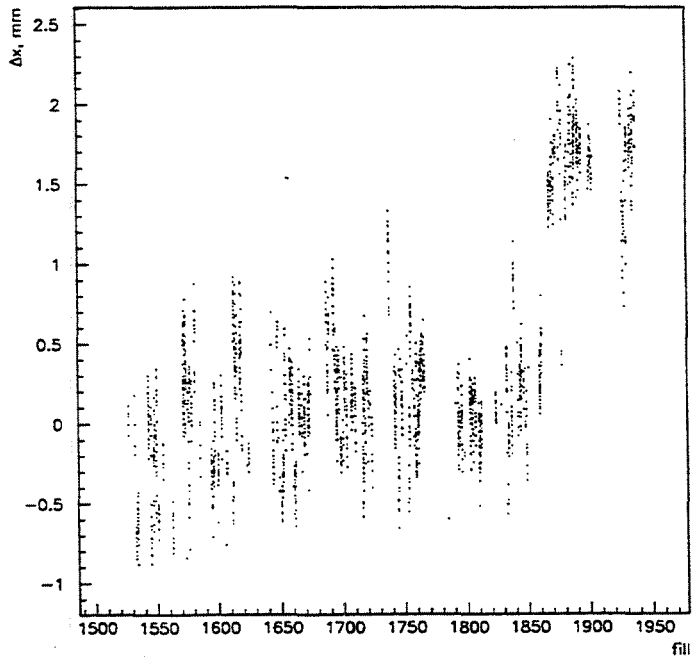

Figure 6: Δx *versus fill.*

In Fig.6 we show the variation of the average value of Δx during 1993 data taking:

each point represents the average value taken over the time needed to write a cassette. It is evident that there is a large variability inside a fill and a definite step of about 1.5 mm in the average value around fill 1870, at the beginning of LEP period 3.

The value of Δx, as seen before, can be affected both by the beam position x_{int} and by the acollinearity and the two effects cannot be disantangled. To obtain x_{int} from the measured Δx values, the effect of the superconducting quadrupole must be taken properly into account as well as the effect of the VSAT acceptance, since Δx_1 and Δx_2 represent average values of rather broad distributions, which are affected in non trivial ways by different beam parameters, such as beam width, divergence and acollinearity. This can only be done by an accurate simulation program and we used to this aim the extended simulations done to calculate the luminosity with the fast simulation program FASTSIM. We used FASTSIM runs (each run had about 40000 bhabhas) done with different x_{int} values, different beam widths, divergences and tilts.

Since we expect that the variations of the beam tilts have a minor effect, we first examine the simulations done with fixed tilts. If we also fix the values of the beam width and divergence, a linear relation is found between Δx and x_{int}:

$$\Delta x = D_0 + f_x x_{int} \tag{7}$$

For different values of the beam width or divergence, the proportionality factor f_x changes, due to the fact that the limited VSAT acceptance cuts in a different way the tails of the Δx distributions depending on the values of these parameters. Since the beam width and divergence affect the value of $R\Delta x$, we can monitor such variations by

the values of $R\Delta x$ and correct f_x directly in terms of $R\Delta x$. The dependence is weak and well fitted by the equation:

$$f_x = 4.36 \pm 0.07 - (0.35 \pm 0.02) \times R\Delta x \tag{8}$$

Taking into account the two equations, we calculated, for each cassette, the average values of x_{int} from the values of Δx and $R\Delta x$. The results are shown in Fig. 7, where x_{int} values calculated by the VSAT data are plotted versus the same variable measured by the Micro Vertex detector.

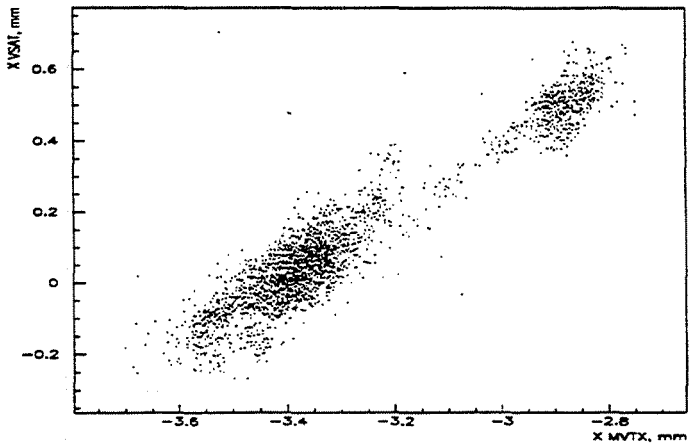

Figure 7: *x_{int} measured by VSAT in the approximation of fixed acollinearity versus the same variable measured by the VD.*

The comparison between the two sets of measurements shows a qualitative agreement within an overall shift of about 3.4 mm. In Fig.8 we plot the difference between VSAT and VD determinations of x_{int}, separately for the two periods. There is a differ-

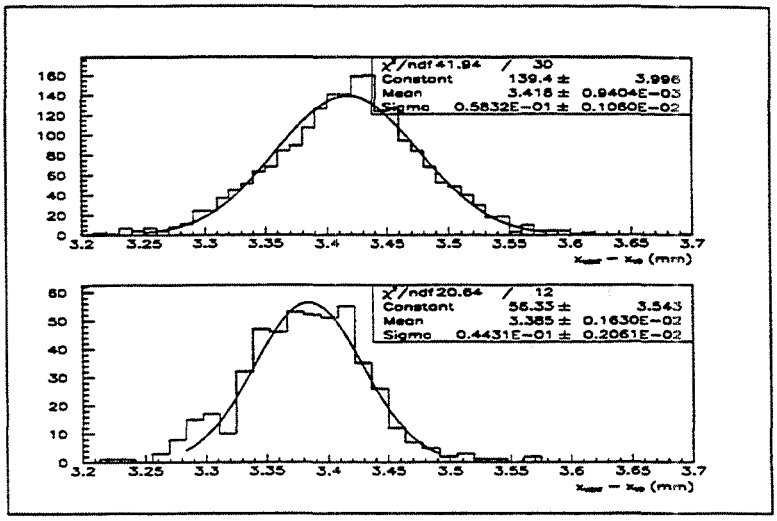

Figure 8: *Difference from the x_{int} values measured by the VSAT and by the VD, for the first two LEP periods (top) and for the last period (bottom).*

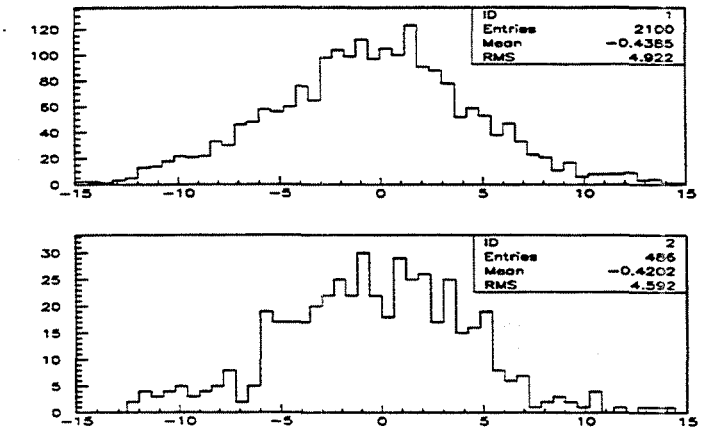

Figure 9: *Difference between the x_{int} values measured by the VSAT and by the VD, normalized to the expected errors, for the first two LEP periods (top) and the last period (bottom).*

ence of about 33 μm between the mean value of the first two periods and that of period 3, which is small compared to the overall fluctuations, but significant. The spread is better for the last period than for the previous ones (44 μm compared to 58 μm), however, also for the last period, the spread is much larger than expected from the estimated errors (about 14 μm for the VSAT and 5 μm for the VD). Indeed, the plots of the pulls for the two periods, shown in Fig.9, indicate that the average fluctuations are about five times the expected values.

This shows that the fluctuations in the acollinearity, which affect the VSAT determination of x_{int} but not that of the VD, though small, give a significant contribution. From FASTSIM simulations done for different beam tilts, we estimate that an average fluctuation in the acollinearity of the order of 15 μrad is sufficient to produce an additional error of about 40 μm in the VSAT determination of x_{int}. Also, a systematic difference in acollinearity of about 12 μrad can explain the shift in the average value determined from the VSAT data in period 3 with respect to the previous periods.

The study of the z coordinate of the interaction point, z_{int}, was carried on in a similar way. As explained in section 2, the value of z_{int} is related to the difference δ between Δx_1 and Δx_2. The relation between z_{int} and δ is much less affected by the values of $R\Delta x$ and of the acollinearity than the similar relation between x_{int} and Δx, since, in the difference, such dependences cancel out. Therefore a simple proportionality law between the two quantities was used.

In Fig.10 the variation of z_{int} determined from VSAT data during 1993 is shown: no step corresponding to the start of period 3 is visible. In Fig.11, the difference

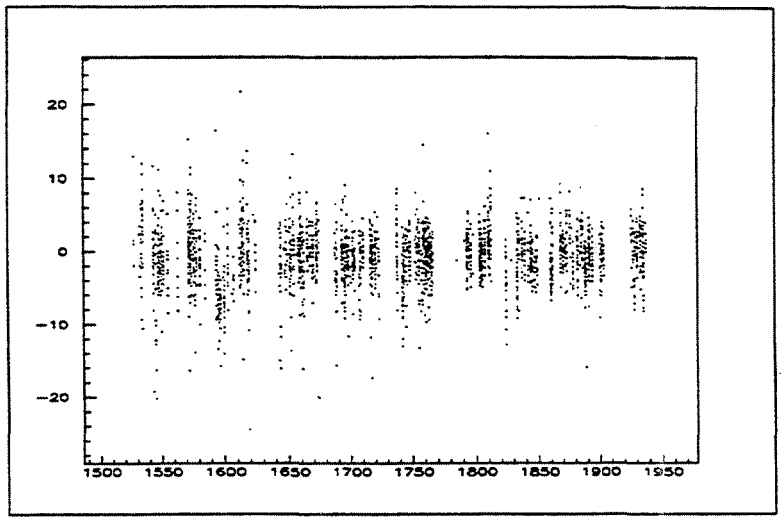

Figure 10: *z_{int} determined by VSAT versus the fill number.*

between VSAT and TPC determinations of z_{int} is shown. There is a systematic shift of about 5 mm, but the agreement is good and the spread is close to the expected value, as confirmed by Fig. 12, where the distribution of the pulls is shown. No significant difference in the mean values between period 3 and the first two periods is observed.

The agreement between VSAT and TPC values confirms the validity of neglecting the effect of variations of $R\Delta x$ and ϵ_x in the determination of z_{int}, at least within the present experimental uncertainties.

We finally comment briefly on the measurement of the y coordinate of the interaction point. The y_{int} determination with the VSAT is in principle similar to the x_{int} measure. However, as mentioned above, the trajectories of the Bhabha electrons are squeezed in the (y, z) plane by the converging effect of the SCQ: as a consequence,

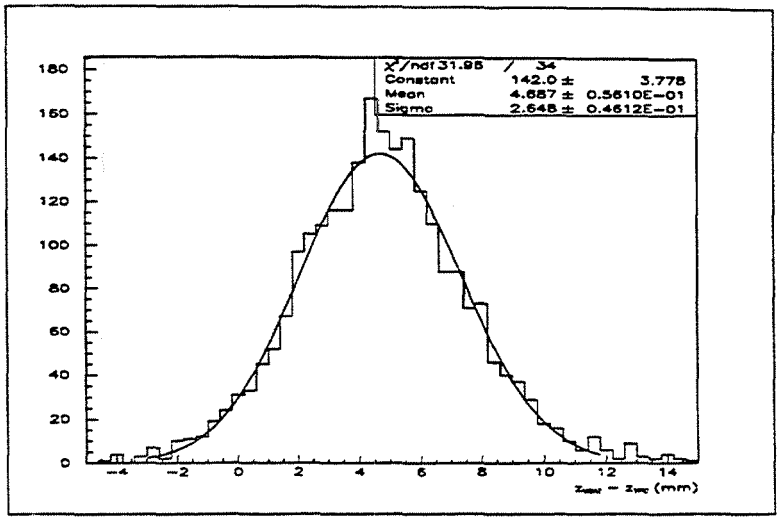

Figure 11: *Difference between the z_{int} determination of the VSAT and z_{int} measured by the TPC.*

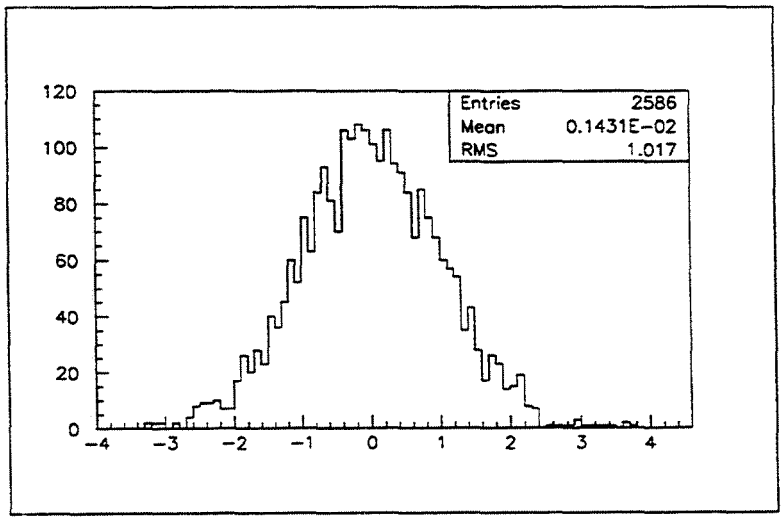

Figure 12: *Pull of the z_{int} values measured by the VSAT and TPC.*

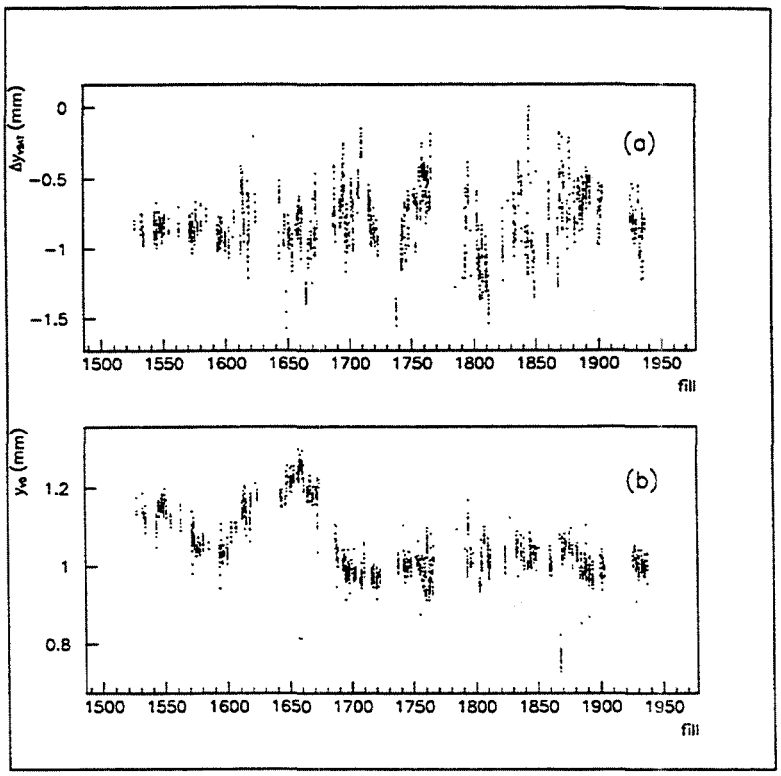

Figure 13: *b) Δy measured by the VSAT versus the fill; b) y_{int} measured by the Micro Vertex detector versus the fill.*

the VSAT sees reduced variations with respect to the real changes of y displacement. Besides, an acollinearity effect is present also in the (y, z) plane, probably larger than the effect in the (x, z) plane due to the larger variability of the tilts in this plane. The combination of the two effects accounts for the lack of correlation between the VSAT and the Micro Vertex measures of y_{int}, evident from the comparison of Fig. 13a and Fig. 13b.

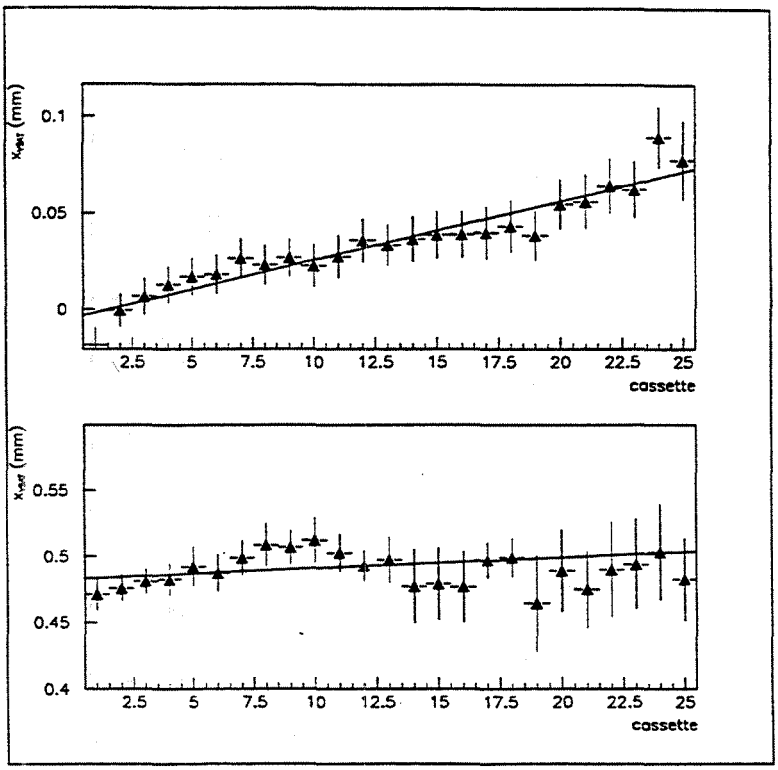

Figure 14: x_{int} *measured by the VSAT versus the progressive cassette number from the start of the fill: top, for the first periods, bottom for period 3.*

4 Variations of the beam parameters during the fill

With the combined VSAT, VD and TPC data, the systematic variations of the beam parameters during the fill lifetime could be studied. The time unit used is again the *cassette*, which corresponds to a time of the order of 20 minutes.

In Fig. 14 we show the variation of x_{int} as measured by the VSAT as a function of the progressive cassette number from the start of the fill (top for the first periods,

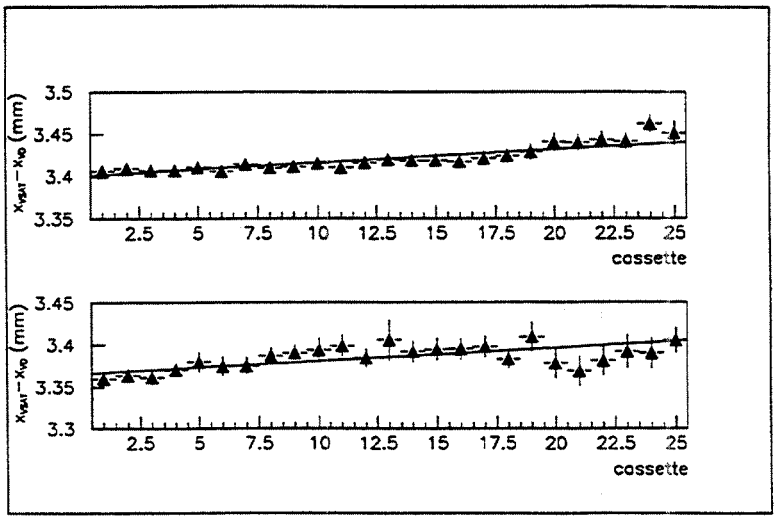

Figure 15: *Difference between x_{int} measured by the VSAT and by VD versus the progressive cassette number from the start of the fill: top, for the first periods, bottom for period 3.*

bottom for period 3). One notices that for the first periods there is an average small systematic shift of x_{int} of the order of 80 μm towards the center of LEP ring from the start to the end of the fill, while there is practically no shift for period 3.

To check wether the shift is due to a real shift of the interaction point or it is a side effect of a variation of the beam acollinearity, we plot in Fig. 15 the difference between the average values determined by the VSAT and the VD: apparently about half of the shift of the first periods might indeed be due to an acollinearity effect. Under this hypothesis, the corresponding variations in acollinearity are of the order of 15 μrad, that is of a quantity close to that expected from the analysis done in section 2 of the spread of the x_{int} difference between VSAT and VD.

No systematic shift is visible in z_{int}, while there is a trend in y_{int}, as shown in

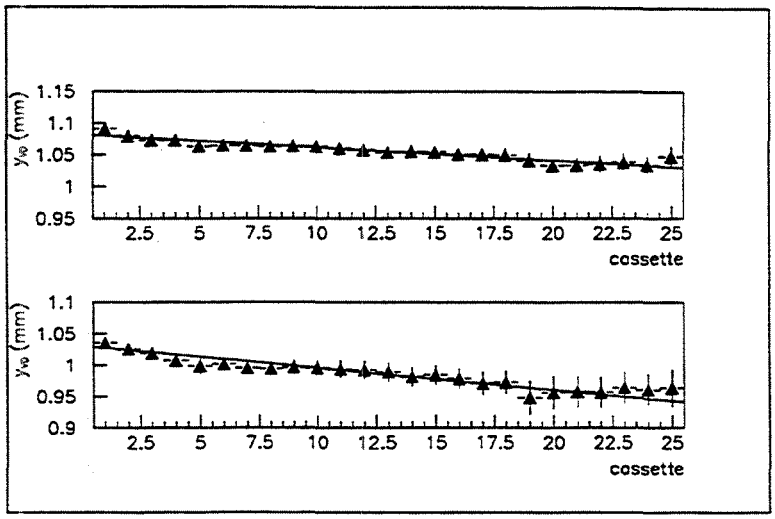

Figure 16: *y_{int} measured by the VD versus the progressive cassette number from the start of the fill: top, for the first periods, bottom for period 3.*

Fig. 16, where the VD data were used, since the resolution in y_{int} of the VSAT data is too poor.

The study of the variations of the counting rate asymmetry A_D between the two diagonal arms of the VSAT during the fill gives indications of possible trends in the variations of the average tilt of the incident beams. Significant variations, of the order of 1%, between the start and the end of the fill are observed (see Fig. 17), which correspond, from FASTSIM studies, to variations of the order of 20 μrad in the average tilt.

Finally, the variations of $R\Delta x$ inside the fill (Figure 18), show a decrease of about 400 μm from the start to the end of the fill. This is expected from the reduction of the beam divergence during the fill which is a consequence of the cooling precedure applied

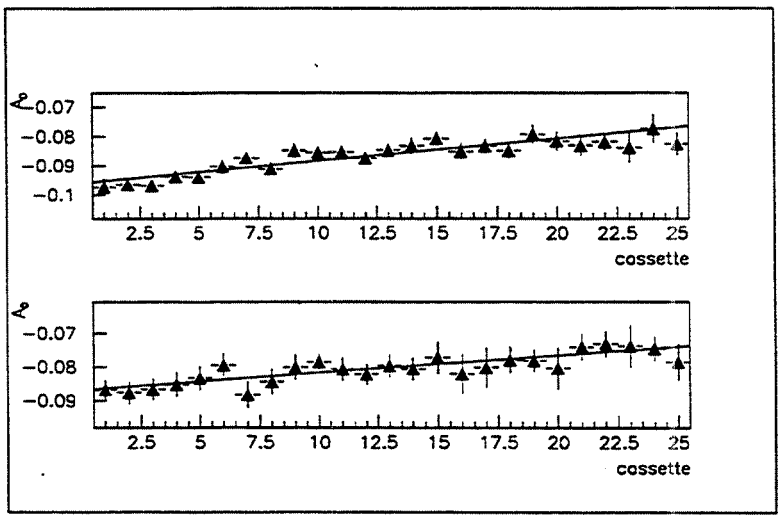

Figure 17: *Counting rate asymmetry A_D between the two diagonal arms of the VSAT versus the progressive cassette number from the start of the fill: top, for the first periods, bottom for period 3.*

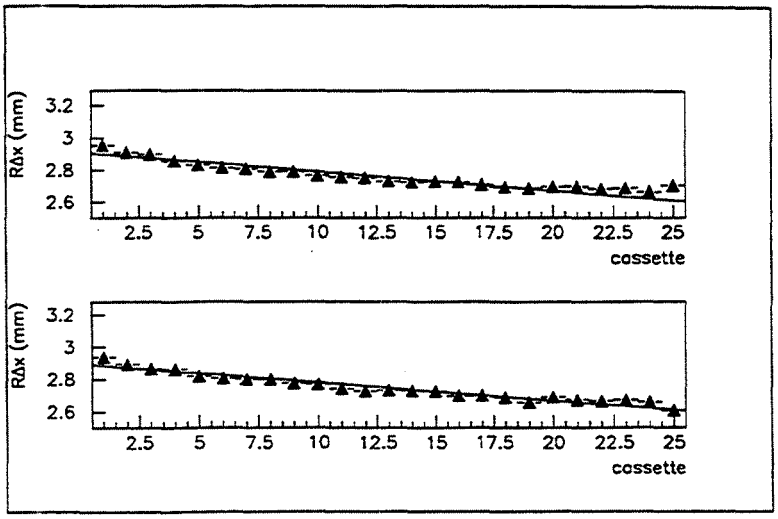

Figure 18: *Variation of the $R\Delta x$ as a function of the progressive cassette number from the start of the fill: top, for the first periods, bottom for period 3.*

to the beams, after reaching stable conditions.

References

[1] Almehed et al., *A silicon tungsten electromagnetic calorimeter for LEP*, **NIM A305 (1991) 320.**

[2] Almehed et al. *High precision relative luminosity measurement with a Very Small Angle Tagger (VSAT) in DELPHI*, **DELPHI 92-77 PHYS 188.**

Appendix B

Measurements of the beam parameter variations in DELPHI with the VSAT

DELPHI Collaboration

DELPHI 95-150 LEDI 2
27 September, 1995

Measurement of the beam parameter variations in DELPHI with the VSAT

S. Almehed[1], F. Cossutti[2], Ch. Jarlskog[1], G. Jarlskog[1], P. Jonsson[1], P. Poropat[2], G. Rinaudo[3], E. Vallazza[4]

Abstract

The beam parameter variation during 1994 data taking, obtained by the measurements of the Very Small Tagger (VSAT) luminometer, are presented; a comparison with 1993 data is shown.

[1]Lund
[2]Trieste
[3]Torino
[4]CERN

Contents

1 Introduction

The Very Small Angle Tagger (VSAT) is an electromagnetic sampling calorimeter for the luminosity measurement in DELPHI. It consists of four rectangular modules placed symmetrically at about 7.7 m from the DELPHI origin, around a short elliptical section of the beam pipe behind the low beta superconducting quadrupoles (SCQ) as shown in fig. 1. The distance between two neighbouring modules is about 12 cm, corresponding to the smaller beam pipe dimension in that region. Since the physical process studied for the luminosity measurement is the Bhabha scattering, where electrons and positrons are emitted back to back, we use the coincidences of signals between a module in the forward region and a module in the backward region, thus defining two diagonals for the trigger: diagonal 1 (modules F1-B2) and diagonal 2 (modules F2-B1).

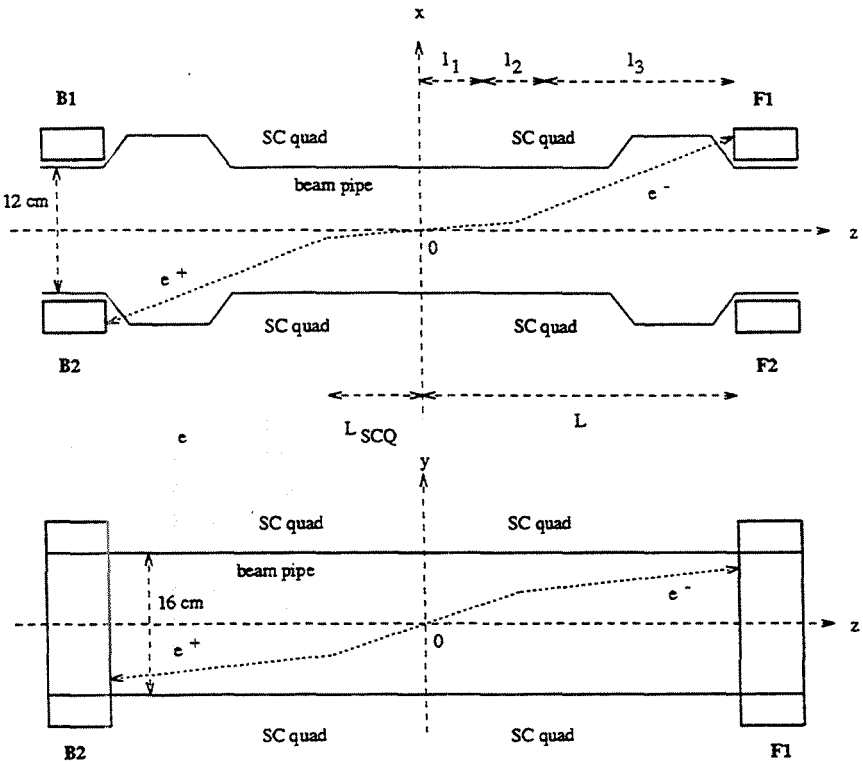

Figure 1: *Layout of the position of the VSAT modules in the (x,z) and (y,z) planes: the distance L_{SCQ} of the center of the superconducting quadrupoles from the DELPHI origin is about 4 m and the distance L of the front of the VSAT modules is about 7.7 m; the distances l_1, l_2 and l_3 define the three regions relevant to the beamspot equations.*

Each VSAT module contains 12 tungsten absorbers ($X_0 = 0.38$ cm) interspaced with 12 silicon planes (Full Area Detectors, (FAD)) for energy measurement (fig. 2). The

dimensions of the calorimeters are 3 cm in the transverse horizontal direction (x), 5 cm in the vertical direction (y) and 24 radiation lengths (about 10 cm) along the beam direction (z). The center of the electromagnetic shower is given by three silicon strip planes with 1 mm pitch placed close to the shower maximum at 5, 7 and 9 X_0; the second plane is used for the y coordinate measurement and the other two planes for the x coordinate measurement. More details are given in references [1], [2], [3] and [4].

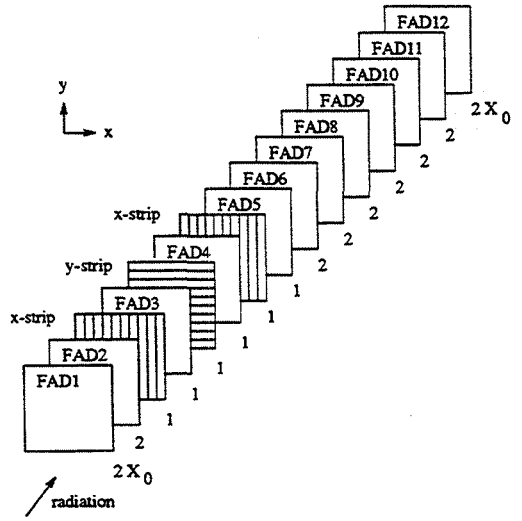

Figure 2: *Layout of the VSAT modules.*

Due to the very small emission angle of the Bhabha events accepted in the VSAT, in spite of the restricted angular acceptance of the detector (between 5 and 7 mrad in polar angle and about 50 degrees in azimuth), the accepted Bhabha cross section is very large (about 500 nb): this allows to monitor with high statistics, besides the luminosity, also the beam background and the variation of beam parameters.

The effect of the variation of beam parameters on the quantites measured by the VSAT will be discussed in section 2. In section 3, the procedure used to obtain the information on the beam parameters will be described and their variation during 1994 will be discussed.

2 Beam parameters monitoring with the VSAT

The beam parameters that are relevant for the following discussion are:

- the average values of the coordinates x_b, y_b and z_b of the interaction point;
- the corresponding beam widths σ_x, σ_y and σ_z;
- the average values of the incident positron and electron beam directions at the interaction point, in the (x,z) and in the (y,z) planes (we will call them briefly *tilts*), respectively θ^x_+, θ^x_-, θ^y_+ and θ^y_-;

- the beam divergence in the two planes, that is the spread around the above average directions.

The quantities measured with the VSAT which are used to extract information on the beam parameters are the x and y coordinates of the impact points of the scattered leptons on the four modules, while their directions cannot be measured. In the following two sections, we will discuss the dependence on the beam parameters of such coordinates.

2.1 Beam parameters in the (x,z) plane

The transport of the positron and the electron from the interaction point to the VSAT module is given by the product of three matrices which describe the trajectory in the three relevant regions shown in fig. 1:

- region 1, of length l_1, from the interaction point to the superconducting quadrupole in the DELPHI solenoid;
- region 2, of length l_2, through the superconducting quadrupole;
- region 3, of length l_3, from the superconducting quadrupole to the VSAT module.

Since the effect of the DELPHI solenoid is completely negligible for the Bhabha electrons in the VSAT, trajectories in region 1, as well as 3, are straight lines and the resulting equations between initial and final coordinates and directions are linear. Explicitly, the x coordinates of the impact points on the four VSAT modules are:

$$\begin{aligned} x_{F1} &= f_x(x_b - z_b(\theta_1^x + \theta_-^x)) + l_x(\theta_1^x + \theta_-^x) \qquad & x_{B2} &= f_x(x_b - z_b(\theta_1^x + \theta_+^x)) - l_x(\theta_1^x + \theta_+^x) \\ x_{B1} &= f_x(x_b + z_b(\theta_2^x - \theta_+^x)) + l_x(\theta_2^x - \theta_+^x) \qquad & x_{F2} &= f_x(x_b + z_b(\theta_2^x - \theta_-^x)) - l_x(\theta_2^x - \theta_-^x) \end{aligned} \tag{1}$$

where x_b, z_b are the x and z coordinates of the interaction point, θ_1^x and θ_2^x are the production angles in diagonal 1 and 2, respectively (always assumed to be positive) and θ_+^x (θ_-^x) is the tilt angles in the (x,z) plane of the incident positron (electron). The coefficients f_x and l_x are functions of the lengths l_1, l_2 and l_3 of the three regions and of the "k-factor" of the superconducting quadrupoles. For the values of 1993 and 1994 periods, their values are:

$$f_x = 2.1 \pm 0.1 \qquad l_x = (12.60 \pm 0.02)m \tag{2}$$

essentially equal for the four modules. Eqs. (1) show that particle trajectories can be treated as straight lines by assuming the modules to be located at an effective distance, l_x, from the center of DELPHI (z_b=0). Fig. 3 illustrates different situations, corresponding to one or more of the four beam parameters (x_b, z_b, θ_+^x, θ_-^x) being different from zero.

From eqs. (1), we see that it is convenient to use the quantities:

$$\begin{aligned} \Delta x_1 &= x_{F1} + x_{B2} = 2 \cdot f_x(x_b - z_b(\theta_1^x + \theta_x)) + \epsilon_x l_x \\ \Delta x_2 &= x_{F2} + x_{B1} = 2 \cdot f_x(x_b + z_b(\theta_2^x - \theta_x)) + \epsilon_x l_x \end{aligned} \tag{3}$$

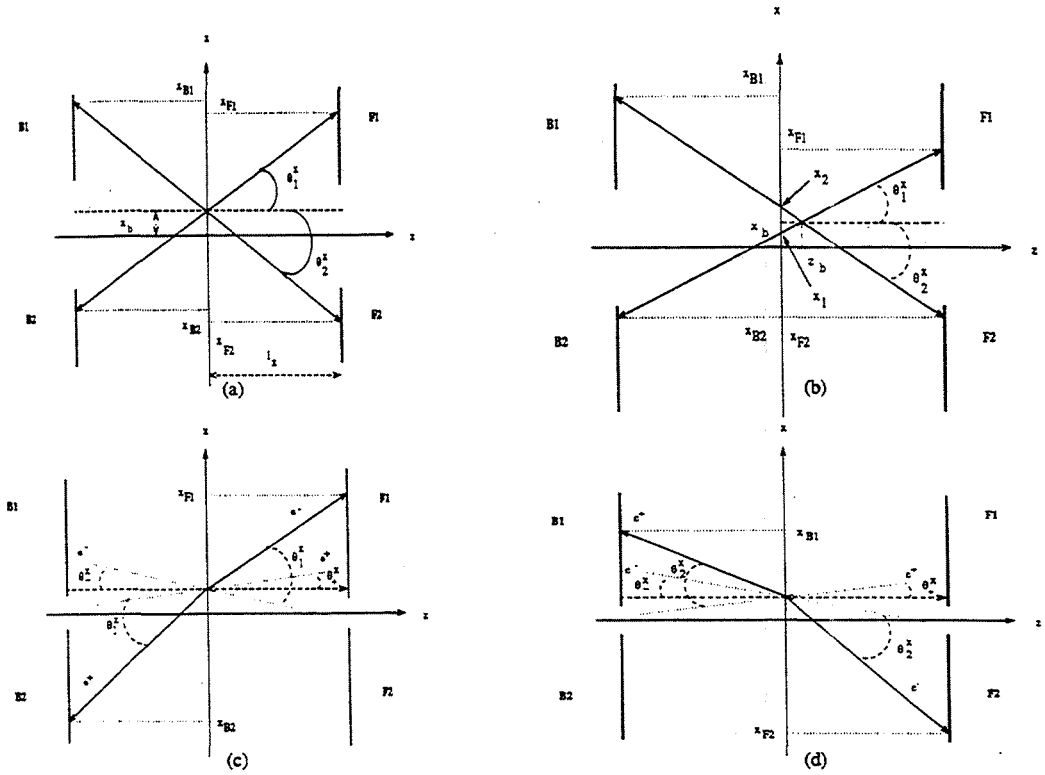

Figure 3: *(a) events with positive x displacement, zero z displacement and zero tilts; (b) events with the same values of x displacement and tilts but with a positive displacement in z; events for which only the z displacement is zero, in diagonal 1 (c) and in diagonal 2 (d).*

where we have defined the average tilt, θ_x, and the acollinearity, ϵ_x, as follows

$$\theta_x = \frac{\theta_+^x + \theta_-^x}{2} \qquad \epsilon_x = \theta_-^x - \theta_+^x \tag{4}$$

Eqs. (3) evidentiate the similarity of the x_b and ϵ_x effects on the impact points. This is more clearly depicted in fig. 4, where we have assumed for simplicity that only the electron beam has a nonzero tilt: the full lines correspond to outgoing particle tracks for $x_b = \theta_-^x = \theta_+^x = 0$, whereas the dotted line shows the case of nonzero acollinearity and x_b=0 and the dashed line shows an event with zero acollinearity but nonzero x_b, which has the same impact points on the modules, showing that the ϵ_x and x_b effects are equivalent, and therefore these two parameters cannot be determined separately using the VSAT information alone.

To better separate the dependence on different beam parameters, we define the following quantities:

$$\Delta x = \frac{\Delta x_1 + \Delta x_2}{2} = 2 \cdot f_x x_b + \epsilon_x l_x + f_x z_b(\theta_2^x - \theta_1^x - 2\theta_x) \tag{5}$$

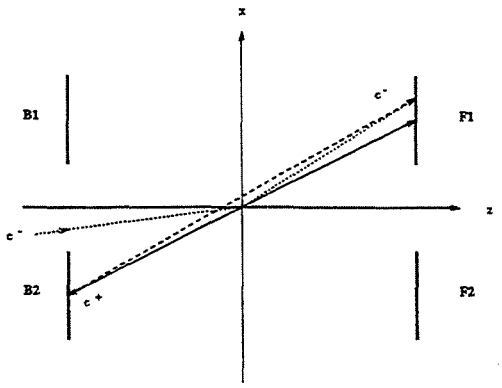

Figure 4: *Effects of the acollinearity and the x displacement on the impact points.*

$$\delta x = \Delta x_2 - \Delta x_1 = 2 \cdot f_x z_b (\theta_1^x + \theta_2^x) \tag{6}$$

By taking the average over a reasonably long period of time (we usually assume the time needed to write a cassette, which is about 20 minutes and corresponds to about 4 K events), we can substitute to θ_1^x and θ_2^x their average values, $\overline{\theta_i^x}$, which are both very close to 5.5 mrad. The equations show that the average value of the δx distribution essentially depends only on the value of z_b. On the contrary, the average value of the Δx distribution essentially measures the combined effect of the beam x displacement and beam acollinearity in the (x,z) plane, since the third term in eq. (5) is completely negligible.

From eq. (5) it also follows that the dispersion $\sigma_{\Delta x}$ of the Δx distribution is related to the dispersion of the distribution of x_b and ϵ_x, i.e. to the beam parameters σ_x and σ_{θ_x}:

$$\sigma_{\Delta x} = 2\, f_x\, \sigma_x + l_x\, \sigma_{\theta_x} + \sigma_m \tag{7}$$

where σ_m is the measurement error on Δx. The first and the third term are small compared to the middle one and are also rather well known, thus $\sigma_{\Delta x}$ can be used to measure the beam divergence, σ_{θ_x}.

However, due to the limited VSAT acceptance, the averaging procedure introduces second order dependences on the beam parameters, which can only be evaluated by an appropriate Monte Carlo simulation. We used to this aim the extensive simulations of different beam conditions which were done with the fast simulation program FASTSIM to determine the VSAT acceptance of Bhabha events for the measure of the luminosity (details of the program are found in [2]). Two major dependences are found: on σ_x and σ_{θ_x}, i.e. on the widths of the x_b and ϵ_x distributions and on the y tilt. Fortunately, both such dependences can be parametrized in terms of quantities directly measured by the VSAT, the former by $\sigma_{\Delta x}$ and the latter by the quantity Δy, which will be introduced below. The resulting corrections to Δx and δx are small and linear. Also, all the effective parameters of eq. (5) and (6), such as f_x and l_x, have been calculated with FASTSIM.

There are two other useful measures that can be done with the VSAT and which are related to the beam tilts. With a view to this, it is helpful to consider events with equal

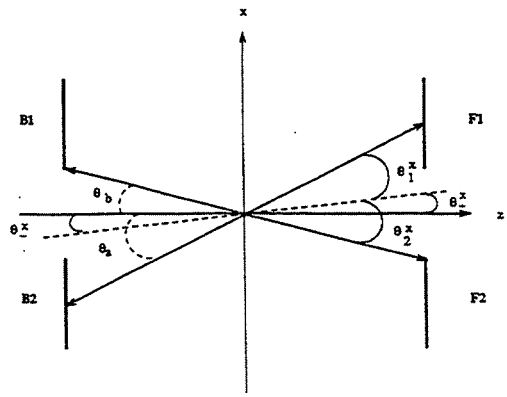

Figure 5: *Effect of the beam tilts on the production angles on the two diagonals.*

(positive) beam tilt angles, θ^x_+ and θ^x_-, as in fig. 5. The figure shows clearly that for the same values of the impact points the production angle on diagonal 1, θ^x_1, is smaller than in the case of zero tilts, where it would be equal to θ_a, while the opposite holds for the production angle on diagonal 2 (θ^x_2 is larger than θ_b). Due to the rapid decrease of the Bhabha cross section with the angle, this induces an opposite variation of the number of accepted Bhabha events on the two diagonals: the number of events on diagonal 1, N_1, will increase, whereas the number of events on diagonal 2, N_2, will decrease. Therefore, we expect to observe a variation of the variable:

$$A_D = \frac{N_1 - N_2}{N_1 + N_2} \tag{8}$$

called *diagonal asymmetry*. It must be noted, however, that the diagonal asymmetry is only affected by the average tilt angle, θ_x, and not by the separate values of θ^x_- and θ^x_+. By consequence, it cannot be used to extract information on the acollinearity, ϵ_x. The relationship between A_D and θ_x has been evaluated by FASTSIM.

2.2 Beam parameters in the (y,z) plane

The transport equations in the (y,z) plane are very similar to those of the (x,z) plane:

$$\begin{aligned} y_{F1} &= f_y(y_b - z_b(\theta^y_1 + \theta^y_-)) + l_y(\theta^y_1 + \theta^y_-) \qquad & y_{B2} &= f_y(y_b - z_b(\theta^y_1 + \theta^y_+)) - l_y(\theta^y_1 + \theta^y_+) \\ y_{B1} &= f_y(y_b + z_b(\theta^y_2 - \theta^y_+)) + l_y(\theta^y_2 - \theta^y_+) \qquad & y_{F2} &= f_y(y_b + z_b(\theta^y_2 - \theta^y_-)) - l_y(\theta^y_2 - \theta^y_-) \end{aligned} \tag{9}$$

There are however two important differences with respect to the (x,z) plane. The first difference is due to the fact that in the y direction the superconducting quadrupoles have a convergent effect, opposed to the divergent effect in the other plane. This gives values for the f_y and l_y parameters which are much smaller than those of the corresponding parameters in the (x,z) plane:

$$f_y = 0.10 \pm 0.02 \qquad l_y = (3.50 \pm 0.02)m \tag{10}$$

In particular, because of the small value of f_y, VSAT measures in the (y,z) plane are practically insensitive to the values of y_b and z_b. The second difference is the small angle of the production angles θ_1^y and θ_2^y, which average to zero.

We define

$$\Delta y_1 = y_{F1} + y_{B2} \qquad \Delta y_2 = y_{F2} + y_{B1} \tag{11}$$

and

$$\Delta y = \frac{\Delta y_1 + \Delta y_2}{2} \tag{12}$$

Taking the average value over one cassette, we obtain

$$\Delta y = 2 f_y y_b + l_y \epsilon_y \tag{13}$$

where we have defined the average acollinearity, ϵ_y, in a similar way as for the (x,z) plane.

Information on the average tilt

$$\theta_y = \frac{\theta_+^y + \theta_-^y}{2} \tag{14}$$

is provided by the difference

$$y_{F1} - y_{B2} \approx y_{F2} - y_{B1} \approx 2\, l_y\, \theta_y \tag{15}$$

We point out that a similar measure is in principle possible also in the (x,z) plane to obtain the value of θ_x, however, due to the narrow acceptance of the VSAT calorimeters, fluctuations in the average production angle completely mask possible effects of θ_x: for this reason in the (x,z) plane we use the diagonal asymmetry, A_D, which provides a much better measure of θ_x.

Finally, the width, $\sigma_{\Delta y}$, of the Δy distribution can be used to obtain the y divergence, σ_{θ_y}, of the beams.

3 Variation of the beam parameters

From VSAT data alone we can estimate the z coordinate of the interaction point using eq. (6), but this is not possible neither for the x nor for the y coordinate. This is due to the fact that, as shown in eq. (5) and (13), the detector variables depend both on the beam displacement and on the acollinearity in those directions. However, we can use eqs. (5) and (13) together with the beamspot values for x and y as they are determined by VD and TPC to obtain information on the variations of acollinearity.

3.1 Estimation of z beamspot

From eq. (6), we have

$$z_b = \frac{\delta x}{2 f_x (\theta_1^x + \theta_2^x)} \tag{16}$$

where δx has been corrected for second order dependence on beam parameters as explained in section 2. The sum of the production angles can be derived from the expressions of the impact points, eq. (1), as follows:

$$\theta_1^x + \theta_2^x = \frac{x_{F1} - x_{B2} - x_{F2} + x_{B1}}{2 \cdot l_x} \tag{17}$$

The distribution of z_b during 1994 is given in fig. 6. We observe an increase by 3 mm during period 1, a decrease of 1 mm during period 3 and small variations in period 2.

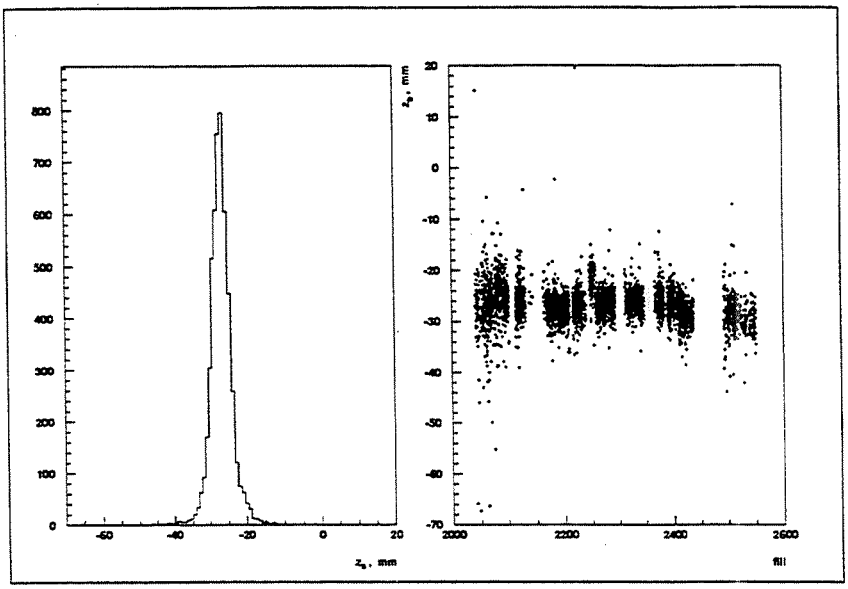

Figure 6: *z beamspot from* Δx_1 *and* Δx_2.

In fig. 7, we have plotted the VSAT versus the TPC measurement for the z beamspot.

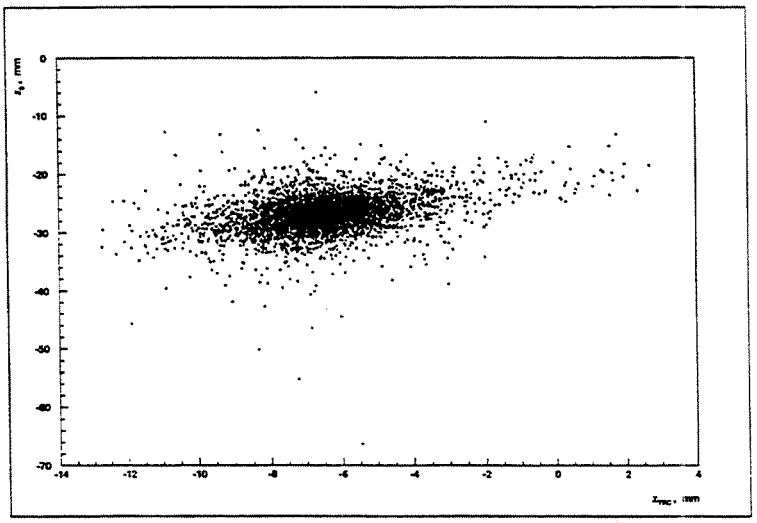

Figure 7: z_b *from VSAT versus* z_{TPC}.

In spite of the much larger error in the VSAT determination, We discern a linear relation, which is seen more clearly in the profile plot of fig. 8. The offset between the two measurements is of the order of 20 mm.

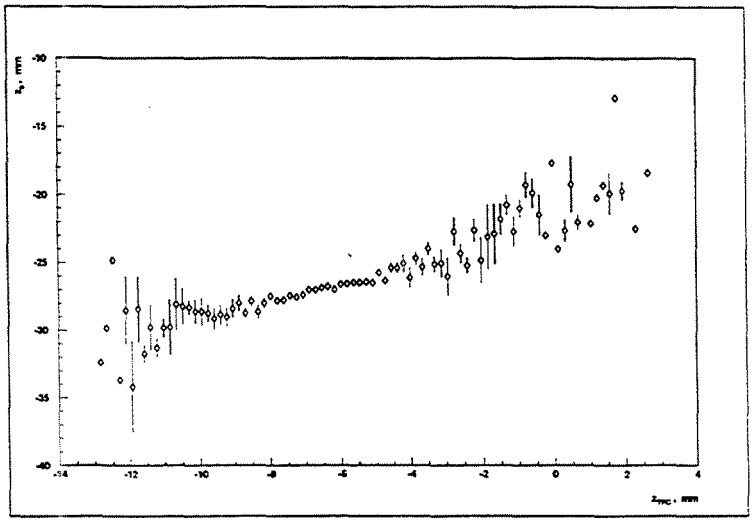

Figure 8: *Correlation between z_b and z_{TPC}, 1994 data.*

The distributions of the pulls of the VSAT and TPC determinations for all 1994 data and for the three periods are given in fig. 9 and 10, respectively and show that our

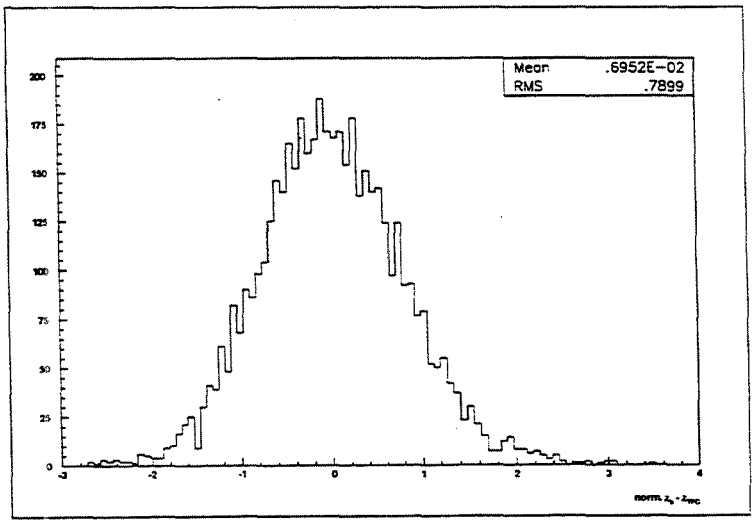

Figure 9: *Normalized difference between z_b and z_{TPC} for all 1994 data.*

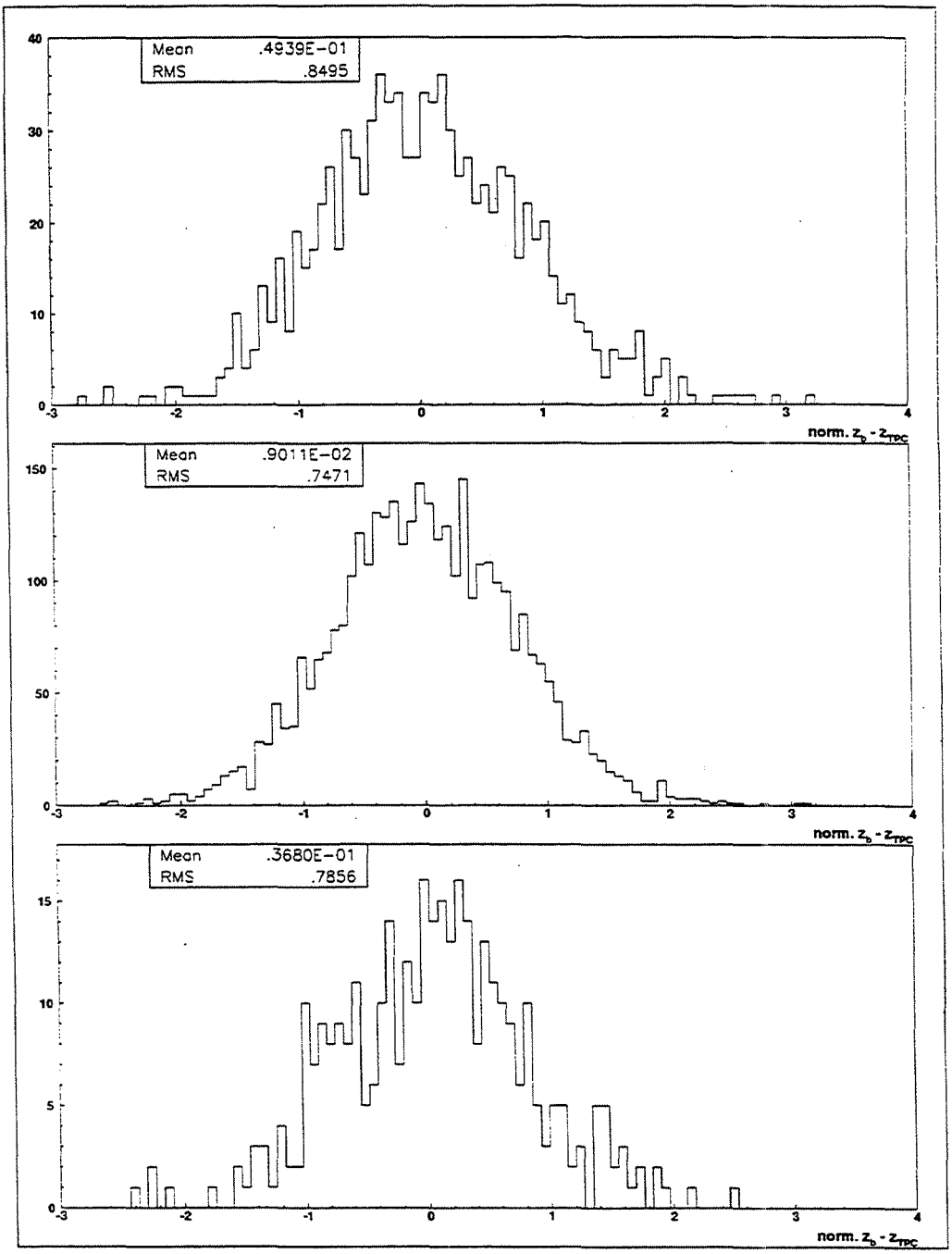

Figure 10: *Normalized difference between z_b and z_{TPC}, 1994 data, periods 1, 2 and 3.*

determination of z_b is compatible within errors with the TPC measure. The distributions of z_b for 1993 data and the corresponding difference from TPC are shown in figs. 11 and 12.

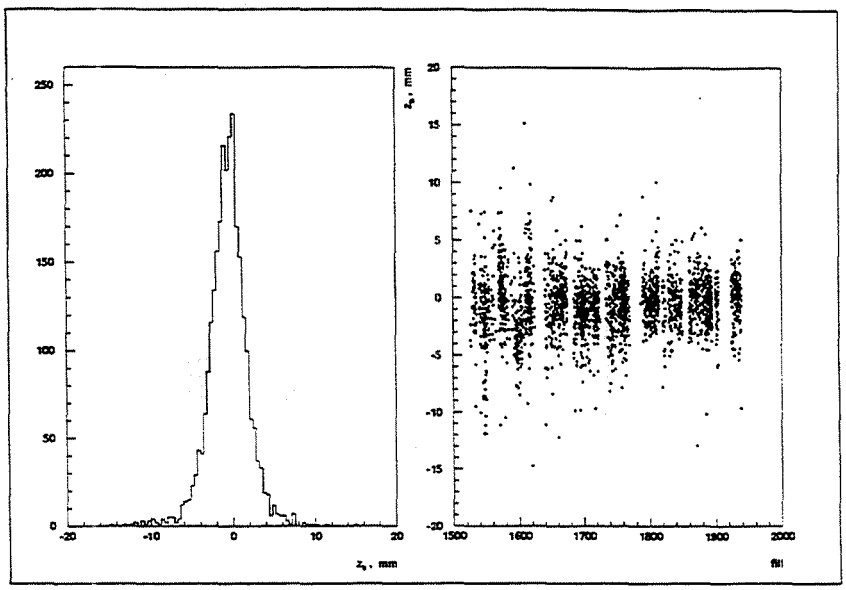

Figure 11: *z_b from 1993 data.*

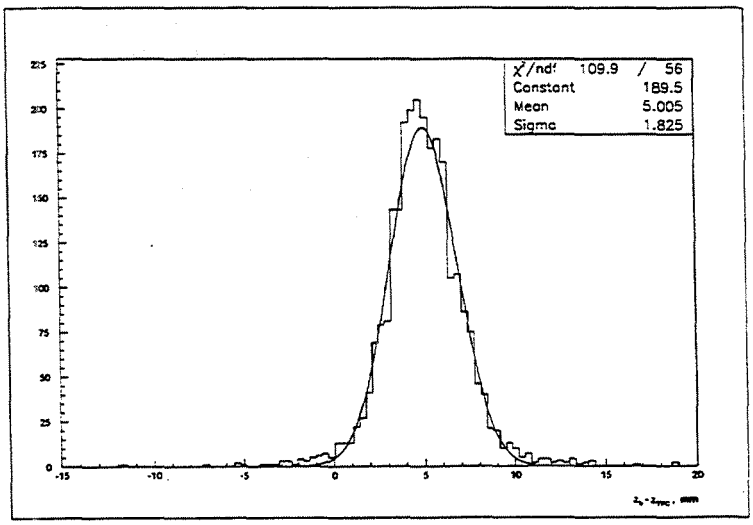

Figure 12: *Difference between z_b and z_{TPC}, 1993 data.*

3.2 Beam divergence, asymmetry and tilt

The variations of the beam width and divergence values are detected in terms of variations of $\sigma_{\Delta x}$. We show the variations of this parameter for 1994 in fig. 13.

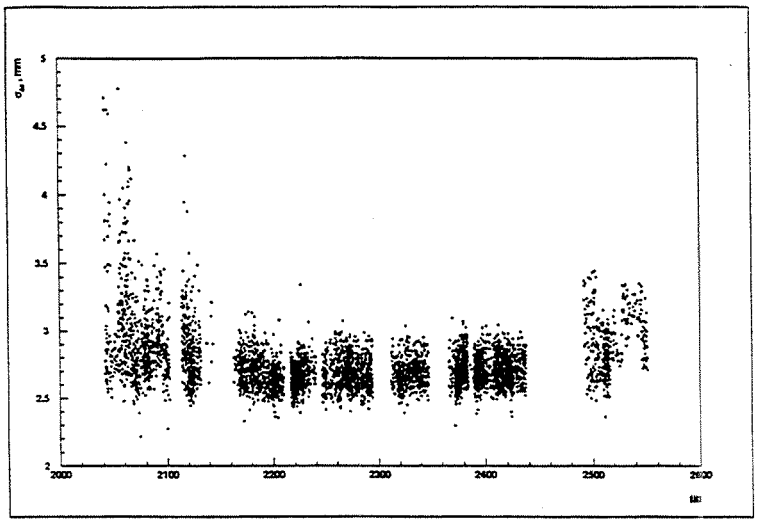

Figure 13: *Variation of $\sigma_{\Delta x}$ during 1994.*

We see that $\sigma_{\Delta x}$ varied from 2.2 mm to 4.8 mm in period 1, 3.4 mm in period 2 and 3.5 mm in period 3. There is an increase of the order of 50 μm during period 2. This variable covered a smaller interval in 1993 than in 1994, i.e. from 2.4 mm to 3.4 mm, within which it manifested more moderate fluctuation than in the following year.

The variations of the tilt angle in the (x,z) plane are monitored by the diagonal asymmetry defined in eq. (8). They are shown in fig. 14 for 1994 data and in fig. 15 for 1993 data.

The mean tilt, θ_y, in the (y,z) plane is monitored by the average y values of the impact points (see eq. 15). The variation of the mean tilt in the (y,z) plane during 1994 is given in fig. 16 and in fig. 17 for 1993 data.

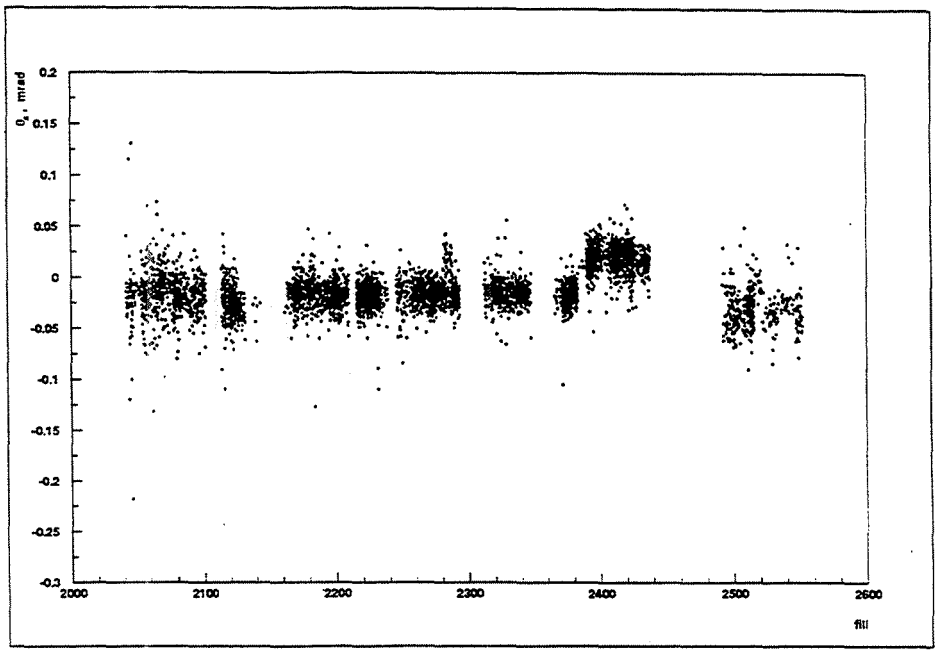

Figure 14: *Variation of θ_x during 1994.*

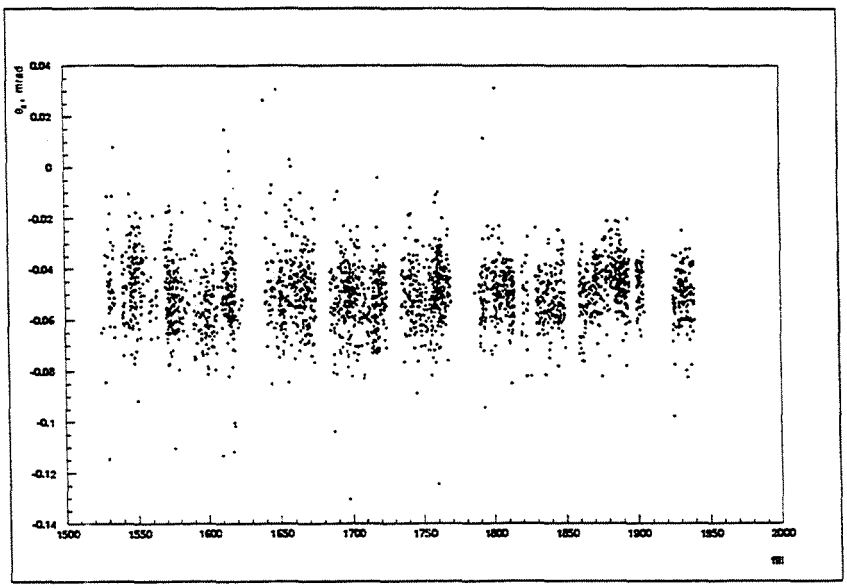

Figure 15: *Variation of θ_x during 1993.*

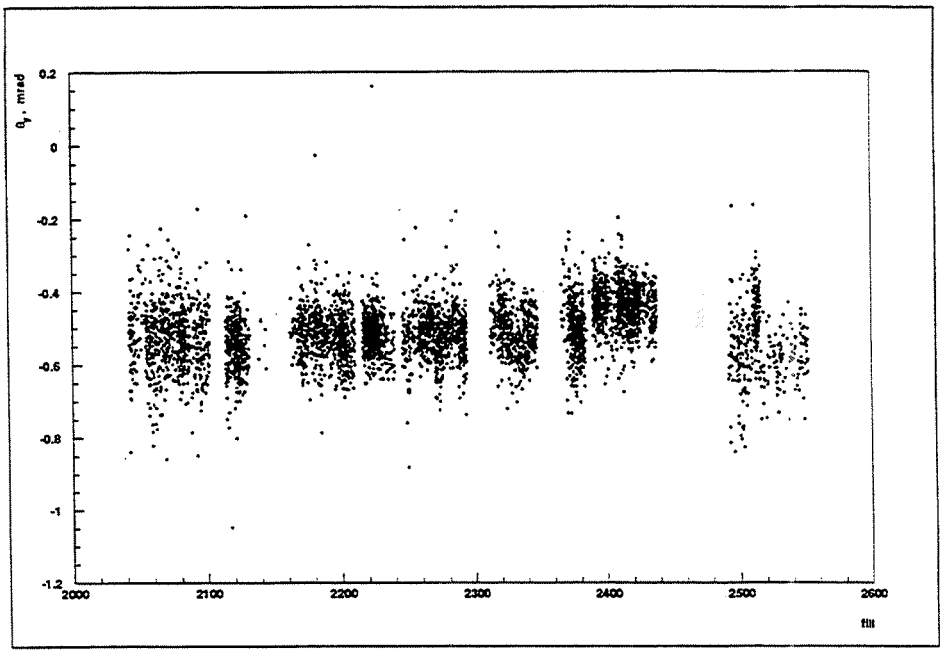

Figure 16: *Variation of θy during 1994.*

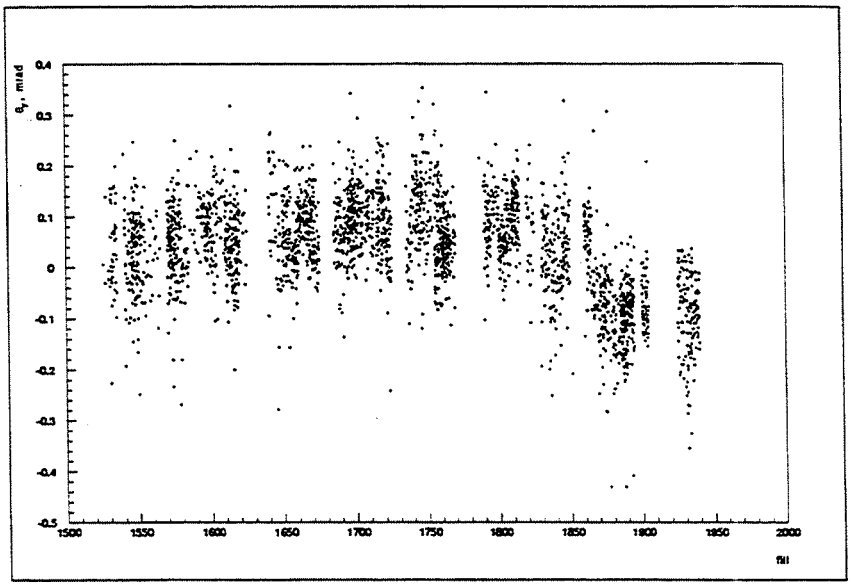

Figure 17: *Variation of θy during 1993.*

3.3 Acollinearity

In order to obtain acollinearity estimations in the (x,z) and (y,z) planes, we introduce the VD values for x beamspot and y beamspot in eqs. (5) and (13), from which we obtain the following expressions:

$$\epsilon_x \approx \frac{\Delta x - 2f_x \cdot x_{VD}}{l_x} \tag{18}$$

and

$$\epsilon_y \approx \frac{\Delta y - 2f_y \cdot y_{VD}}{l_y} \tag{19}$$

Fig. 18 shows ϵ_x for 1994 data. The most significant features are the increase of ϵ_x of the order of 50 μrad in period 1 and the rather large fluctuations in period 3. In fig. 19, the ϵ_x data for 1993 are shown: the range of ϵ_x fluctuations in 1993 was clearly smaller than in 1994.

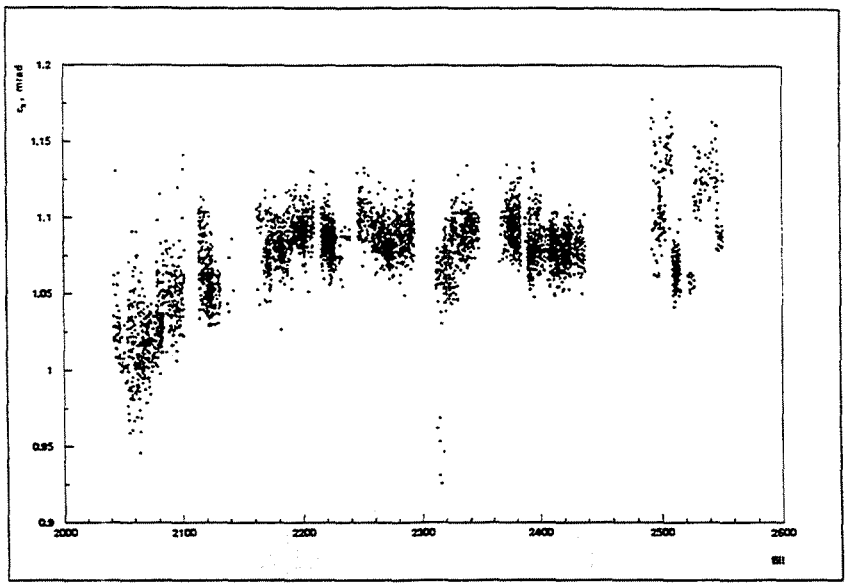

Figure 18: *Variation of ϵ_x during 1994.*

The 1994 variations of the acollinearity in the (y,z) plane are shown in fig. 20. The variations are much larger than those of ϵ_x with a large step of about 0.4 mrad between period 2 and periods 1 and 3. The ϵ_y variations in 1993 data are shown in fig. 21, where no sharp variation is observed.

In figs. 22-25, we give the corresponding distributions of figs. 18-21 for the results presented by LEP. Apart from an overall shift of the mean values, the agreement between the VSAT and LEP determination of the acollinearity in both planes and during both years is very good.

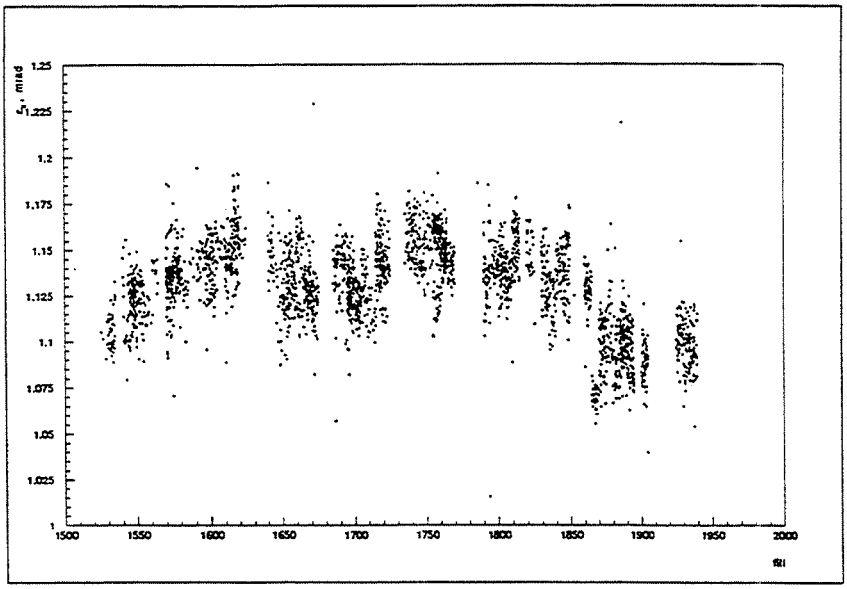

Figure 19: *Variation of ϵ_x during 1993.*

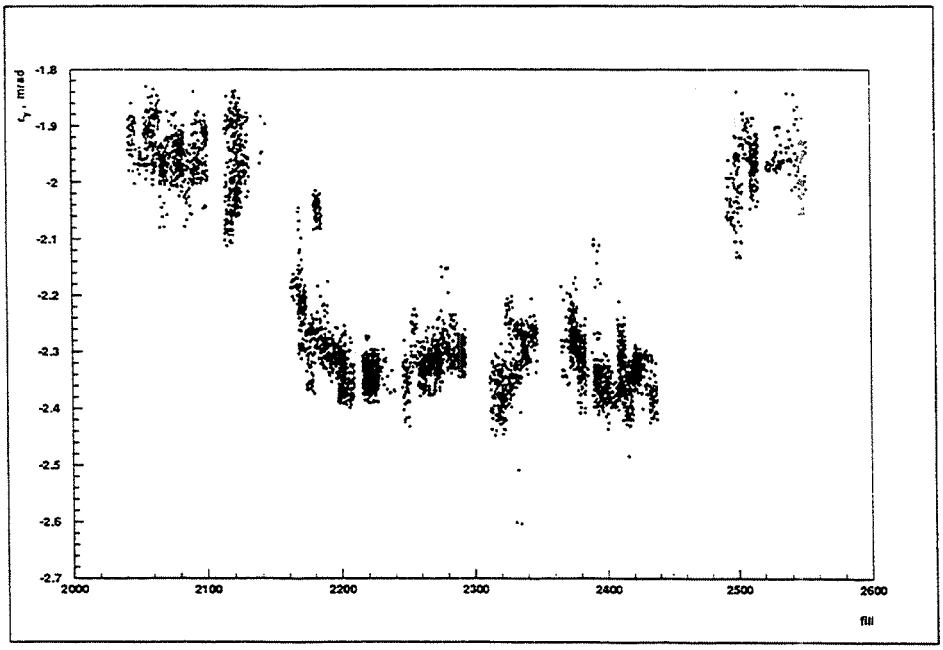

Figure 20: *Variation of ϵ_y during 1994.*

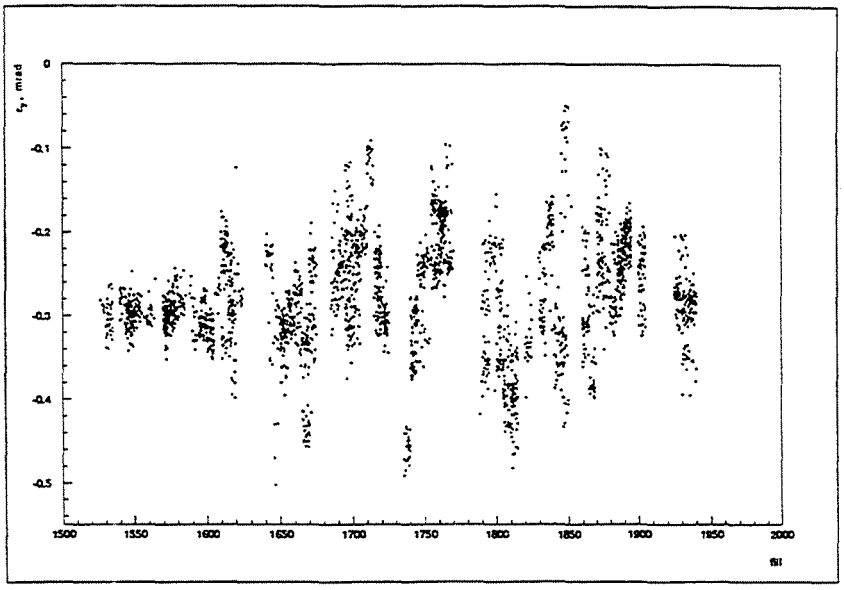

Figure 21: *Variation of ϵ_y during 1993.*

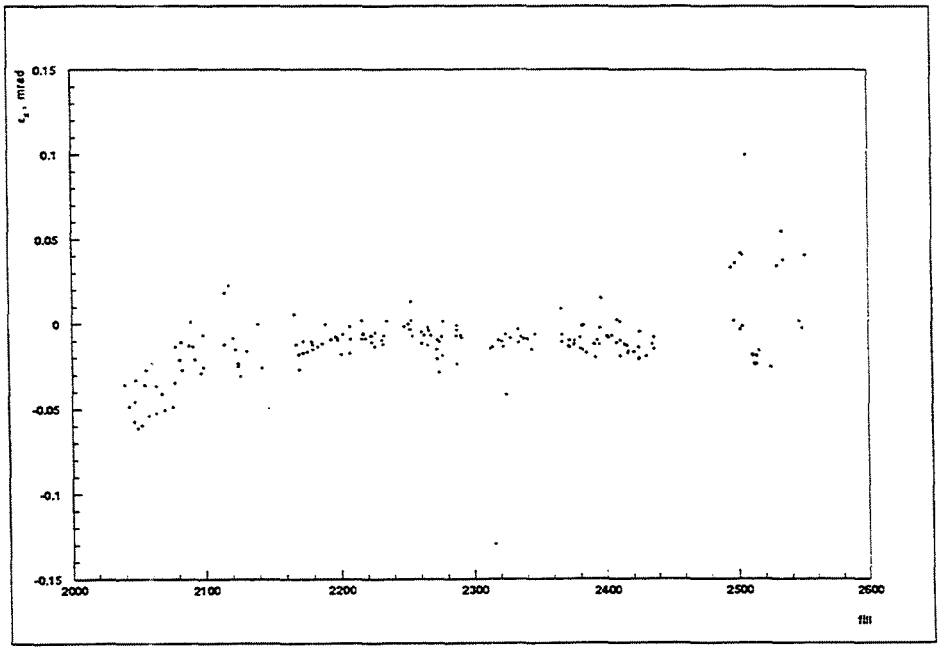

Figure 22: *ϵ_x from LEP during 1994.*

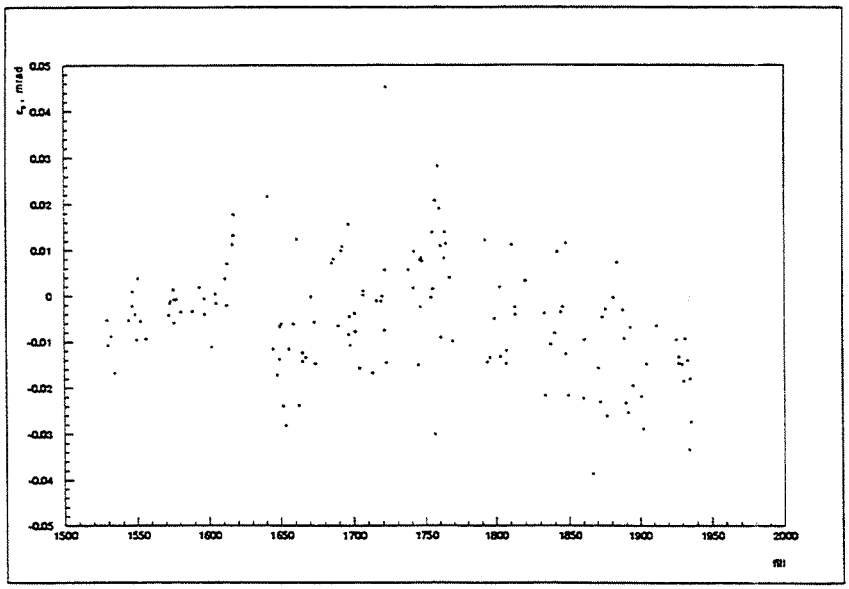

Figure 23: ϵ_x *from LEP during 1993.*

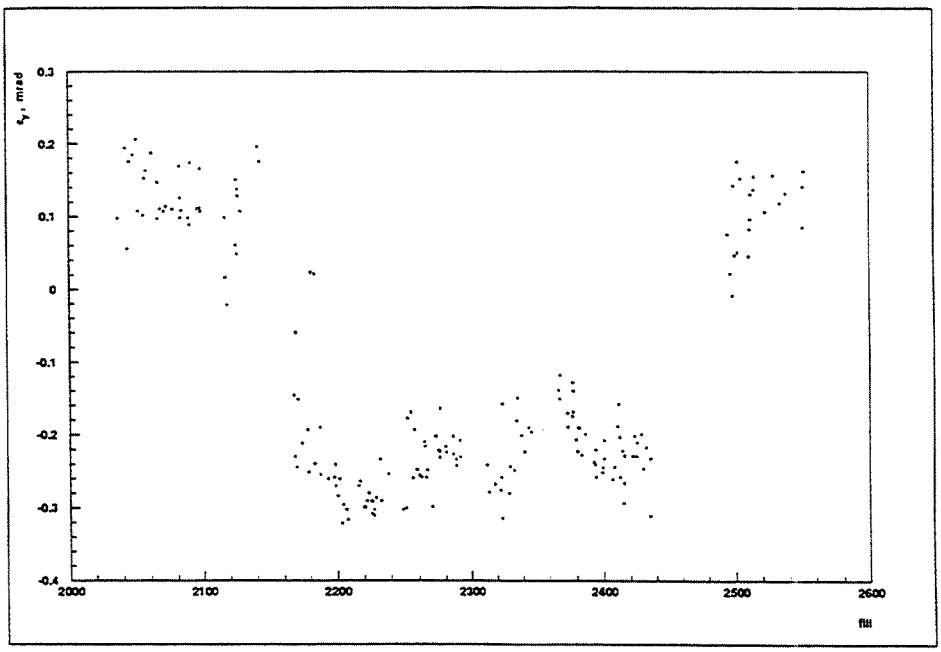

Figure 24: ϵ_y *from LEP during 1994.*

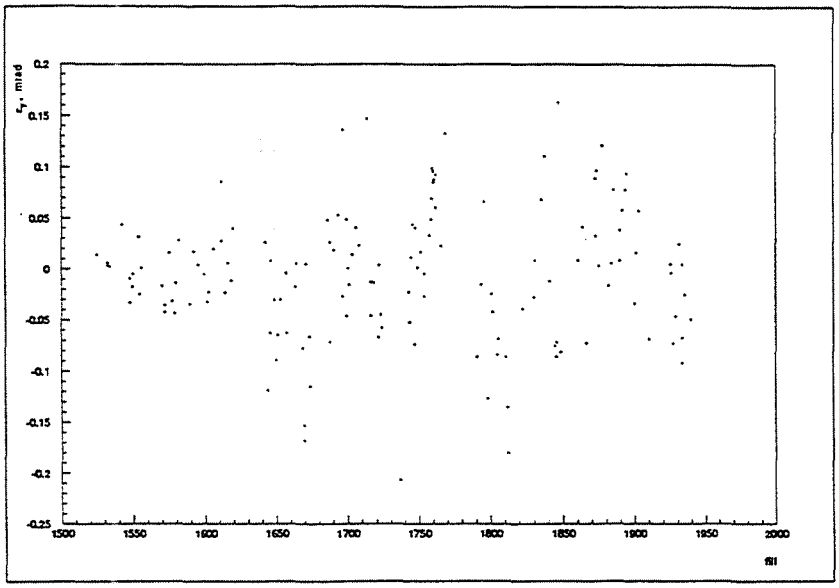

Figure 25: ϵ_y *from LEP during 1993.*

4 Conclusions

The position of the VSAT allows for high accuracy measurements of variation in time of LEP beam parameters. In particular, we have shown that the VSAT measurements, combined with the measurements of the beam spot done by TPC and VD, give useful information on tilt and acollinearity of beams. This information cannot be obtained easily from other detectors in DELPHI and it is very useful for a better understanding of the beam conditions at the DELPHI interaction point, which are relevant for many physics analyses.

References

[1] Almehed et al., *A silicon tungsten electromagnetic calorimeter for LEP.*

[2] Almehed et al., *High precision relative luminosity measurement with a Very Small Angle Tagger (VSAT) in DELPHI*, DELPHI 92-77 PHYS 188

[3] Almehed et al., *Beam parameter monitoring and interaction point measurement in DELPHI with the VSAT* DELPHI 94-144 PHYS 453

[4] Ch. Jarlskog, *Interaction point estimation and beam parameter variations in DELPHI with the VSAT*, LUNF D6/(NFFL-7110)/1995

Appendix C

Precision Determination of the Z^0 Resonance Parameters

DELPHI Collaboration

DELPHI 95-62 PHYS 497
30 June, 1995

Precision determination of the Z^0 resonance parameters

DELPHI Collaboration

Paper submitted to the "EPS-HEP95" Conference
Brussels, **27th July to 2nd August 1995**

EPS-HEP 95 Ref. eps0520
Submitted to Pa 1, Pa 15
Pl 18, Pl 19

DELPHI 95-62 PHYS 497
30 June, 1995

Precision Determination of the Z^0 Resonance Parameters

Preliminary

DELPHI Collaboration

S.Almehed, D.Bardin, M.Bigi, L.Bugge, T.Burgsmüller, M.Calvi, T.Camporesi, P.Checchia, F.Cossutti, P.J.Holt, P-S.Iversen, G.Jarlskog, P.Jonsson, A.Koch-Mehrin, M.Koratzinos, F.Glege, R.Lindner, J.MacNaughton, F.Mandl, G.Myatt, V.Nikolaenko, V.Obraztsov, A.Olchevski, M.Paganoni, P. Ratoff, A.Read, D.Reid, R.Reinhardt, P.Renton, G.Rinaudo, J.Strauss, T.Todorov, E.Vallazza, M.Verlato, H.Wahlen, G.R.Wilkinson, M.Winter, K.Yip, L.Zanini.

Abstract

During 1993 LEP was run at 3 energies near the Z^0 peak in order to give improved measurements of the mass and width of the resonance. DELPHI accumulated data corresponding to an integrated luminosity of 30.4 pb^{-1} during the dedicated scan with frequent measurements of the LEP energy, and 5.7 pb^{-1} at the Z^0 peak before the start of the scan. Analyses have been carried out on the hadronic cross sections and the cross sections and forward–backward asymmetries in the leptonic channels, using the most precise evaluations of the LEP energies. During 1994 LEP operated only at the Z^0 peak, and preliminary results are available on the hadronic and leptonic channels. Model independent fits to the totality of DELPHI lineshape and asymmetry data have been carried out and give values of the resonance parameters with significantly smaller errors than those previously published.

1 Introduction

This note reports on the cross section and the leptonic forward–backward asymmetry analyses of the DELPHI data taken during the 1993 LEP energy scan and that taken at a single energy near the Z^0 peak in 1994. In 1993 LEP operated at the peak energy and at ± 1.76 GeV above and below (the so–called "± 2 GeV"points). Before the scan with carefully monitored energies commenced data was taken at the peak (the "pre–scan" point). The analyses are still at a preliminary stage and not all channels have been investigated in the 1994 data at this time. Therefore the statistical and some of the systematic errors can be reduced with further study. Nevertheless the data give values of the Z^0 resonance parameters with significantly smaller errors than those previously published by DELPHI [1, 2]. All cross sections were corrected for the rms energy spread of the LEP beams.

2 Determination of the LEP Energies

During 1993 the energies of a sample of the "± 2 GeV" fills were systematically measured by resonant depolarization at the end of physics [3]. For fills where there was no direct measurement the energy was calculated from the NMR magnetic field measurement in the reference magnet, using the nearest depolarization measurement for an absolute scale [3]. This interpolation is one of the main sources of error. A (random fill–to–fill) uncertainty is assigned to the energy of each off–peak fill for which an energy calibration was not performed. This uncertainty has a value of of ± 2.9 MeV for the peak+2 points and ± 7.0 MeV for the peak-2 points. Within the framework of the Working Group on LEP Energy [3], a file was produced which gave an estimate for the LEP energy at 15 minute intervals during each fill using the NMR readings, the nearest polarization measurement, the best estimates of tide and temperature effects, and corrections for radio frequency cavity trips. This was in turn converted within DELPHI to an average energy per cassette of raw data. For the 1994 data, which was all at the same energy as the peak scan point in 1993, a preliminary energy error of ± 4 MeV was used [4].

The net effect of the LEP energy uncertainties and their correlations is to give systematic errors, common between the LEP experiments, of 1.5 MeV on the mass and 1.7 MeV on the width of the resonance, when data from all years is combined.

3 Determination of the Luminosity

For the 1993 data the absolute measurement of the luminosity was based on the Small Angle Tagger (SAT) calorimeter, but the relative luminosity at the off–peak points was taken from the Very Small Angle Tagger (VSAT) data, thus making a significant reduction in the statistical errors on the cross sections. Due primarily to a better geometrical definition of the masks and improved understanding of the data, the systematic errors in the SAT measurement were lower than in previous years and amounted to ($\pm 0.21\%$) in the experimental cross section, to be combined with the ($\pm 0.17\%$) uncertainty on the theoretical Bhabha cross section calculated with the program BHLUMI4.02 [6]. The total uncertainty in the luminosity determination of 1993 is therefore $\pm 0.27\%$.

For the 1994 data taking the luminosity was measured using the Small Angle Tile Calorimeter (STIC) of DELPHI. This detector is described in detail in ref. [5]. It consists of towers of scintillating tiles, sandwiched between lead plates and read out using wavelength shifting fibres and vacuum phototetrodes. The luminosity measurement is based on the mask technique used previously by DELPHI, but due to a better definition of the inner acceptance edge of the mask a higher precision is achieved. The overall experimental uncertainty is $\pm 0.09\%$, to which the largest contribution is $\pm 0.06\%$ due to the uncertainty on the position of the interaction point. The Bhabha cross section observed by the STIC is computed using the program BHLUMI4.02 [6] and assigned a theoretical uncertainty of $\pm 0.16\%$. The total uncertainty in the luminosity determination of 1994 is therefore $\pm 0.18\%$.

4 Hadronic Cross Sections

As in previous analyses [1, 2] the event selection was based on charged tracks only, having momentum greater than 0.4 GeV and polar angle between 20° and 160°. The charged multiplicity, N_{ch} was required to be greater than 4, and charged energy E_{ch} greater than 12% of the centre–of–mass energy.

A total of 687,000 events was selected in 1993 data. The selection efficiency was found from Monte Carlo simulation to be $(95.18 \pm 0.11)\%$. The simulation was carried out only for those events in which the generated hadronic energy was greater than $0.1\sqrt{s}$. This cut is introduced explicitly into the fitting procedure used to extract the Z^0 parameters and is estimated to have a negligible effect on the systematic errors. The $\tau^+\tau^-$ and e^+e^- backgrounds were evaluated from simulation and by inspection of distributions sensitive to the contaminations. The $\tau^+\tau^-$ background was found to be $(0.57 \pm 0.05\%)$ at each energy, whereas the e^+e^- background was evaluated as 0.05%, 0.03% and 0.03% at 89.4 GeV, 91.2 GeV and 93.0 GeV respectively, with an uncertainty of $\pm 0.03\%$. The two-photon background was estimated to be 16 ± 3 pb from Monte Carlo simulation.

A preliminary determination has been made of the hadronic cross section using a partial sample of 1,144,000 events from the 1994 data and the STIC luminosity. At this stage of the analysis the systematic uncertainty in the cross section due to efficiencies and backgrounds is estimated to be 0.15%, of which $\pm 0.10\%$ is common to the results of previous years.

5 Cross Sections and Forward–Backward Asymmetries in the e^+e^- Channel

The analysis of 1993 data followed the procedures described in [2]. Two different methods were used, one relying largely on the barrel electromagnetic calorimeter (HPC) for event selection with the efficiency being determined by simulation, and the second using two independent selections whose efficiencies could be determined from the data. Because the HPC was not stable during the early part of 1993, the first method was not used for the "pre–scan" data. In both methods the electron and positron were required to be in the polar angle range $44° < \theta < 136°$, and the acollinearity was required to be smaller than 10°. A total of 24,228 events was selected. Apart from the luminosity, systematic errors

arise from the event selection and from the t–channel subtraction. For these preliminary results the systematic uncertainties are estimated to be $\pm 0.80\%$, $\pm 0.44\%$ and $\pm 0.53\%$ at the centre–of–mass energies of 89.4 GeV, 91.2 GeV and 93.0 GeV respectively.

The forward–backward asymmetries have been determined with the same samples of events. Systematic errors arise because of charge confusion, forward–backward acceptance differences and the t–channel subtraction and are estimated to be ± 0.016, ± 0.003 and ± 0.004 at centre–of–mass energies of 89.4 GeV, 91.2 GeV and 93.0 GeV respectively.

6 Cross Sections and Forward–Backward Asymmetries in the $\mu^+\mu^-$ Channel

For the cross section measurement the μ^- was required to be in the polar angle range $20^\circ < \theta < 160^\circ$ and events were required to have two charged particles of momentum greater than $5 \times \sqrt{s}/91.188$ GeV and acollinearity less than 20°. Each particle had to be identified as a muon, using either the muon chambers (MUB and MUF), or the Hadron Calorimeter (HCAL), or the HPC or the Forward Electromagnetic Calorimeter (FEMC). Unlike in previous anaslyses [1, 2] the selection of $\mu^+\mu^-$ candidates involved the use of the variable $P_{rad} = \sqrt{P_1^2 + P_2^2}$, where P_1 and P_2 are the momenta of the highest momentum charged particle in each hemisphere. A requirement of $P_{rad} > 39.6 \times \sqrt{s}/91.2$ GeV reduced the $\tau^+\tau^-$ background by one half while increasing the $\mu^+\mu^-$ efficiency slightly, compared to the cuts on muon momentum used previously. A total of 28,994 events was selected in 1993 data. Reconstruction and identification efficiencies were measured from the data, as was the cosmic ray background. The latter was found to be $(0.33 \pm 0.07)\%$, $(0.11 \pm 0.03)\%$ and $(0.23 \pm 0.05)\%$ at energies of 89.4 GeV, 91.2 GeV and 93.0 GeV respectively. The $\tau^+\tau^-$ background was estimated from simulation and by fitting to discriminating variables to be $(1.06 \pm 0.11)\%$. At this stage of the analysis the systematic uncertainty in the cross section determination from efficiencies and backgrounds was estimated to be $\pm 0.28\%$.

For the forward–backward asymmetry determinations the polar angle range was extended to $11^\circ < \theta < 169^\circ$, except for the "pre–scan" period when problems with the Forward Chamber A required the range to be reduced to $18^\circ < \theta < 162^\circ$. A total of 27,492 events was selected. The differential cross sections of the $\mu^+\mu^-$ events at the three centre–of–mass energies of the scan points are shown in figure 1. The figure shows the large angular acceptance of the DELPHI detector for this channel, and the significant asymmetries above and below the peak are clearly visible. The asymmetry was calculated using a maximum likelihood fit of the lowest order form of the angular distribution. At this stage of the analysis an uncertainty of ± 0.0009 is assigned to the asymmetry to allow for possible detector and charge acceptance asymmetries.

A sample of 49,748 $\mu^+\mu^-$ events obtained at the peak energy in 1994 has been analysed to give preliminary results for the cross section and 54,300 events for the forward–backward asymmetry. At this stage of the analysis the systematic errors on the cross section and forward–backward asymmetry are estimated at $\pm 0.4\%$ and ± 0.0015 respectively.

The Z^0 parameters are obtained from the DELPHI data using the program ZFITTER [7]. The parameter P_{rad} cannot be used explicitly in ZFITTER, however it was verified using the Monte Carlo generators DYMU3 [8] and KORALZ [9] and studies of the momentum measurements in DELPHI that the uncertainty due to corrections for this

cut was only ±0.04% in the cross section.

7 Cross Sections and Forward–Backward Asymmetries in the $\tau^+\tau^-$ Channel

The selection of $\tau^+\tau^-$ events in 1993 data was similar to that described in Ref. [2]. Events were required to be of low multiplicity and to consist of two well isolated jets, in order to remove background from $q\bar{q}$ events. The thrust axis, computed using charged and neutral energy, was required to lie in the polar angle range $43° < \theta < 137°$. Selections on the variables P_{rad}, E_{rad} (a similar variable defined using the energies in the electromagnetic calorimeters within a cone of half-angle 30° around the thrust direction in each hemisphere) and the total charged and neutral energy E_{vis}, reduced the backgrounds from e^+e^-, $\mu^+\mu^-$ and two-photon events. The selection efficiency was determined by simulation to be $(48.5 \pm 0.3)\%$. The two-photon background was estimated to be 3.3 ± 0.2 pb, that due to $q\bar{q}$ events $(0.45 \pm 0.15)\%$ and that due to $\mu^+\mu^-$ events $(0.39 \pm 0.07)\%$ at all energies. The cosmic ray background was estimated to be $(0.34 \pm 0.03)\%$, $(0.11 \pm 0.01)\%$ and $(0.23 \pm 0.02)\%$ and the e^+e^- background to be 15 ± 1 pb, 16 ± 1 pb and 12 ± 1 pb, at the centre–of–mass energies of 89.4 GeV, 91.2 GeV and 93.0 GeV respectively. A total of 17,225 events was selected. For these preliminary results the systematic error due to selections and backgrounds is estimated to be ±0.8%, in addition to the systematic error on the luminosity.

The forward–backward asymmetries were measured using the likelihood method on the events of the 1–N and 3–3 topologies. Systematic errors arise from the e^+e^- subtraction and from charge confusion and are estimated to be ±0.008, ±0.002 and ±0.002 at centre–of–mass energies of 89.4 GeV, 91.2 GeV and 93.0 GeV respectively.

8 Cross Sections and Forward–Backward Asymmetries in the Inclusive Lepton Channels

As in Refs. [1, 2] for the cross section determination events were required to have between 2 and 6 charged particle tracks with momentum greater than 0.2 GeV, at least two of them lying in the polar angle range $43° < \theta < 137°$. At least one hemisphere was required to contain one charged particle, and the other between 1 and 5. The acollinearity, defined by the isolated charged particle and the resultant momentum of the particles in the opposite hemisphere, was required to be less than 20°, and one charged particle was required to have momentum greater than 3 GeV (at the peak, scaled with $\sqrt{s}$ off the peak). Using these criteria a total of 65,544 events was selected in 1993 data. The selection efficiencies for e^+e^- and $\mu^+\mu^-$ events were determined from the data, whereas that for $\tau^+\tau^-$ events was obtained from simulation. Hadronic and two-photon backgrounds were estimated by simulation and were found to be $(0.12 \pm 0.01)\%$ and 6.1 ± 0.3 pb respectively. The background from cosmic rays was measured from the data and was found to be $(1.62 \pm 0.06)\%$, $(0.65 \pm 0.02)\%$ and $(1.51 \pm 0.05)\%$ at 89.4 GeV, 91.2 GeV and 93.0 GeV respectively. The t–channel contribution to the e^+e^- cross section was computed and subtracted leading to an additional sytematic error of ±0.22%. The overall systematic

error from efficiencies and backgrounds in the s–channel cross section was estimated to be $\pm 0.35\%$.

For the determination of the forward–backward asymmetry, only the 51,198 events of the 1–1 topology were used. Corrections were applied for cosmic ray and two–photon backgrounds, and the e^+e^- t-channel contribution was subtracted. Systematic errors arise from the t–channel subtraction and charge confusion and are estimated to be ± 0.0020.

The inclusive lepton results were compared to those of sections 5, 6 and 7 using lepton identification. The lepton–identified results were corrected to 4π acceptance and for the cuts on momenta and acollinearity using the program ZFITTER [7]. The weighted mean of the lepton–identifed results was then computed at each energy. Similarly the the mean of the differences of the lepton–identified forward–backward asymmetries and those measured in the inclusive lepton channel was found. These comparisons can be seen in Table 1. Given the different angular ranges of the analysed data and the different correction factors involved, the good agreement supports the validity of the lepton–identified results.

Collision energy (GeV)	Cross section ratios identified/inclusive	Asymmetry differences identified–inclusive
91.297	1.0010 ± 0.0057	0.0108 ± 0.0120
89.433	0.9910 ± 0.0069	0.0107 ± 0.0143
91.192	0.9932 ± 0.0052	0.0030 ± 0.0084
93.016	0.9925 ± 0.0062	0.0046 ± 0.0133

Table 1: Comparison of the inclusive lepton cross sections and forward–backward asymmetries with the weighted averages of the flavour identified results. The errors shown include the systematic plus uncorrelated statistical errors.

9 Fits to the Data and Interpretation of the Results

Fits to the preliminary 1993 and 1994 data on the hadronic and leptonic cross sections and the leptonic forward–backward asymmetries, and to all the previously published DELPHI data [1, 2] have been made using the program ZFITTER [7]. Full account was taken of the LEP energy uncertainties and their point–to–point correlations. Detailed study [3] has shown that the uncertainties on the LEP energy determinations in 1991, 1992 and 1993 can be considered as having negligible correlation.

A 9–parameter fit, allowing independent couplings for the three lepton species, was carried out. The resulting parameters are:

$$
\begin{aligned}
M_Z &= 91.1849 \pm 0.0034 \text{ GeV} \\
\Gamma_Z &= 2.4913 \pm 0.0053 \text{ GeV} \\
\sigma_0 &= 41.39 \pm 0.10 \text{ nb} \\
R_e &= 20.88 \pm 0.16 \\
R_\mu &= 20.70 \pm 0.09 \\
R_\tau &= 20.61 \pm 0.16
\end{aligned}
$$

$$
\begin{aligned}
A_{FB}^{0,e} &= 0.0233 \pm 0.0069 \\
A_{FB}^{0,\mu} &= 0.0166 \pm 0.0030 \\
A_{FB}^{0,\tau} &= 0.0210 \pm 0.0057 \\
\chi^2/DF &= 151/133.
\end{aligned}
$$

where $A_{FB}^{0,f}$ is defined as:

$$
A_{FB}^{0,f} = 3\frac{g_{V_e} g_{A_e}}{(g_{V_e}^2 + g_{A_e}^2)} \frac{g_{V_f} g_{A_f}}{(g_{V_f}^2 + g_{A_f}^2)}.
$$

Note that according to the recommendation of the LEP Electroweak Working Group [10] $A_{FB}^{0,f}$ is defined in terms of the real parts of the couplings, whereas the leptonic partial widths are defined in terms of their magnitudes. The differences are insignificant with present experimental uncertainties, but are in any case correctly taken into account in the fits. The correlation coefficients for the parameters of the 9-parameter fit are given in Table 2. The uncertainty on Γ_Z does not include an additional ± 0.0010 GeV, common to all LEP experiments, due to the uncertainty of ± 5 MeV on the LEP centre–of–mass energy spread. There is an additional uncertainty on M_Z due to the imprecise knowledge of the distance between the radio frequency stations in points 2 and 6. However this error is totally correlated between ALEPH and DELPHI and disappears when an average is made over the experiments.

Since the parameters are in good agreement with lepton universality, we carry out a 5-parameter fit assuming flavour independence of the couplings. The resulting parameters are:

$$
\begin{aligned}
M_Z &= 91.1849 \pm 0.0034 \text{ GeV} \\
\Gamma_Z &= 2.4913 \pm 0.0053 \text{ GeV} \\
\sigma_0 &= 41.40 \pm 0.10 \text{ nb} \\
R_l &= 20.71 \pm 0.07 \\
A_{FB}^{0} &= 0.0182 \pm 0.0025 \\
\chi^2/DF &= 155/139.
\end{aligned}
$$

The correlation coefficients of the parameters of the 5-parameter fit are given in Table 3. Here R_l is defined for the Z^0 decay into a pair of massless charged leptons and is treated consistently throughout. The results of the 9–parameter and 5–parameter fits are in good agreement with those published by the other LEP collaborations [11, 12, 13].

In figure 2 the result of the 5–parameter fit is shown together with the DELPHI data on the hadronic cross sections. In figure 3 and figure 4 respectively are shown the DELPHI data on leptonic cross sections and forward–backward asymmetries, compared to the results of the 5–parameter fit. The leptonic data shown is all corrected for the acollinearity and momentum cuts and extrapolated to the full solid angle where necessary.

From the results of the preceeding fits the following parameters can be derived:

$$
\Gamma_e = 83.48 \pm 0.36 \text{ MeV}
$$

$$
\begin{aligned}
\Gamma_\mu &= 84.22 \pm 0.51 \text{ MeV} \\
\Gamma_\tau &= 84.60 \pm 0.74 \text{ MeV} \\
\Gamma_l &= 83.83 \pm 0.23 \text{ MeV} \\
g^2_{V_l} &= (1.54 \pm 0.21) \times 10^{-3} \\
g^2_{A_l} &= 0.2507 \pm 0.0007 \\
\Gamma_{inv} &= 503.9 \pm 4.1 \text{ MeV} \\
\Gamma_{had} &= 1.7360 \pm 0.0052 \text{ GeV}.
\end{aligned}
$$

Assuming the Minimal Standard Model value for Γ_ν/Γ_l:

$$\Gamma_\nu/\Gamma_l = 1.992 \pm 0.002$$

and using our result:

$$\Gamma_{inv}/\Gamma_l = 6.010 \pm 0.046$$

the number of light neutrino species can be deduced. The result is:

$$N_\nu = 3.017 \pm 0.023.$$

	Γ_Z	σ_0	R_e	R_μ	R_τ	$A_{FB}^{0,e}$	$A_{FB}^{0,\mu}$	$A_{FB}^{0,\tau}$
M_Z	0.05	-0.01	-0.02	-0.05	-0.03	0.03	0.08	0.04
Γ_Z	–	-0.15	0.01	0.00	0.01	0.01	0.00	0.00
σ_0		–	0.06	0.15	0.05	0.00	0.00	-0.01
R_e			–	0.04	0.03	0.00	0.00	0.00
R_μ				–	0.04	0.00	0.01	0.00
R_τ					–	0.00	0.00	0.02
$A_{FB}^{0,e}$						–	0.02	0.01
$A_{FB}^{0,\mu}$							–	0.02

Table 2: The correlation coefficients for the parameters of the 9-parameter fit.

	Γ_Z	σ_0	R_l	A_{FB}^0
M_Z	0.05	-0.01	-0.06	0.10
Γ_Z	–	-0.15	0.00	0.00
σ_0		–	0.16	0.00
R_l			–	0.01

Table 3: The correlation coefficients for the parameters of the 5-parameter fit.

The leptonic vector and axial-vector couplings correspond to a value of the weak mixing angle of

$$\sin^2\theta^{lept}_{eff} = 0.2304 \pm 0.0014.$$

References

[1] DELPHI Collaboration, P. Abreu et al., Nucl. Phys. **B417** (1994) 3.

[2] DELPHI Collaboration, P. Abreu et al., Nucl. Phys. **B418** (1994) 403.

[3] The working group on LEP energy, R. Assmann et al., Z. Phys. **C66** (1995) 567.

[4] Working Group on LEP Energy, meeting summaries (1994).

[5] S.J. Alvsvaag et al.,"The Small Angle Tile Calorimeter Project in DELPHI", 4^{th} International Conference on Advanced Technologies in Particle Physics, Como, Italy, (1994).

[6] S. Jadach et al.,"Higher–Order Radiative Corrections to Low–Angle Bhabha Scattering: The YFS Monte Carlo Approach", preprint CERN-TH/95–38 (1995).

[7] D. Bardin et al.,"ZFITTER: An Analytical Program for Fermion Pair Production in e^+e^- Annihilation", preprint CERN-TH 6443 (1992) and references therein.

[8] J.E. Campagne and R. Zitoun, Z. Phys **C43** 1989) 469.

[9] KORALZ S. Jadach, B.F.L. Ward and Z. Wąs,
Comput. Phys. Commun. **66** (1991) 276.

[10] LEP Electroweak Working Group Minutes (May 1995).

[11] ALEPH Collaboration, D. Buskulic et al., Z. Phys. **C62** (1994) 539.

[12] L3 Collaboration, M. Acciarri et al., Z. Phys **C62** (1994) 551.

[13] OPAL Collaboration, R. Akers et al., Z.Phys. **C61** (1994) 19.

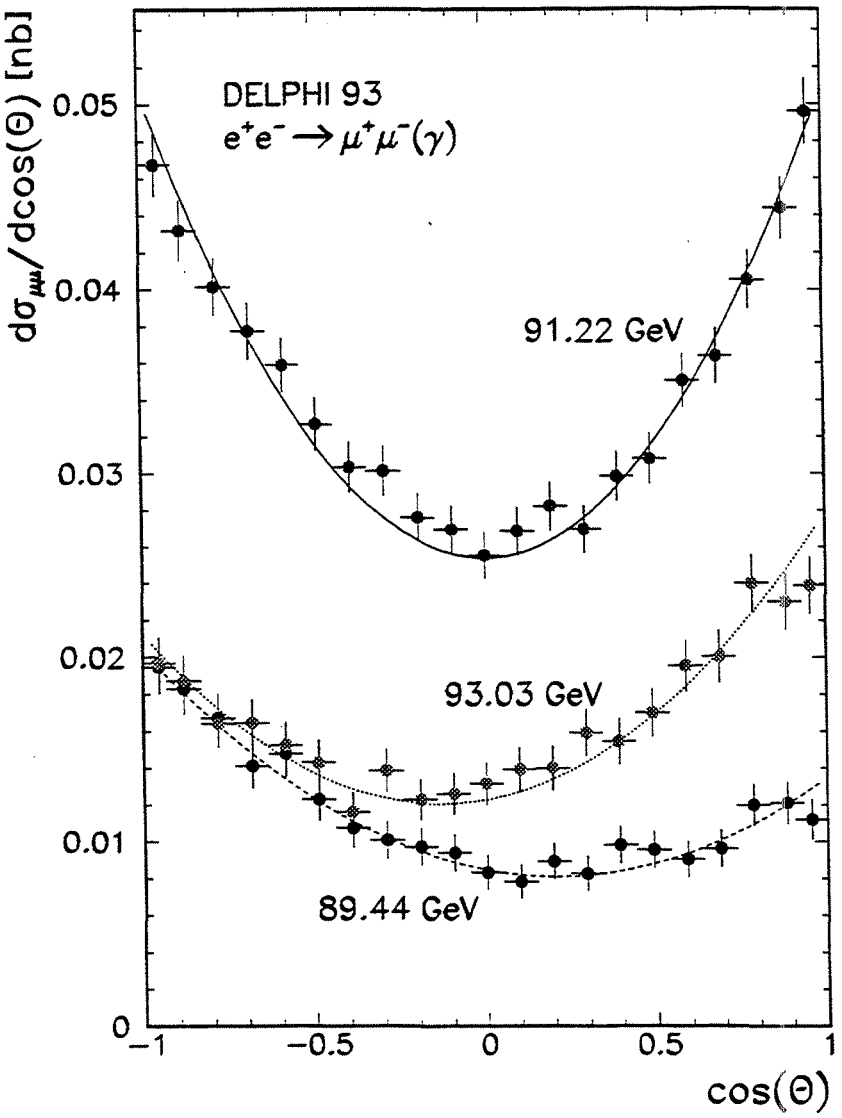

Figure 1: The differential cross sections in the $\mu^+\mu^-$ channel for the 1993 data at the three energy values. The curves are fits to the lowest order form of the angular distribution.

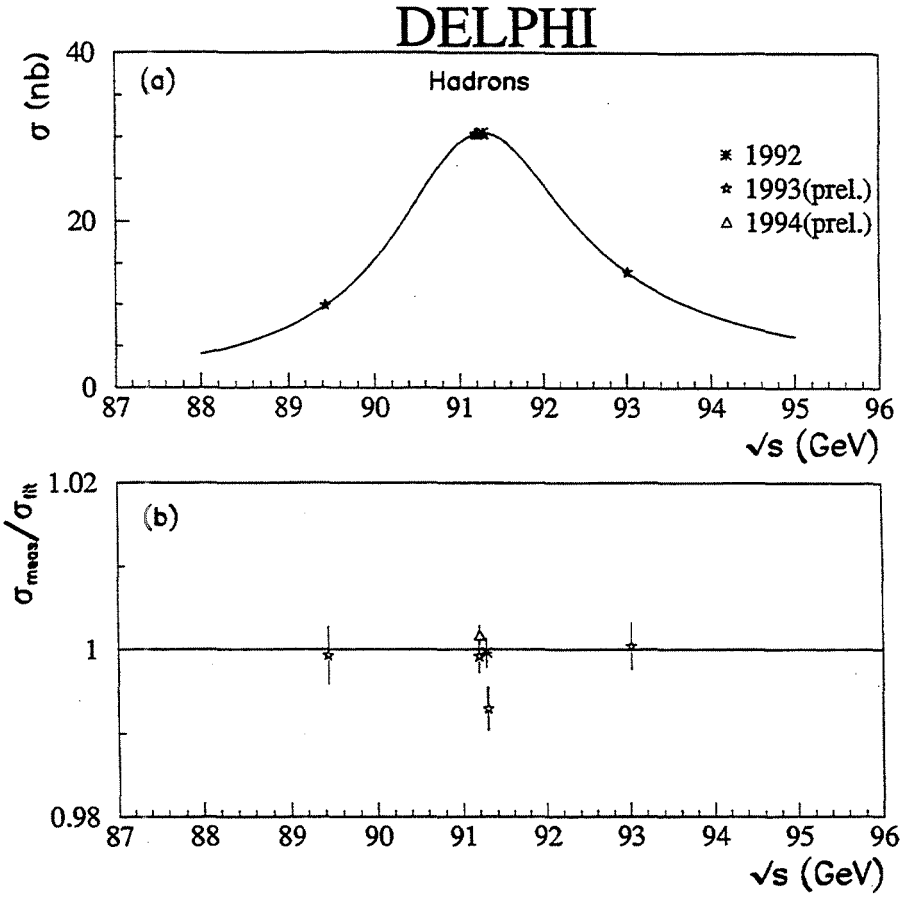

Figure 2: Hadronic cross sections from 1992 and preliminary 1993 and 1994 data. The errors shown are statistical only. In (a) the data are shown together with the result of the 5-parameter fit described in Section 9. Plot (b) shows the ratio of the measurements to the best fit values.

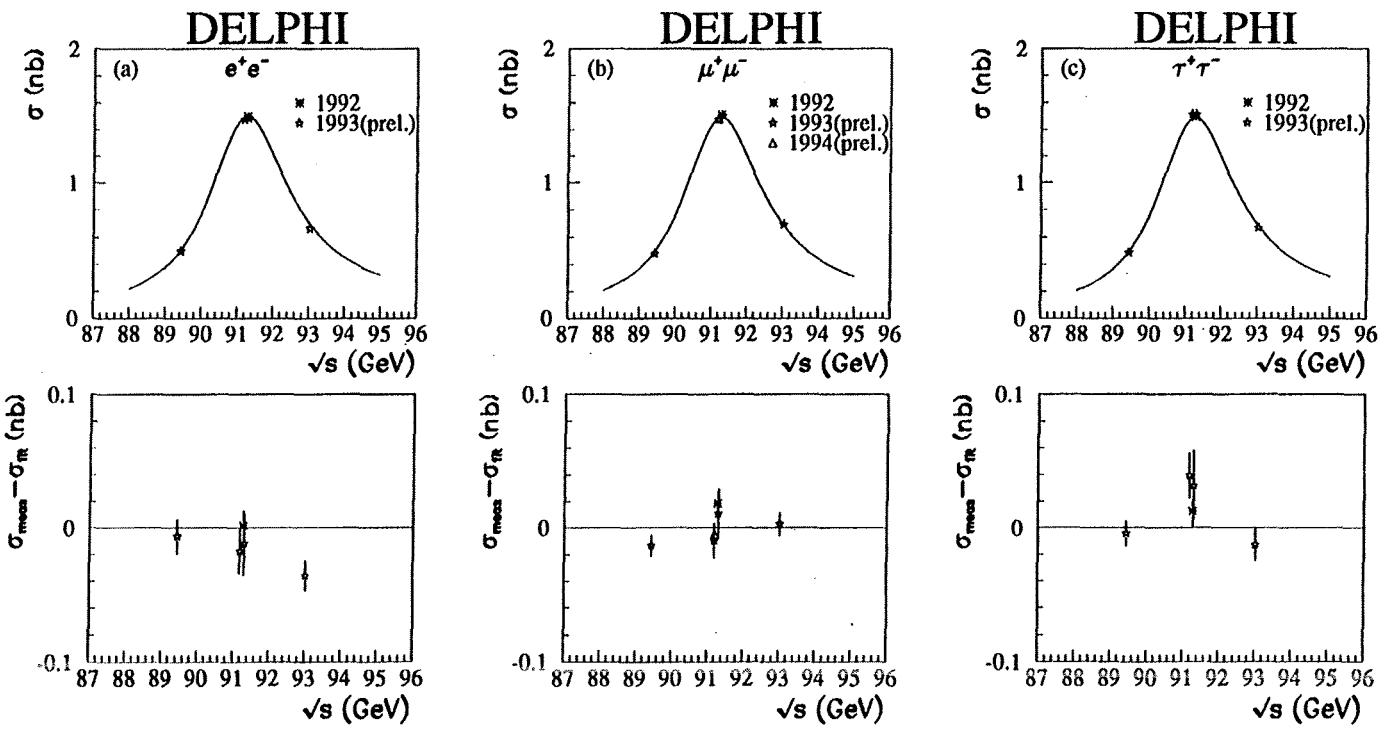

Figure 3: Cross sections in the (a) e^+e^-, (b) $\mu^+\mu^-$ and (c) $\tau^+\tau^-$ channels from 1992 and preliminary 1993 and 1994 data. The cross sections are extrapolated to the full solid angle and corrected for the acollinearity and momentum cuts. Only statistical errors are shown. The lower plots show the differences between the measured points and the best fit values. The curves are the results of the 5-parameter fit described in Section 9.

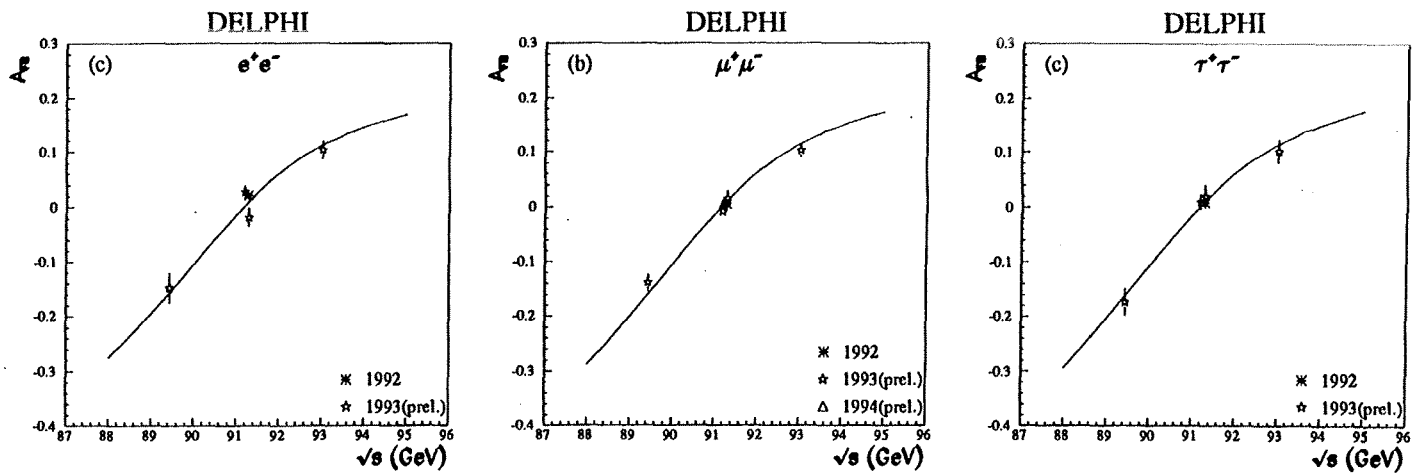

Figure 4: Forward–backward asymmetries in the (a) e^+e^-, (b) $\mu^+\mu^-$ and (c) $\tau^+\tau^-$ channels from 1992 and preliminary 1993 and 1994 data. The asymmetries are extrapolated to the full solid angle and corrected for the acollinearity and momentum cuts. The curves are the results of the 5–parameter fit described in Section 9.

Appendix D

Study of multihadron production in two-photon collisions at LEP1 and LEP2

Study of multihadron production in two-photon collisions at LEP1 and LEP2

S. Almehed [1], *G. Jarlskog* [1], *P. Jonsson,* [1] *F. Kapusta* [2], *I. Tyapkin* [3], *N. Zimin* [1,3], *A. Zinchenko* [3]

[1] *Department of Physics, University of Lund, Sweden*
[2] *LPNHE, IN2P3-CNRS, Universités Paris VI et VII, France*
[3] *JINR, Dubna, Russian Federation*

Abstract

Results of an experimental study of the reaction $e^+e^- \to e^+e^- + hadrons$ are presented. The data were obtained by the DELPHI detector at LEP1 and LEP2. Together with Monte Carlo predictions they illustrate the evolution of the two-photon process under no-tag conditions. Double-tag events with both scattered e^+ and e^- measured by the DELPHI VSAT detector were observed for the first time at LEP1. The total $\gamma\gamma$ hadronic cross-section is estimated for the $\gamma\gamma$ centre of mass energy up to 35 GeV.

1 Introduction

Multihadron production in $\gamma\gamma$ reaction has been studied in many previous experiments, more recently at KEK [1] and LEP [2, 3]. According to those studies a correct leading order description of the experimental data has to combine three components: a soft interaction term described by the generalized Vector meson Dominance Model (VDM), a perturbative term described by the Quark Parton Model (QPM) with a direct quark exchange, and a term for the hard scattering of the partonic constituents of the photon, the so-called Resolved Photon Contribution (QCD-RPC). All these models were realized in the TWOGAM generator which describes DELPHI data reasonably well for both the no-tag and single tag cases. The QPM and VDM events are generated with the same parameters as in previous DELPHI analyses [3]. The QCD-RPC was treated using leading order QCD factorization: a hard scattering subprocess gives the dominant scale p_T^2, taken also as the factorization scale. Since such subprocesses are considered as perturbative, a single free parameter, p_T^{min}, the transverse momentum of the outgoing partons has to be specified and used in order to separate the RPC from the non-perturbative contribution. These values of p_T^{min} were found for parton density functions from the requirement to reproduce the visible experimental two-photon cross-section at Z^0 peak. The Gordon-Storrow (GS2 with $p_t^{min}(GS2) = 1.88 \pm 0.020\ GeV/c$) and Glück-Reya-Vogt (GRV with $p_t^{min}(GRV) = 1.58 \pm 0.018\ GeV/c$,) parameterizations of the parton density functions have been shown to reproduce data better and were chosen for simulation. Errors come from statistical errors in the experimental data and those of the simulated samples. The generated events were processed by the full detector simulation program and then subjected to the same selection procedure as the experimental data. A description of the DELPHI detector together with basic criteria used to select $\gamma\gamma$ hadronic events can be found in ref. [3, 4].

2 No tag visible cross-section behaviour

The experimental data analyzed were collected during 1995 and 1996 LEP runs. They correspond to integrated luminosities of 29.4 pb^{-1}, 5.8 pb^{-1} and 7.9 pb^{-1} for centre-of-mass energies of $\simeq$ 91, $\simeq$ 135 and $\simeq$ 172 GeV, respectively. The configuration of the DELPHI detector was quite stable during that period providing an opportunity to look at the evolution of the $\gamma\gamma$ process at different energies. In order to select hadronic two-photon events at least 4 charged particles in the event with an energy below 20 GeV are required together with invariant mass of the hadronic system in the range 4-30 GeV/c^2 and total transverse momentum of the events below 3 GeV/c. Those criteria suppress the Z^0 decay background at peak, the background from $\tau\tau$ pairs and beam-gas interactions and remove the $\gamma\gamma$ resonance energy region. To validate trigger conditions a total energy of the charged particles greater than 3 GeV was also required together with a momentum of the most energetic particle that was greater than 1 GeV/c. In order to use a neutral component of the hadronic system and hence to provide better rejection of the background and increase the sensitivity to the parton distribution function behaviour, all calorimetric information was included in the analysis The visible cross-section (Fig.1) for the events meeting the selection criteria was calculated for each LEP energy point. A simulation was used to check the visible $\gamma\gamma$ cross-section due to Z^0 background. A visible Z^0 background corresponds to $\sigma_Z^{MC} = 92.9 \pm 5.7$ pb (averaged over points around the peak) and only 2.5$\pm$0.5 pb at $\simeq$ 135 GeV. The cross-section of the beam-gas background was estimated to be below 1 pb for all samples using events originated far from the interaction point. The remaining background contribution was found to be negligible. After bin-by-bin subtraction of the background the visible $\gamma\gamma$ cross-section at the Z^0 peak was found to be $\sigma_{\gamma\gamma}^{exp} = 658.6 \pm 7.6$ pb, which is in agreement with our previous studies [3]. The experimental values are well fitted by the combination of a linear term and Cahn's formula [5], describing the shape of the Z^0 peak. An indication that there is an excess of Monte Carlo predictions is seen for higher energies. The errors of the simulated points come from the uncertainty of p_t^{min} determinations and statistical errors of the simulated samples. Systematic errors relevant for comparing different parton density parameterizations are highly correlated and move the points in the same direction. Different experimental distributions were produced and compared with a simulation shown in Fig.2. It can be seen that the Monte Carlo predicts perfect agreement at $\simeq$ 91 GeV and slightly exceeds data at $\simeq$ 172 GeV. The increasing activity in the forward direction comes mainly from the QCD-RPC processes (Fig.2f) and is more pronounced for the GRV parton density parameterization. Estimation of errors

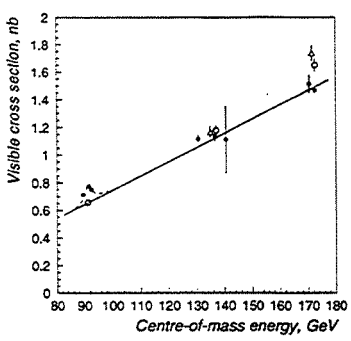

Figure 1: Visible cross-section of the process $e^+e^- \rightarrow e^+e^- + hadrons$ for no-tag events. Points are experimental results, white circles - simulation with GS2 parton density function, white triangle - the same with GRV parameterization. Also shown is the result of the fit by the combination of Cahn's formula and a linear term (dashed line). The solid line shows the linear term alone expressed as $\sigma_{\gamma\gamma} = \sigma_{\gamma\gamma}^Z + d\sigma/dE \times (E_{cms} - 91.25)$, where $\sigma_{\gamma\gamma}^Z = 658.6\pm7.6$ pb, $d\sigma/dE = 10.3\pm0.2$ pb/GeV and E_{cms} is the centre-of-mass energy in GeV.

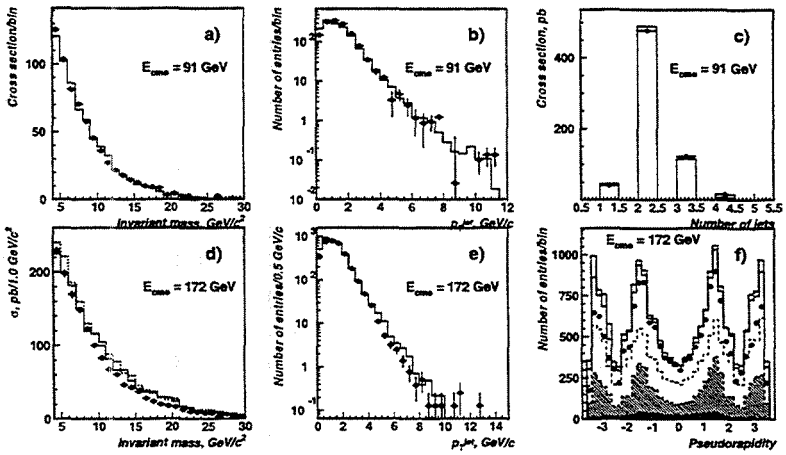

Figure 2: Distributions of event variables. a) and d) invariant mass, b) and e) transverse momentum of jets c) number of reconstructed jets, f) energy flow. Points are data, solid and dotted lines are the full VDM + QPM+RPC predictions with GS2 and GRV parton density functions correspondently while dashed line is QCD-RPC contribution for GS2, hatched histogram is VDM part, double hatched - QPM part.

affecting the level of agreement of the simulated and experimental samples is much more complicated. It was found that the main disagreement comes from the events with a low energy of charged particles and a low fraction of transverse energy, where detector effects (tracking and trigger efficiencies, calorimeter thresholds) are very important and hard to simulate. These effects are still being studied.

3 Double tagged events

Full statistics collected at LEP1 with corresponding integrated luminosity of 101 pb^{-1} are used in the analysis. Four electromagnetic luminometers, the so-called Very Small Angle Taggers (VSAT) [6], are used for energy and angle reconstruction for both scattered e^+ and e^- that was measured. They are placed symmetrically $\simeq$7.7 m downstream of the DELPHI interaction point behind the superconducting quadrupoles at $\simeq$ 60 mm from the beam line covering polar angles θ between 4-15 mrad. Despite the low angles measured the visible cross-section for double tag events is small due to the acceptance of modules (3 cm in X and 5 cm in Y-directions). Moreover, the reconstruction of θ and ϕ angles is quite sensitive to LEP beam parameters, many run-time corrections should be defined and then applied (incident angles of beams for each fill, beam spot position for each run). After all corrections are applied the energy resolution was found to be $\simeq$ 7%, accuracy of angle reconstruction $\sigma_\theta = 0.6$ mrad and $\sigma_\phi = 9°$. Due to a high cross-section of Bhabha scattering for diagonal modules, it is important to have sufficient rejection of background, to avoid random coincidence mainly with the no-tag events measured by DELPHI. Specific cuts were applied to do so: the difference in X and Y coordinates measured for both scattered leptons $\leq 2 \times \sigma$ of the corresponding narrow distributions found for Bhabha events (due to their specific kinematics) for each fill, the energy measured in each module $\leq$

$0.7 \times Ebeam$. Together with the requirement for total event energy measured $\leq 115\ GeV$, 99% of bhabha events are rejected with only 1% for double tagged events. Outer modules are also populated by off-momentum electrons located narrowly around the horizontal plane. This fact can be used for the relative alignment of those modules and thus, with the use of collinearity of Bhabha events, for the relative alignment of internal modules as well. To eliminate possible background from leptonic $\gamma\gamma$ production for the hadronic part of event $3 \leq N_{Charged} \leq 15$, energy of the charged particles below 12 GeV and total energy of the hadronic system below 20 GeV are required. The procedure described above is used for full simulation of double tagged events. Only GS2 parameterization is used for the QCD-RPC part. The VSAT part of the events was treated by specific programs used for luminosity studies. Only 43 events met all selection criteria. Different distributions obtained for such events are shown in Fig.3. Reasonable agreement is shown

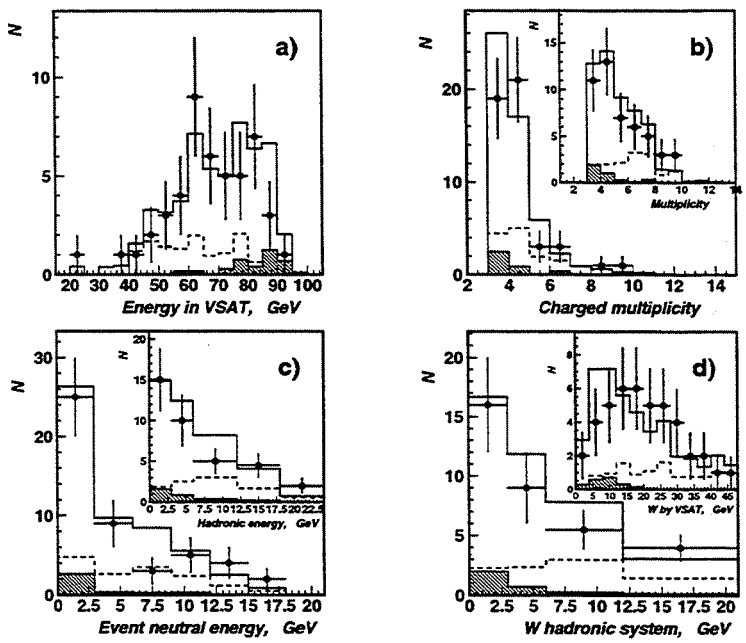

Figure 3: Double tag events. a) energy of scattered e^+ and e^-, b) event multiplicity, c) energy of hadronic system, d) invariant mass reconstructed. Points are data, solid lines are the full VDM+QPM+RPC predictions, dotted lines are the QPM+RPC and hatched histogram -QPM part.

between data and simulation predictions both for the VSAT measurements (Fig.3a) and hadronic component of events shown in Fig.3b-3d. There is an indication that an unfolding procedure should be adopted for better reconstruction of invariant mass from the scattered leptons measured by VSAT (upper part of Fig. 3d) but it is of greatest importance for the lower range. It is clear that due to the very low Q^2 range covered the main contribution comes from the VDM while the QCD-RPC has $\simeq$22% and the QPM only 5%. Taking these fractions into account it becomes possible to estimate a total effective $\gamma\gamma$ hadronic cross-section from those components implemented in the TWOGAM generator. For points combined in the range of $\gamma\gamma$ invariant mass 20-30 GeV and 30-48 GeV results are shown in Table 1, with only statistical errors presented.

Table 1: Effective total $\gamma\gamma$ hadronic cross-section

$\sqrt{s}$ GeV	No of events	Total $\sigma^{\gamma\gamma}_{Tot}$ nb
25	16	356 ± 90
35	10	325 ± 105

4 Conclusions

We have studied hadronic events produced in two-photon collisions at centre-of-mass energies $\sqrt{s} \simeq 91$, 135 and 172 GeV. The visible cross-section of the process $e^+e^- \rightarrow e^+e^- + hadrons$ with the anti-tag condition as a function of e^+e^- centre-of-mass energy is well described by the linear function. Different experimental distributions can be reproduced by the simulation with reasonable accuracy and can be used to evaluate the role of the two-photon process as a background for some physics analyses. At higher energies a certain indication of the increased simulated activity is observed in the forward direction due to QCD-RPC processes which is higher for the GRV parton density parameterization. Preliminary results have been obtained for double tagged events at LEP1 energies. Reasonable agreement with Monte Carlo predictions was shown for such events with very low measured Q^2. The effective total $\gamma\gamma$ cross-section is estimated for $\gamma\gamma$ centre-of-mass energy up to 35 GeV. The forthcoming higher energy LEP runs will contribute to a better understanding of two-photon phenomena.

References

[1] AMY Coll., R. Tanaka et al., *Phys. Lett.* **B277** (1992) 215;
TOPAZ Coll., R. Enomoto et al., KEK-93-107, KEK-93-215.

[2] ALEPH Coll., D. Buskulic et al., *Phys. Lett.* **B313** (1993) 509;
OPAL Coll., R. Akers et al., *Z. Phys. C* **61** (1994) 119;
L3 Coll., O. Adriani et al., *Phys. Lett.* **B318** (1993) 575.

[3] DELPHI Coll., P. Abreu et al., *Z. Phys. C* **62** (1994) 357.

[4] DELPHI Coll., P. Abreu et al., *Nucl. Instr. Meth.* **A378** (1996) 57.

[5] R.N. Cahn, *Phys. Rev.* **D36** (1987) 2666.

[6] DELPHI Coll., P. Abreu et al., *Phys. Lett.* **B342** (1995) 402.

ERRATA

- page 40, equation 3.5

$$\sigma_{acc} = \sigma_0[1 - A(\Delta x - \overline{\Delta x})^2 - B(\Delta x - \overline{\Delta x}) - C(\sigma\Delta x - \overline{\sigma\Delta x}) \\ -D(\Delta y - \overline{\Delta y}) - E(A_D - \overline{A_D})]$$

- page 58, Table 4.1

Correction	Size	Uncertainty	$\Delta\phi$	$\Delta\theta$ (mrad)
Energy reconstruction	<5 GeV	3 GeV	1°	0.15
Geometrical survey (x,y,z)	$\approx$ 1 mm	200 μm	0.5°	0.07
Off-momentum electron position (y)	$\approx$ 1 mm	600 μm	1.5°	0.1
Interaction point correction (x)	$\approx$ 3 mm	20 μm	-	0.03
Beam angles correction	$\approx$ 200 μrad	$\approx$ 50 μrad	0.5°	0.05
Angles reconstruction procedure	-	-	8°	0.6